Model Based Control of Refrigeration Systems

Ph.D. Thesis

Lars Finn Sloth Larsen

Central R & D
Danfoss A/S
DK-6430 Nordborg, Denmark.

ISBN 87-90664-29-9
November 2005

Printing: Budolfi tryk Aps

To my wife

Helena

Preface and Acknowledgments

The work presented in thesis has been carried out under the Industrial Ph.D. programme supported by the Danish Ministry of Science Technology and Innovation. The thesis is submitted in partial fulfillment of the requirements for the Degree of Doctor of Philosophy at the Department of Control Engineering, Aalborg University, Denmark. The work has been carried out at the Central R&D - Refrigeration and Air Conditioning, Danfoss A/S and at the Department of Control Engineering, Institute of Electronic Systems, Aalborg University during a 3 year period from October 2002 to November 2005. Professor Jakob Stoustrup, Associate Professor Henrik Rasmussen and Research Engineer Claus Thybo has supervised the work.

I would especially like to express my gratitude to my good friend, dive mate, college and supervisor Claus Thybo, for his invaluable help, support and inspiration. His guidance and support has truly been ideal. Without his presence this project would not have been at all and it wouldn't have been so enjoyable. I would like to thank Jakob Stoustrup for sharing of his profound knowledge within control theory, that has improved the academic level of this thesis. Moreover I would like to thank Henrik Rasmussen, who has more than a lifetimes experience within application of control theory. His sincere and eager interest in my work has truly been a source of inspiration.

I would like to thank Professor Manfred Morari for giving me the opportunity to stay at the Automatic Control Laboratory, ETH Zürich and for giving me valuable guidance while I was there. I was amazed by the unique scientific milieu and the high academic level there. I would especially like to thank Tobias Geyer, who contributed with many ideas and a lot of help, while I was at the ETH. I would furthermore like to thank him for taking of his valuable time at the ending of his Ph.D.-study to come and visit Danfoss and Aalborg University. I would like to thank the people at the department of ETH; Johan, Helfried, Miroslav and Frank for making it a really enjoyable and memorable stay.

Finally, I want to acknowledge the financial support from the Danish Ministry of Science, Technology and Innovation and Danfoss A/S.

November 2005, Nordborg, Denmark

Lars Finn Sloth Larsen

Summary

The subject for this Ph.D. thesis is model based control of refrigeration systems. Model based control covers a variety of different types of controls, that incorporates mathematical models. In this thesis the main subject therefore has been restricted to deal with system optimizing control. The optimizing control is divided into two layers, where the system oriented top layers deals with set-point optimizing control and the lower layer deals with dynamical optimizing control in the subsystems. The thesis has two main contributions, i.e. a novel approach for set-point optimization and a novel approach for desynchronization based on dynamical optimization.

The focus in the development of the proposed set-point optimizing control has been on deriving a simple and general method, that with ease can be applied on various compositions of the same class of systems, such as refrigeration systems. The method is based on a set of parameter depended static equations describing the considered process. By adapting the parameters to the given process, predict the steady state and computing a steady state gradient of the cost function, the process can be driven continuously towards zero gradient, i.e. the optimum (if the cost function is convex). The method furthermore deals with system constrains by introducing barrier functions, hereby the best possible performance taking the given constrains in to account can be obtained, e.g. under extreme operational conditions.
The proposed method has been applied on a test refrigeration system, placed at Aalborg University, for minimization of the energy consumption. Here it was proved that by using general static parameter depended system equations it was possible drive the set-points close to the optimum and thus reduce the power consumption with up to 20%.

In the dynamical optimizing layer the idea is to optimize the operation of the subsystem or the groupings of subsystems, that limits the obtainable system performance. In systems with a distributed control structure, the cross-couplings are not naturally incorporated in the design of the controllers. The disturbances caused by the individual subsystems might be insignificant, however if the effect from all of the subsystems is synchronized it might cause a sever deterioration in the system performance. In the part of the thesis covering dynamical optimization, the main emphasis is laid on analyzing the phenomena of synchronization of hysteresis controlled subsystems. The propose

method for desynchronization is based on a model predictive control setup. By formulating a cost function that penalizes the effects of synchronization hard, an optimal control sequence for the subsystems can be computed that desynchronizes the operation. A supermarket's refrigeration system consists of a number of refrigerated display cases located in the supermarkets sales area. The display cases are connected to a central refrigeration system, moreover the temperature control in the display cases is carried out by hysteresis controller. Practice however shows that the display cases have a tendency to synchronize the temperature control. This cause periodically high loads on the central refrigeration system and thereby an increased energy consumption and wear. By studying a nonlinear system model it has been analyzed, which parameter that are important for the synchronization. Applying the proposed method on the nonlinear system model has proved that it is capable of desynchronizing the operation of the display cases.

Sammenfatning

Emnet for denne Ph.D.-afhandling er modelbaseret regulering af kølesystemer. Modelbaseret regulering er et bredt område der stort set kan indbefatte alle former for regulering, hvor man benytter matematiske modeller. I denne afhandling har hovedemnet dog været indskrænket til at omhandle system optimerende regulering. Optimeringen opdeles på to niveauer, hvor det øverste system orienterede niveau tager sig af sæt-punkts optimering og det nederste niveau tager sig af dynamisk optimering i de enkelte delsystemer. Afhandlingen har to hovedbidrag, nemlig en metode til sæt-punkts optimering samt en dynamisk optimerende metode til desynkronisering.

I sæt-punkts optimeringen er hovedvægten lagt på at udvikle en simpel og generel metode, der nemt kan anvendes på en mangfoldighed af forskellige system indenfor det samme område, såsom kølesystemer. Metoden baserer sig på et sæt af parameter afhængige statiske systemligninger der beskriver en given proces. Ved at adaptere parametrene til den givne proces, prædiktere den statiske tilstand og beregne en statisk kostfunktionsgradient kan processen drives kontinuert mod nul gradienten, dvs. mod optimum (hvis kostfunktionen er konveks). Metoden medtager ydermere system begrænsninger ved at indføre barrierefunktioner, således at den bedst mulige performance under de givne begrænsninger, eksempelvis ved ekstreme driftssituationer, kan blive opnået. Den udviklede metode blev anvendt på et testkøleanlæg opstillet på Aalborg universitet, til minimering af energiforbrug. Her viste metoden sig i stand til, ved brug af generelle statiske parameterafhængige ligninger, at drive anlæggets sæt-punkter tæt på det virkelige optimum og dermed mindske energiforbruget med op til 20%.

I det dynamiske optimerings niveau er tanken at optimere driften af det eller de delsystemer der udgør flaskehalse for den opnåelige systemperformance. I systemer med en distribueret reguleringsstruktur er krydskoblinger i systemet ikke naturligt inkorporeret i reguleringsdesignet. Forstyrrelserne fra de enkelte delsystemer er måske enkeltvis ubetydelig men synkroniseres effekten fra alle delsystemer kan det betyde alvorlige forringelser i systemperformancen. Hovedvægten i den dynamiske optimerings del er lagt på at undersøge synkroniseringsfænomener i hysterese regulerede delsystemer. Den foreslåede metode til desynkronisering baserer sig på et model prædiktivt reguleringssetup. Ved at opstille en kostfunktion der vægter effekten af synkronisering hårdt kan en

optimal styresekvens til de enkelte delsystemer blive beregnet således at synkronisering og effekten heraf kan minimeres. Supermarkedskøleanlæg består af et antal kølemøbler opstillet i foretningens salgsområde. Kølemøblerne er tilsluttet et centralt køleanlæg og temperatur reguleringen i det enkelte møbel foregår ved en hysterese regulering. Det viser sig i praksis at der er en tendens til at disse kølemøbler synkronisere deres temperaturregulering. Dette medfører imidlertid periodevis store belastninger på det centrale køleanlæg og dermed et forhøjet energiforbrug og slid på anlægget. Ved at benytte en ikke-linear systemmodel blev det undersøgt, hvilke parametre der er betydende for at kølemøblerne synkronisere, samt det blev vist at den forslåede metode er i stand til at desynkronisere driften af kølemøblerne.

Contents

List of Figures

List of Tables

Nomenclature

Symbols

Symbols and parameters used in refrigeration system models

$C_{p,air}$	Specific heat capacity of air
$C_{p,goods}$	Specific heat capacity of goods in display case
$C_{p,wall}$	Specific heat capacity of evaporator wall in display case
C_v	Specific heat capacity of refrigerant
$comp_i$	The i'th compressor capacity
f_q	Heat loss factor in compressor
h_{ad}	Specific enthalpy at outlet of compressor, adiabatic compression
h_{ic}	Specific enthalpy at inlet condenser
h_{ie}	Specific enthalpy at inlet evaporator
h_{is}	Specific enthalpy at outlet of compressor, isentropic compression
h_{lat}	Latent heat capacity of refrigerant
h_{oc}	Specific enthalpy at outlet condenser
h_{oe}	Specific enthalpy at outlet evaporator
$h_{out-suc}$	Specific enthalpy at outlet of suction manifold
h_{sen}	Sensible heat capacity of refrigerant
$K_{1,CF}$	Constant in power consumption in condenser fan
$K_{1,EF}$	Constant in power consumption in evaporator fan
$K_{2,CF}$	Constant in mass flow rate of air across condenser
$K_{2,EF}$	Constant in mass flow rate of air across evaporator
k_{offset}	Offset in expression for power consumption in condenser fan
$\dot{m}_{air,C}$	Mass flow rate of air across condenser
$\dot{m}_{air,E}$	Mass flow rate of air across evaporator
M_{goods}	Mass of goods in display case
$\dot{m}_{ref}$	Mass flow rate of refrigerant
M_{ref}	Mass of liquid refrigerant in the evaporator in the display case
M_{wall}	Mass of evaporator wall in display case
m_C	Exponent in over all heat transfer coefficient, condenser
m_E	Exponent in over all heat transfer coefficient, evaporator
N_{CF}	Rotational speed of the condenser fan

N_{EF}	Rotational speed of the evaporator fan
N_C	Rotational speed of the compressor
OD	Opening degree of the expansion valve
P	Pressure
P_c	Condensing pressure
P_e	Evaporating pressure
P_{suc}	Suction pressure
$\dot{Q}_{airload}$	Heat load from surrounding on display case
$\dot{Q}_{air-wall}$	Heat flux from air to evaporator wall in display case
$\dot{Q}_c$	Heat flux in condenser
$\dot{Q}_{goods-air}$	Heat flux from goods to air in display case
$\dot{Q}_{load}$	Heat load from water heater
Q_1, Q_2, Q_3	Weight matrices
$\dot{Q}_e$	Heat flux in the evaporator (cooling capacity)
R	Gas constant of refrigerant
T	Temperature
T_a	Ambient temperature
T_{air}	Temperature of air in display case
T_{aoc}	Temperature of air out of condenser
T_{aoe}	Temperature of air out of evaporator
T_c	Condensing temperature
T_{cr}	Temperature in cold storage room. Water temperature in water heater
T_e	Evaporating temperature
T_{goods}	Temperature of goods in display case
T_{ic}	Temperature of the refrigerant at the inlet of the condenser
T_{oc}	Temperature of the refrigerant at the outlet of the condenser
T_{oe}	Temperature of the refrigerant at the outlet of the evaporator
$t_{open,i}$	Opening time of inlet valve to evaporator in the i'th disp. case
T_{samp}	Sample time
T_{sat}	Saturation temperature
T_{sc}	Subcooling
T_{sh}	Superheat
T_{wall}	Temperature of evaporator wall in display case
$UA_{air-wall}$	Overall heat transfer coefficient, air -> evap. wall in disp. case
UA_C	Overall heat transfer coefficient for condenser
$UA_{goods-air}$	Overall heat transfer coefficient, goods -> air in disp. case
$UA_{wall-ref}$	Overall heat transfer coefficient, evap. wall -> refrig. in disp. case
$\dot{V}_{comp,i}$	Volume flow created by the i'th compressor
V_{suc}	Volume of suction manifold
V_d	Displacement volume in compressor
$\dot{W}_C$	Power consumption in compressor
$\dot{W}_{CF}$	Power consumption in condenser fan
$\dot{W}_{EF}$	Power consumption in evaporator fan
α_C	Constant in over all heat transfer coefficient, condenser
α_E	Constant in over all heat transfer coefficient, evaporator
δ_{comp_i}	Binary variable describing the i'th compressor

δ_{valve_i}	Binary variable describing the i'th inlet valve
η_{is}	Isentropic efficiency
η_{vol}	Volumetric efficiency
ρ_{ref}	Density of refrigerant
ρ_{suc}	Density of refrigerant in suction manifold
τ_{CF}	Torque on the shaft of the condenser fan
τ_{fil}	Time constant approximating the emptying time of the evaporator

Symbols and parameters used in the set-point optimizing control

b_u	Constant used in the description of linear inequality constrains, inputs
b_x	Constant used in the description of linear inequality constrains, states
$c_{o,j}$	Approximation of $\frac{\partial u_{ss}}{\partial o_{ss}}\Big\|_{x_{ss}\in\partial_j\tilde{\mathcal{U}}} f_j^T$
$c_{x,j}$	Approximation of $\frac{\partial u_{ss}}{\partial x_{ss}}\Big\|_{o_{ss},x_{ss}\in\partial_j\tilde{\mathcal{U}}} f_j^T$
E	Matrix describing linear inequality constrains
e_i	The i'th row of E
F	Matrix describing linear inequality constrains
f	Steady state model
f_j	The j'th row of F
g	Nonlinear inequality constrain
h	Nonlinear equality constrain
J	The cost function
o_{ss}	Steady state control objectives
R	Weight on control objectives
t	Relative weight between barrier function and cost function
u_{ss}	Steady state value of the control signals
v_{ss}	Steady state value of the disturbances
x_{ss}	Steady state value of the states
ϕ	Barrier function
θ_{ss}	Steady state parameters
$\mathcal{F}$	Feasible set
$\mathcal{O}$	Set of solutions to $o_{ss}=0$
$\mathcal{U}$	Set of control variables
$\tilde{\mathcal{U}}$	Set of control variables mapped into the x_{ss}-space
$\mathcal{V}$	Set of disturbances
$\mathcal{X}$	Set of states

Symbols and parameters used in the dynamical optimizing control

A	State-space matrix, in MLD model
A_i, B_i, C_i, D_i	Linear system matrices of the i'th subsystem
A_u, B_u, C_u, d_u	Linear system matrices of the describing dynamics of u_{sub}
B_α	Linear matrix containing the coupling strength of all subsystems
B_1, B_2, B_3	State-space matrices, in MLD model
c_i, d_i	Affine terms in the i'th subsystem
D_1, D_2, D_3	State-space matrices, in MLD model
$E_1, ..., E_5$	Inequality constraint matrices, in MLD model
f_i	Dynamical model of the i'th subsystem

K	Desynchronizing state feedback matrix
K_i	Coupling strength of the i'th Kuramoto oscilator
M	Over estimate
m	Under estimate
N	Prediction horizon
Q_1, Q_2, Q_3	Weight matrices
U	Vector containing a N-step control sequence
u_{exo}	Exogenous control input
u_{sub}	Input to subsystems
u_i, u_i	Controllable upper and lower bounds of the i'th subsystem
x_i	The state vector of the i'th subsystem
x_u	The state vector for u_{sub}
y_i	Output vector of the i'th subsystem
$\bar{y}_i$	Upper bound on y_i
$\underline{y}_i$	Lower bound on y_i
z	Auxiliary variable, in MLD model
α_i	Coupling strength of the i'th subsystem
δ_i	Binary switch, $\delta \in \{0, 1\}$, of the i'th subsystem
$\delta_{\bar{u}_i}$	Binary switch guarding upper bound of the i'th subsystem
$\delta_{\underline{u}_i}$	Binary switch guarding upper bound of the i'th subsystem
θ_i	The phase of the i'th Kuramoto oscilator
$\mathcal{N}_i$	Neighbors of the i'th subsystem

Mathematical symbols

$\succeq, \preceq$	Elementwise $\geq, \leq$
$\leftrightarrow$	Logical iff
$\wedge$	Logical and
$\vee$	Logical or
$\cap$	Intersection
$\cup$	Union
$\emptyset$	The empty set
$\mathbb{N}_0$	Non-negative integers
$\mathbb{R}$	Real numbers
$\mathbb{R}^n$	Space of n-dimensional real vectors
$\mathbb{R}^{n \times m}$	Space of n by m real vectors
I	Identity matrix
R^T	Matrix transpose
R^{-1}	Inverse of the square matrix

Abbreviations

CCC	Constant condensing pressure control
CEC	Constant evaporating pressure control
CFTOC	Constrained finite time optimal control
HVAC	Heating ventilation and air conditioning
LTA	Condensing pressure controlled as linear function of T_a
LQR	Linear quadratic regulator

MI-LP	Mixed integer linear program
MLD	Mixed logical dynamical
MPC	Model predictive control
OCC	Optimal condensing pressure control
OEC	Optimal evaporating pressure control
QSC	Quasi strongly conected
UQSC	Uniformly quasi strongly conected

Chapter 1

Introduction

1.1 Background and Motivation

This project was started-up by Danfoss A/S. Danfoss is a global industrial company, with approximately 17.500 employees and an annual turnover of 15.434 mill. DKK (2003)[1]. Danfoss consists of three business areas, namely: Refrigeration & Air Conditioning (RA), Heating & Water and Motion Controls. The RA-division is by far the largest of the three division, it makes out roughly 50% of the company concerning as well employees as annual turnover. Danfoss is a manufacturer and provider of equipment and controls for refrigeration systems. Especially controls for supermarkets refrigeration systems is one of the major markets for Danfoss. In this thesis it is especially the supermarkets refrigeration systems that is considered.
Application of control algorithms in refrigeration systems is an area that is relatively unknown within the community of control engineering; only few publications can be found. Traditionally most of the development of control algorithms for refrigeration systems has been carried out by refrigeration specialists. The complexity of the refrigeration process, the huge number of different system designs and lack of mathematical models, has made it hard for a non-refrigeration specialist to contribute to the development of control algorithms. Today the refrigeration control system consist of a number of self-contained distributed control loops that during the past years has been optimized to obtain a high performance of the individual subsystems, thus disregarding cross-coupling. The supervisory control of the supermarket refrigeration systems therefore greatly relies on a human operator to detect and accommodate failures, and to optimize system performance under varying operational condition. Today these functions are maintained by monitoring centers located all over the world. Initiated

[1] Annual report Danfoss A/S, 2003

by the growing needs for automation of these procedures, that is to incorporate some "intelligence" in the control system, Danfoss started to look into model based methods for FDI (Fault Detection and Identification) and system optimization. The later issue, that is model based methods for system optimizing control in supermarket refrigeration, is the topic of this thesis.

1.1.1 Vision of a System Optimizing Control

In the traditional (present) control structure the human operator is essential for optimizing the refrigeration systems performance according to varying operational conditions, such as changing ambient temperatures, changing cooling demands etc., that is by adjusting the set-points, see Figure 1.1. However in order to ensure even a remotely close to optimal operation of the refrigeration system, the intervention frequency from the operator has to be quite high. It is therefore not realistic that an operator does these adjustments in practice, why the most refrigeration systems operate with constant set-points.

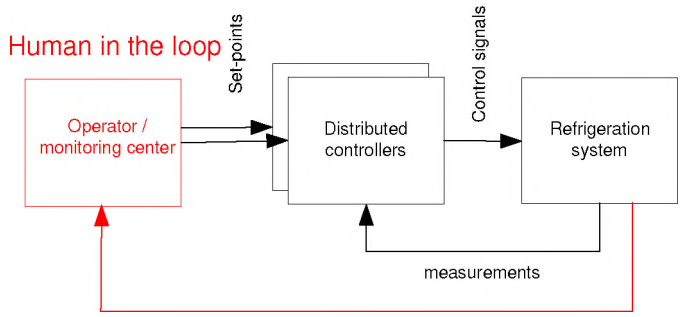

Figure 1.1: The traditional control structure.

The idea of implementing a system optimizing control is to let an optimization procedure take over the task of operating the refrigeration system and thereby replace the role of the operator in the traditional control structure. In this thesis, in the context of refrigeration systems, the idea is to divided the optimizing control structure into two parts. A part optimizing the steady state operation "set-point optimizing control" and a part optimizing dynamic behaviour of the system "dynamical optimizing control", see Figure 1.2. The dynamical optimizing control optimizes the control performance taking the dynamics of the system into account. At this level the optimization is aimed at improving control performance e.g. by minimizing variations on the controlled variables, minimizing the control actions, minimizing response time etc. The set-point optimizing control optimizes the static or quasi-static operation of the system e.g. by minimizing

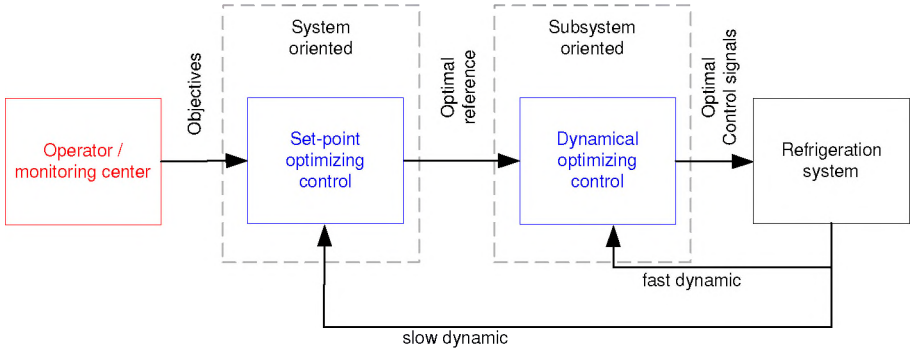

Figure 1.2: The optimizing control structure.

energy consumption, operational costs etc. This way of decomposing the control system results in a cascaded structure where the inner loop (dynamical optimizing control) suppresses the fast disturbances and ensures stability of the system, the slow outer loop (set-point optimizing control) reacts on the slow varying disturbances that have an impact on steady state performance. By comparing Figure 1.1 and 1.2 it can be seen that the role of the operator has changed. His position in the control system has shifted to lower intervention frequency and his input to the system has changed as well. Instead of feeding set-points to the system his task is to give the objectives, that is whether the system should be operated at e.g. minimal power consumption or minimal operational costs etc.
The idea of dividing the system optimization into a static and dynamical part is motivated mainly by three things. Firstly; the dynamical optimizing control can be focused at the group of *subsystems*, where the distributed control structure fails, that is where dynamics of the cross-couplings plays an important part. Large part of the traditional distributed control system can then be maintained ensuring a clear and simple control layout. Secondly; the set-point optimization becomes independent of the control system. At this level the *system* performance is optimized. Thirdly; the modelling effort can be divided into much simpler static *system* models and dynamical models of *subsystems*.
The vision of a system optimizing control and the idea of dividing it into a dynamical and a set-point optimizing part has been the driving force behind this project work and what ties this thesis together.

1.2 Objectives

The main objective of this thesis is to investigate the possibilities of using models in the control of supermarkets refrigeration systems such that as well the control performance

in the distributed control loops as the overall system performance can be optimized.

Set-point Optimizing Control
For many years supermarkets refrigeration systems has been operated with constant set-points. Within the recent years it has been proved by Jakobsen *et al.* (2001) and Larsen and Thybo (2004*b*) that the potential energy savings using optimal set-points in refrigeration systems are substantial. This has increased the interest for methods applicable to refrigeration systems for set-point optimization. The objective in this thesis is to derive a general applicable set-point optimization method for refrigeration system that can drive the set-points towards optimal energy efficiency, while respecting the system limitations.

Dynamical Optimizing Control
A supermarkets refrigeration system consist of a number of subsystems each controlled by a distributed controller. This however neglects the effects of the cross-couplings in the system. However for refrigeration systems with continuous valued control actions this in many cases does not lead to a severe performance degradation, this has among others been investigated by Larsen and Holm (2002). In supermarkets refrigeration systems, consisting of a number of hysteresis controlled subsystems, cross-couplings however have a tendency to make the subsystems synchronize, causing periodically high loads on the system, see Chapter 6. An effect of this is a reduced efficiency and excessive wear on the system. The objective in this part of the thesis is to analyze the phenomenon of synchronization and derive a method for desynchronizing the operation of the distributed controllers.

1.3 Contributions and Publications

The contributions in this thesis fall in two parts concerning respectively set-point optimization and dynamical optimizing control.
The main contribution in the area of set-point optimization.

- Indication of the potential energy savings in refrigeration systems using optimal condensation pressure. Published in Larsen and Thybo (2004*b*).
- Formulation of the energy optimization of refrigeration systems in the context of set-point optimization. Published in Larsen *et al.* (2003).
- A novel approach for on-line set-point optimization is proposed. The approach uses a model based prediction of the steady state cost function gradient to drive the system towards the optimal steady state operation. Published in Larsen *et al.* (2004).

- A novel approach for maintaining operational feasibility under extreme operational conditions.

The main contribution in the area of dynamical optimization.

- Description of the phenomena of synchronization in systems with hysteresis based controllers.
- Novel approach for desynchronization of hysteresis based controllers utilizing hybrid model predictive control. Published in Larsen *et al.* (2005) and Larsen and Thybo (2004*a*).
- A new switched linear model of a supermarket refrigeration system. Published in Larsen *et al.* (2004).

1.4 Thesis Outline

The thesis is divided in two parts, Part I that deals with set-point optimization and Part II that deals with dynamical optimization. Throughout the thesis the Figure 1.2 is used as the main thread connecting the two parts. The reader will therefore find this figure as front page of part I and II. The outline of the two parts are alike, they both gives an overview of existing methods within the area, a formulation of a generalized class of problems originated from refrigeration systems, a derivation of a method to solve that class of problems, and finally a case from a refrigeration system illustrating the problem and the derived method.

The thesis is organized as follows:
Chapter 1: Introduction

Chapter 2: The Vapour-Compression Cycle Process and Supermarket Refrigeration Systems
In this chapter the fundamental thermodynamic terminology is went over and the basics of a simple vapour compression cycle is explained. Furthermore a description of a test refrigeration system that has been constructed as a part of this project is given. Last part of the chapter gives a brief introduction to the typical layout of a supermarkets refrigeration system and the control structure to match.

Part I: SET-POINT OPTIMIZING CONTROL
Chapter 3: Set-point Optimizing Control
This chapter presents an overview of existing methods for set-point optimizing control. An on-line optimization method is proposed that uses a model based prediction of the steady state cost function gradient to drive the system towards the optimal steady state

operation.

Chapter 4: Energy Minimizing Set-point Control of Refrigeration Systems
The objective of this chapter is to formulate energy optimization of refrigeration systems as a set-point optimization problem, furthermore to indicate the potential energy saving using an energy optimal control strategy. Finally the energy optimization is formulated in the novel on-line optimizing framework introduced in Chapter 3 and experimental results are presented.

Part II: DYNAMICAL OPTIMIZING CONTROL
Chapter 5: Dynamical Optimizing Control
The purpose of this chapter is to give an overview of problems that should be handled in the dynamical optimization layer furthermore which methods that are available. Especially one problem coursed by dynamical interactions in the system are investigated namely synchronization. Furthermore a short introduction of the concept of model predictive and discrete time hybrid models is given. Especially the framework of Mixed Logical Dynamical models for hybrid systems and the link to model predictive control is emphasized. Finally a novel approach for desynchronization using model predictive control is presented.

Chapter 6: Desynchronizing Control of Supermarkets Refrigeration Systems
This chapter has three objectives. Firstly to introduce the problem of synchronization in supermarkets refrigeration systems. Secondly to introduce a non-linear and a piecewise affine system model. Thirdly to illustrate the effect of using the hybrid model predictive desynchronizing approach introduced in Chapter 5.

Chapter 7: Discussion and Recommendations

1.5 Reading the Thesis

The content of this thesis covers matters within as well of refrigeration technic as control theory. During the preparation the main emphasis has thus been laid on the control theory, rather than on the refrigeration technics. The reader is therefore expected to have some knowledge within the field of control engineering whereas no or little previous knowledge of refrigeration technic is anticipated. Some effort has therefore been made to explain the requisite fundamentals of the vapour compression refrigeration cycle which takes place within the refrigeration systems considered in this thesis.

Chapter 2

The Vapour-Compression Cycle Process and Supermarket Refrigeration Systems

Refrigeration systems are widely used and can be found in various places such as in supermarkets, in buildings for air conditioning, in domestic freezer etc. These systems in principle all work the same way, they utilize a vapour-compression cycle process to transfer heat. In the first part of this chapter a brief introduction to the most common thermodynamical properties and relations will be given, subsequently the vapour compression cycle and the basic control strategy will be described. Last part of the chapter describes the most common supermarket refrigeration system layout and describes the basic control system.

2.1 Fundamentals of Thermodynamics

Before we turn to describe the vapour-compression refrigeration cycle some fundamental thermodynamical relations, that is used throughout the thesis are briefly recalled.

The First Law of Thermodynamics

The first law of thermodynamics describes conservation of energy, that is for an insulated system, the change of internal energy ΔU equals the sum of the applied work W and heat Q.

$$\Delta U = W + Q \tag{2.1}$$

The Specific Enthalpy

The specific enthalpy (h) is a refrigerant specific property that only depends on the state of the refrigerant, i.e. pressure, temperature and quality. The specific enthalpy is defined as:

$$h \equiv u + Pv, \tag{2.2}$$

where u is the specific internal energy, P is the pressure and v is the specific volume. The enthalpy of a refrigerant can be interpreted as the quantity of energy supplied to the refrigerant to bring it from a certain initial reference state to its current state. The enthalpy of by large all refrigerants can be computed by using various software programs e.g. EES (Klein and Alvarado (2002)).

By applying first law of thermodynamics on a finite volume with an entering ($\dot{m}_i$) and exiting ($\dot{m}_o$) mass flow, the internal energy increase of the volume can be written as (neglecting the potential and kinetic energy (Sonntag *et al.* (1998))):

$$\frac{dU}{dt} = \dot{Q} + \dot{W} + (\dot{m}_i h_i - \dot{m}_o h_o), \tag{2.3}$$

For a steady state and steady flow process this gives:

$$\dot{Q} + \dot{W} = \dot{m}(h_o - h_i), \tag{2.4}$$

Eq.(2.3) and Eq.(2.4) are two important equations that will be used throughout this thesis for model derivation.

The Second Law of Thermodynamics and Entropy

The second law of thermodynamic can be somewhat hard to grasp, but it basically states that energy stored as heat, cannot be converted to the equivalent amount of work. This means that the efficiency of a process that involves transforming heat to work can not under even ideal conditions become 1. If we focus on the compression process which among others takes place in the vapour compression cycle process in a refrigeration system, then the theoretically best one can do is to do the process reversible, such that the increase of the involved entropy is 0. The specific entropy (s), is as the enthalpy a refrigerant specific property only dependent on the state of the refrigerant. By using the definition introduced in Sonntag *et al.* (1998), the entropy can be defined as:

$$dS \equiv \left(\frac{\partial Q}{T}\right)_{rev}, \tag{2.5}$$

where T is the temperature and the subindex rev means it is defined in terms of a reversible process.

To get a true measure on how close the compression process is to the theoretical most efficient, that is to a reversible isentropic process, the isentropic efficiency (η_{is}) is introduced. The isentropic efficiency is defined as (for a process where work is added (Sonntag *et al.* (1998))):

$$\eta_{is} = \frac{W_{is}}{W_{real}}, \tag{2.6}$$

where W_{is} is the required work for performing an isentropic compression process and W_{real} is the real work added.

2.2 The Vapour-Compression Cycle Process

The purpose of the vapour-compression cycle process is basically to remove heat from a cold reservoir (e.g. a cold storage room) and transfer it to a hot reservoir, normally the surroundings. The main idea is to let a refrigerant circulate between two heat exchangers, that is an evaporator and a condenser, see Figure 2.1. In the evaporator the

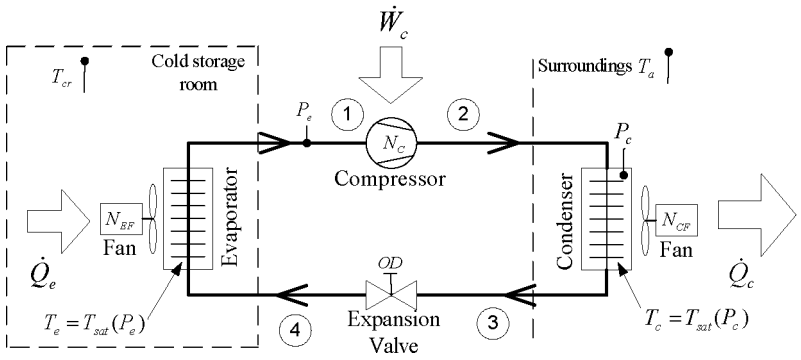

Figure 2.1: The layout of a basic refrigeration system

refrigerant "absorbs" heat from the cold reservoir by evaporation and "rejects" it in the condenser to the hot reservoir by condensation. In order to establish the required heat transfer, the evaporation temperature (T_e) has to be lower than the temperature in the cold reservoir (T_{cr}) and the condensation temperature (T_c) has to be higher than the temperature in the hot reservoir (normally the surroundings T_a), i.e. $T_e < T_{cr}$ and $T_c > T_a$. The refrigerant has the property (along with other fluids and gasses) that the saturation temperature (T_{sat}) uniquely depends on the pressure. At low pressure the corresponding saturation temperature is low and vice versa at high pressure. This property is exploited in the refrigeration cycle to obtain a low temperature in the evaporator and a high temperature in the condenser simply by controlling respectively the evaporating pressure (P_e) and the condensing pressure (P_c). Between the evaporator and the condenser is a compressor. The compressor compresses the low pressure refrigerant (P_e) from the outlet of the evaporator to a high pressure (P_c) at the inlet of the condenser, hereby circulating the refrigerant between the evaporator and the condenser. To uphold the pressure difference ($P_c > P_e$) an expansion valve is installed at the outlet of the condenser. The expansion valve is basically an adjustable nozzle that helps upholding a

pressure difference.

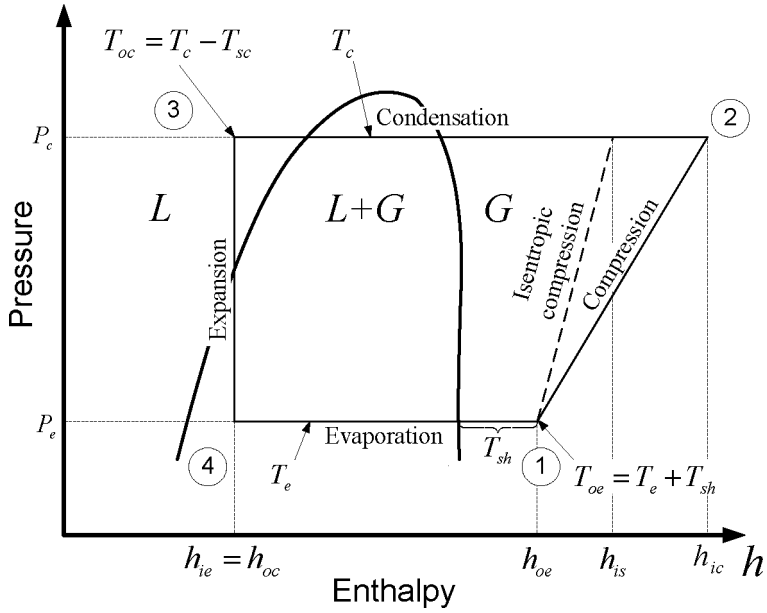

Figure 2.2: The vapour compression cycle in a $h - log(p)$-diagram. The numbers indicate the state points in the cycle

In Figure 2.2 the vapour compression cycle is sketched in a h-$log(P)$-diagram. The diagram is specific for a given refrigerant and gives a general view of the process cycle and the phase changes that takes place. In the h-$log(P)$-diagram, Figure 2.2, the specific enthalpy at the different state points of the refrigeration cycle is denoted by the subindexes i and o for "inlet" and "outlet", plus e and c denoting "evaporator" and "condenser", i.e. h_{oe} is the specific enthalpy at the outlet of the evaporator. This notation will be used throughout the thesis. In the following we will refer to this diagram as we go through the vapour compression cycle. The vapour compression cycle consists of 4 connected subprocesses namely a compression, a condensation, an expansion and an evaporation. We will go through each the processes following the numbers depicted in Figure 2.1 and 2.2.

Compression; State Point 1-2

At the inlet of the compressor the refrigerant is in a gas phase (G) at low pressure and temperature. By compressing the refrigerant, the temperature as well as the pressure increases.

The required work for the compression can be found by forming a control volume around

the compressor, assuming it is insulated (adiabatic compression) and using Eq. 2.4:

$$\dot{W}_C = \dot{m}(h_{ad} - h_{oe}), \tag{2.7}$$

where $\dot{m}$ is the mass flow of refrigerant. If the compression is not adiabatic, then $h_{ic} \neq h_{ad}$ i.e. some heat is transmitted to the surroundings during the compression. In that case it is common to introduce a heat loss factor f_q, to compensate the measurements at the outlet of the compressor for the heat losses. f_q is normally defined as the heat fraction of the applied compressor work that is transmitted to the surroundings (Sonntag *et al.* (1998)):

$$f_q = \frac{h_{ad} - h_{ic}}{h_{ad} - h_{oe}} \tag{2.8}$$

The work applied to the compressor (W_C) can then using Eq.(2.7) and Eq.(2.8) be written as:

$$\dot{W}_C = \frac{1}{1 - f_q} \cdot \dot{m}(h_{ic} - h_{oe}) \tag{2.9}$$

Furthermore the isentropic efficiency η_{is} can be computed using Eq.(2.6):

$$\eta_{is} = (1 - f_q) \cdot \frac{h_{is} - h_{oe}}{h_{ic} - h_{oe}} \tag{2.10}$$

Condensation; State Point 2-3
Form the outlet of the compressor the refrigerant flows into the condenser. The condenser enables a heat transfer ($\dot{Q}_c$) from the hot gaseous refrigerant to the surroundings. Because of the high pressure (the condensing pressure P_c) the refrigerant starts to condense at constant pressure changing its phase from gas into liquid (state point 2-3). A fan blowing air across the condenser helps increasing the heat transfer. Through the last part of the condenser, the refrigerant temperature is pulled down below the condensing temperature (T_c), creating a so-called subcooling (T_{sc}). This subcooling ensures that all of the refrigerant is fully condensed when it passes on to the expansion valve (state point 3). This is important because even a small number of gas bubbles in the liquid refrigerant would lower the mass flow through the valve dramatically, causing a major drop in the cooling capacity ($\dot{Q}_e$).
The heat rejected in the condenser ($\dot{Q}_c$) can be computed forming a control volume around the condenser and using Eq.(2.4):

$$\dot{Q}_c = \dot{m}(h_{ic} - h_{oc}) \tag{2.11}$$

Using the first law of thermodynamics on the system the heat rejected in the condenser can also be computed as:

$$\dot{Q}_c = \dot{Q}_e + \dot{W}_C - \dot{W}_C \cdot f_q \tag{2.12}$$

Recall that the heat $\dot{W}_C \cdot f_q$ is rejected in the compressor.

Expansion; State Point 3-4

The expansion valve separates the high pressure side from the low pressure side. When the refrigerant passes the valve (state point 3-4), it is therefore exposed to a large pressure drop causing some of the refrigerant to evaporate. In Figure 2.2 this can be seen as the process moves from the liquid phase (L) in state point 3, into the two-phase region ($L + G$) in state point 4. This partial phase change causes the temperature to drop down to the evaporation temperature (T_e), determined by the low pressure (P_e). From the expansion valve the refrigerant flows to the evaporator.

Since no work is done when the refrigerant passes the expansion valve ($\dot{W} = 0$) and the expansion valve is assumed insulated ($\dot{Q} = 0$) then according to Eq.(2.4) the inlet enthalpy (h_{oc}) to the valve equals the outlet enthalpy (h_{ie}), i.e. $h_{oc} = h_{ie}$.

Evaporation; State Point 4-1

In the evaporator the low inlet temperature (T_e) enables a heat transfer from the cold reservoir (the cold storage room) to the refrigerant. Hereby the remaining part of the liquid refrigerant evaporates at a constant temperature (T_e) under heat "absorption" from the cold storage room. Like in the condenser a fan helps increasing the heat transfer by blowing air across the evaporator. At the outlet of the evaporator (state point 1) all of the refrigerant has evaporated and the temperature has increased slightly above the evaporating temperature (T_e). This small temperature increase is called the superheat (T_{sh}). The superheat is important to maintain, as it ensures that all of the refrigerant has evaporated, such that no liquid gets into the compressor (state point 1). The liquid could otherwise cause a breakdown of the compressor.

The cooling capacity ($\dot{Q}_e$) can be computed forming a control volume around the evaporator and using Eq.(2.4):

$$\dot{Q}_e = \dot{m}(h_{oe} - h_{oc}) \tag{2.13}$$

The refrigerant has now completed the vapour compression cycle and returns to the inlet of the compressor, state point 1.

2.2.1 Basic Control Structure for a Simple Refrigeration System

The two essentially important set-points to control in a refrigeration system is the high and low pressure, that is the condensing (P_c) and evaporating pressure (P_e). Recall that these pressures uniquely determine the condensing and evaporating temperatures, therefore these has to be kept at a level that enables the proper heat transfers ($\dot{Q}_e$ and $\dot{Q}_c$). Normally the condensing pressure is controlled by a fan blowing air across the condenser (N_{CF}) and the evaporating pressure is controlled by the compressor (N_C), see Figure 2.3. The suction pressure is measured at the inlet of the compressor (in the suction line), if there is no pressure drop in the suction line the suction pressure equals the evaporating pressure.

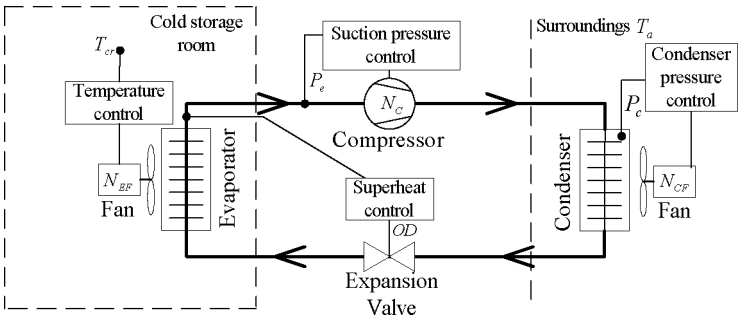

Figure 2.3: The basic control structure in a refrigeration system

As mentioned earlier it is important to uphold a certain superheat to prevent liquid refrigerant from entering the compressor. However the efficiency of the evaporator, that is the ability to absorb heat from the cold storage room, depends on the overall heat transfer coefficient in the evaporator. In general the overall heat transfer coefficient for a liquid flow is much better than for a gas flow. This means that it is preferable to fill the evaporator with as much liquid refrigerant as possible, thereby obtaining a high heat transfer coefficient. In other words it is preferable to run the system with low (ideally zero) superheat. Normally the set-point would be around $5 - 10$ K such that a certain safety margin is upheld. The superheat is controlled by adjusting the inlet of refrigerant to the evaporator by manipulating the opening degree of the expansion valve (OD). Finally the temperature in the cold storage room is controlled by adjusting the evaporator fan speed (N_{EF}). In a typically refrigeration system the control structure is decentralized as depicted in Figure 2.3.

2.3 Supermarket Refrigeration Systems

Refrigeration systems for supermarkets can be constructed in a vast number of ways. It is not realistic within the scope of this thesis to introduce all these system layouts, therefore only the most common layout will be introduced.

2.3.1 Supermarket Refrigeration System Layout

In a supermarket many of the goods need to be refrigerated to ensure preservation for consumption. These goods are normally placed in open refrigerated display cases that are located in the supermarkets sales area for self service. The goods are stored prior to the transfer to the store area, in walk-in storage areas. Figure 2.4 depicts a layout of a

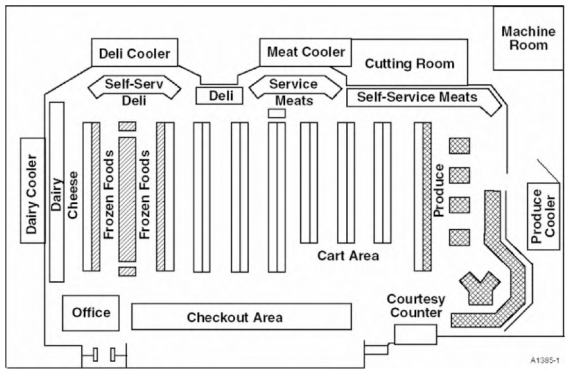

Figure 2.4: Layout of refrigerated display cases in a supermarket (Faramarzi (2004)).

typical supermarket. In general, the refrigeration system in a supermarket can be divided into a low temperature part for storage of frozen food and a medium/high temperature part for refrigerated non-frozen foods. Here, we will consider only the medium/high temperature part.

A supermarket refrigeration system basically works the same way as the simple refrigeration systems described above, Figure 2.3. The number of components is just increased. A simplified supermarket refrigeration circuit is shown in Figure 2.5. The heart of the system is the compressors. In most supermarkets, the compressors are configured as compressor racks, which consist of a number of compressors connected in parallel. The compressors compress the low pressure refrigerant from the suction manifold, which is returning from the display cases. From the compressors, the refrigerant flows to the condenser unit, where the refrigerant condenses; from here the liquid refrigerant flows on to the liquid manifold. The evaporators inside the display cases are fed in parallel from the liquid manifold through an expansion valve. The outlets of the evaporators lead to the suction manifold and back to the compressors thus closing the circuit.

2.3.2 Control System

The control systems used in today's supermarket refrigeration systems is basically like described for the simple systems, i.e. a distributed control layout. The compressor rack is equipped with a suction pressure controller, the condenser unit is equipped with a condensing pressure controller and each of the display cases is equipped with a superheat and a temperature controller.

Turning on and off the compressors in the compressor rack controls the suction pressure. To avoid excessive compressor switching, a dead band around the reference of the suction pressure is commonly used. When the pressure exceeds the upper bound, one or

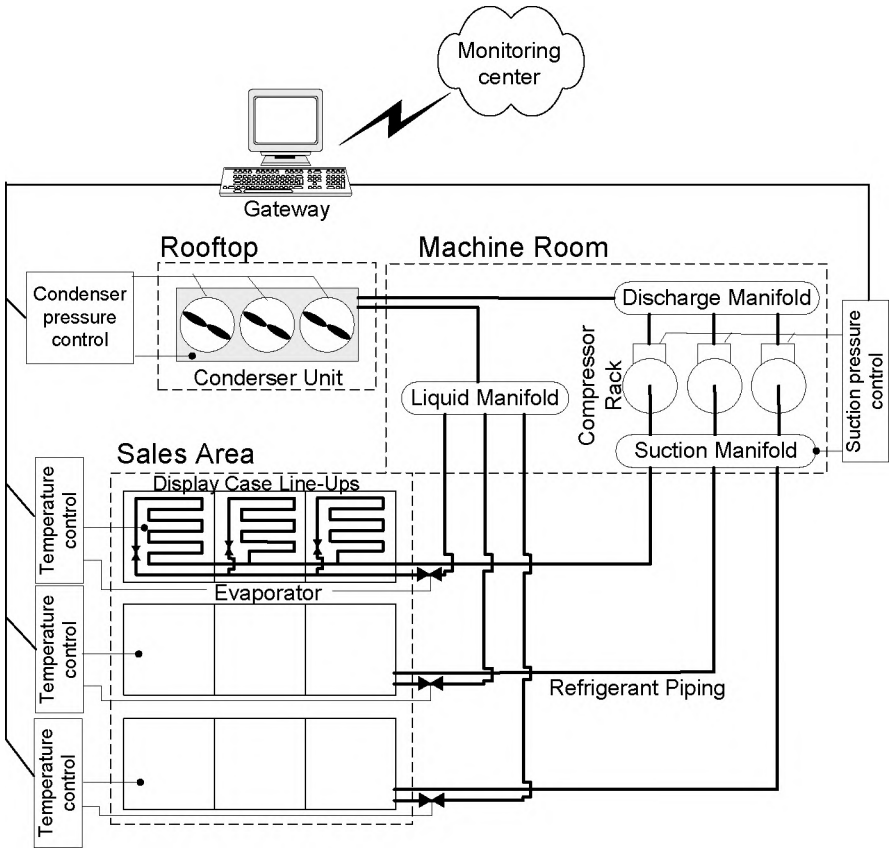

Figure 2.5: A typical layout of a supermarket refrigeration system.

more additional compressors are turned on to reduce the pressure, and vice versa when the pressure falls below the lower bound. In this way, moderate changes in the suction pressure do not initiate a compressor switching (Danfoss A/S (2004*a*)). In some cases one of the compressors can be equipped with a frequency converter, thus facilitating continuous value control actions.

The condensing pressure control is carried out much like the suction pressure control, i.e. the condensing pressure is controlled by turning on and of a number of fans. Also here frequency converters can be used to obtain continuous value control actions.

Normally the superheat is controlled by a mechanical expansion device located at the inlet of the evaporator. Connected in series to the mechanical expansion device is an electronic on/off inlet valve. The display case temperature is controlled by a hysteresis controller that opens and closes the inlet valve. This means that when a certain upper

temperature bound is reached the valve is opens and the temperature decreases until the lower temperature bound is reached and the valve is closed again (Danfoss A/S (2004*b*)). The hysteresis bounds are set according to the required storing temperature of the goods in the display case. Normally the display cases are not equipped with a controllable fan that could otherwise be used in the temperature control.
Figure 2.5 depicts the distributed control structure with the local control loops, furthermore the infrastructure with the lines of communication are depicted. The supermarkets refrigeration control system is normally connected to a central monitoring center. The monitoring center receives process data from each of the local controllers, such that actions can be taken if problems arise in the operation of system. The monitoring center furthermore has the possibility to change set-points and control parameter in the local control loops. However the current infrastructure allows only limited sharing of information directly between the local control loops.

2.4 Models and Test System

The first part of the work in the thesis deals with set-point optimizing control of refrigeration systems. As a part of the preparation of this work a test refrigeration system has been constructed. The test refrigeration is a simple refrigeration system much like the one depicted in Figure 2.1, below the structure of the test system is briefly described. A more thorough description can be found in Appendix A and at the refrigeration laboratory homepage [1]). The basic functionality of a simple refrigeration system, like the test system, is much like a supermarket refrigeration system. Instead of having single components i.e. compressor, condenser etc. the supermarket system has multiple. If the effects of the individual component are accumulated, these can be perceived as single components. Therefore a simple refrigeration system like the test system is suitable for testing system level controls such as set-point optimizing control, which is investigated in the first part of this thesis.
Second part of the thesis concerns dynamical optimizing control. Here the focus is on the subsystems and the dynamical cross-couplings in between them, more specifically on the cross-couplings between the compressors and the display cases. The test system is not usable for such kinds of experiments and therefore no experiments have been conducted related to this part of the work. A simulation model has therefore mainly been used. The used simulation model has been developed for prototyping of refrigeration control systems at Danfoss. In Chapter 6 details of this model will be explained.

[1] `http://www.control.auc.dk/koelelab/"`

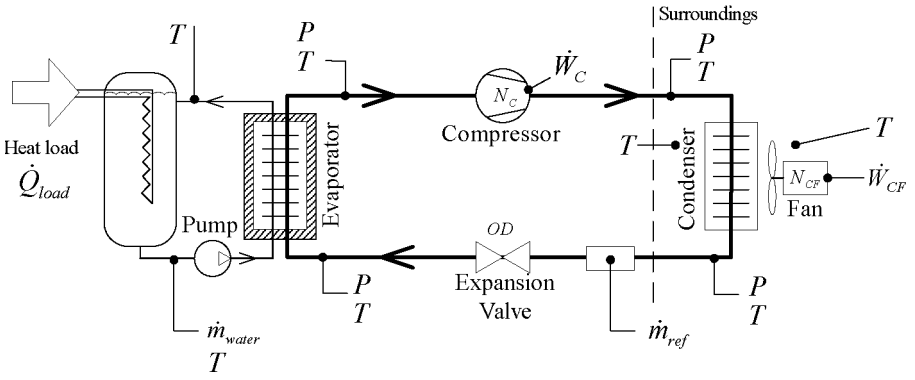

Figure 2.6: Layout of the constructed test refrigeration system.

2.4.1 Test Refrigeration System

As mentioned above a test refrigeration system was constructed, mainly for testing energy optimizing control schemes. Figure 2.6 depicts the basic layout of the system.
The test system is a simple refrigeration system as described above, however instead of air on the secondary side of the evaporator, water is circulated through the evaporator. The heat load on the system is maintained by an electrical water heater with an adjustable power supply for the heat element. The compressor, the evaporator fan and the condenser pump are equipped with variable speed drives such that the rotational speed can be adjusted continuously. The system is furthermore equipped with an electronic expansion valve that enables a continuous variable opening degree. The system is moreover equipped with temperature and pressure sensors on each side of the components in the refrigeration cycle. Mass flow meters measures the mass flow of respectively refrigerant in the refrigeration cycle and water on the secondary side of the evaporator. Temperature sensors measures the in- and outlet temperature of the secondary media on respectively the evaporator and the condenser. The applied power to the condenser fan and the compressor is measured. Finally the entire test system is located in climate controlled room, such that the ambient temperature can be regulated.
For constructing the data acquisition and control interface the XPC toolbox for SIMULINK been used.

Part I

Set-point Optimizing Control

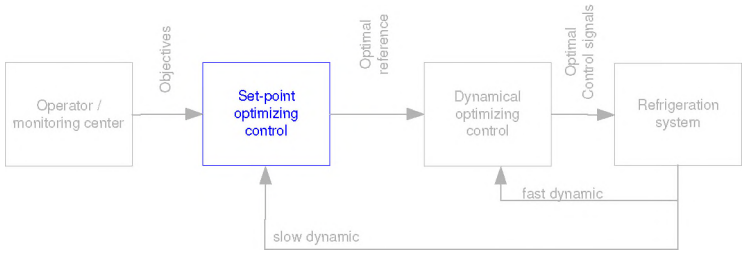

Chapter 3

Set-Point Optimizing Control

Most process plants have complex structures with various subprocesses that have to be coordinated such that the overall control objective is obtained. The classic way to handle the control design for such systems is to divide it into subsystems that are controlled by local stabilizing controllers. Overall stability is then attained by either making the local control robust towards cross-couplings or designing a reference governor for the whole system (Bemporad (1997)). The set-points for the local controllers can normally be chosen within some degree of freedom in a bounded area while still obtaining the objective for the given process. Often these plants operate for long periods in a close to steady state mode, i.e. the local control objective is more or less just disturbance rejection. Systems with this specific enable the possibility for set-point optimization. The objective function to be optimized could encapsulate various things such as production costs, energy consumption, use of raw materials and so forth. Many controllers for larger process plants already utilize these degrees of freedom. In the top-layer of the control hierarchy various kinds of advanced optimization tools for calculating optimal set-points are implemented. For instance in power plant controllers (Mølbak (2003)) where the power production is planned such that economical objectives are optimized taking into account forecasted demands, weather forecasts and so forth, other examples can be found in Yaqun *et al.* (2002), Chang and Shih (2005), Gharb (2001) and Efstratiadis *et al.* (2004). These optimization procedures are often very complicated and involve specialized solvers. For cheaper and mass-produced plants such as refrigeration systems, it is not realistic to implement such complex optimizing controllers, but the need for an intelligent way to continuously track the optimal set-points is thus still present. The requirement to an optimizing control for these systems differs in the way that it should be less complex and apply more generally to various compositions of the same class of systems, such as for instance refrigeration systems. In this chapter the design of such an optimizing control strategy will be addressed. That is an optimizing

control strategy that seeks the optimal set-points while meeting the plant limitations and furthermore adopts the control objective to maintain operational feasibility.

3.1 State of the Art; On-line Set-Point Optimization

In on-line set-point optimization the optimal set-points are continuously evaluated. Hereby it is ensured that the set-points adapt to changing operational conditions due to persistent low frequency disturbances. For such an optimizing control scheme to make sense the system should mainly operate in a nearby steady state mode and have at least *one* degree of freedom. The degree of freedom here refers to the (free) number of set-points that can be varied while upholding the overall control objective. Besides the available degrees of freedom, the *operability* has to be considered, that is the ability of the process to perform satisfactorily under operation away from the nominal design set-point. This latter issue has e.g. been considered in Grossmann and Morari (1984), where a measure of the *flexibility* or *static resiliency* is introduced.
A counterpart to on-line optimization is off-line optimization. Here the optimal set-points are generated before the process plant is started up, based either on models or experiments. The advantage of this is that no complex solvers has to run on-line and perhaps most important a feasible solution is always available. However off-line solutions are not considered here since it requires a considerable installation time and a re-tuning whenever the plant characteristics changes. This is not realistic for smaller mass produced plants such as refrigeration systems.

Process plants normally have complex natures with dynamic and static cross-couplings. When designing the control, the plant has to be decomposed into suitable subsystems in order to compose a clear control layout and to reduce the mathematical complexity. A natural way to decompose the control system is in a hierarchical manner proposed in Lefkowitz (1966), which is motivated by the presence of disturbances with varying frequencies and impact on the "operational cost", other ways of decomposing are reported e.g. in Morari *et al.* (1980), Edgar and Himmelblau (2001) and Skogestad (2000). Figure 3.1 depicts a decomposition of the control system into 4 layers comprising self-organization, adaptation, optimization and regulation. The regulatory task in the top layers is to ensure operability and to keep the set-points at the optimum under influence of "slow" disturbances. The "fast" disturbances are taken care of in the regulatory level by the distributed controllers. Consequently as one moves up in the hierarchic structure the demand to control performance decrease in frequency. This way of decomposing the control system according the frequency (Figure 3.1) fits the distinction between set-point and dynamical optimization that is made in this thesis. That is the dynamical optimization is handled at the regulatory level, whereas the set-point optimization is handled in the optimization layer. By assuming that the "fast" disturbances are dealt with at the regulatory level, the process can be considered to be at a quasi-steady-state at the optimization level. By disregarding the remaining "slow" dynamics, the optimal control

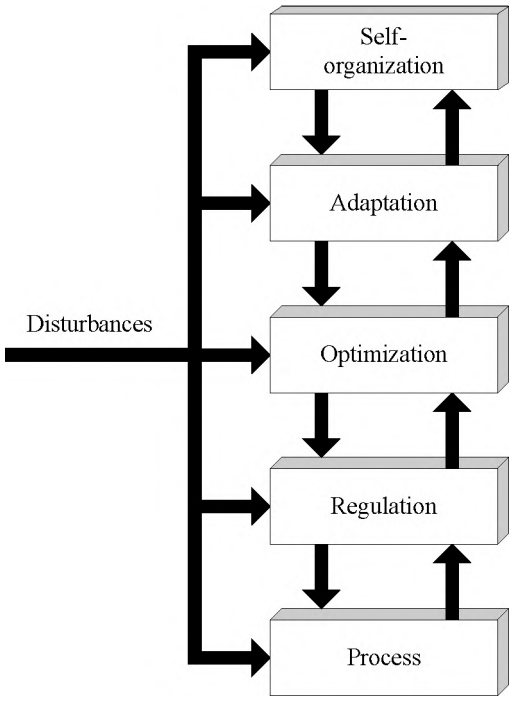

Figure 3.1: Multilayered decomposition of the control system Lefkowitz (1966)

problem (at this level) can be formulated as steady state optimization problem:

$$\begin{aligned} & \min_{u_{ss}} J(x_{ss}, u_{ss}, v_{ss}) \\ \text{Subject to:} \quad & h(x_{ss}, u_{ss}, v_{ss}) = 0 \\ & g(x_{ss}, u_{ss}, v_{ss}) \leq 0, \end{aligned} \tag{3.1}$$

where x_{ss} is a vector containing the relevant states, u_{ss} is the control signal and v_{ss} is the disturbance to the system; the subscript ss denotes steady state. J is a cost function weighting the relevant performance indexes. h and g are vectors describing operational constraints.

Various methods for on-line optimization of this steady state cost function (Eq.(3.1)) are reported. Roughly these methods can be categorized in two classes, namely direct and indirect search methods (Edgar and Himmelblau (2001)).

3.1.1 Direct Methods

The basic idea in the direct methods is to impose small changes in the steady state operation. Based on these experiments, the cost function gradient can be estimated and a step towards a lower cost function value can be taken. One of the advantages with this method is that very little previous knowledge of the system is needed beforehand and no advanced optimization procedure is needed either. Moreover the generality of the method applies to a broad class of systems. The drawback with the method is that for many systems it takes a considerable amount of time for the system to settle at a steady state. Consequently the system can only slowly be driven towards a less expensive steady state (referring to the cost function value). It might not even be fast enough to adapt to the varying operational conditions. Furthermore detecting a steady state is in itself not a simple task e.g. as indicated in Jiang *et al.* (2003) and Liavas *et al.* (1998).

3.1.2 Indirect Methods

Indirect methods or model based methods comprises all the methods that utilizes a model for estimating the optimum, examples of that can be found in Halvorsen and Skogestad (1998) . To the group of indirect methods also belongs the so called self optimizing control. Self optimizing control structures utilizes the characteristics of the system to find and pick out suitable control variables, such that acceptable performance can be obtained with constant set-points in Skogestad (2000). In this way a control structure can chosen that "automatically" keeps the system close to the optimal steady state operation. The model based methods utilizes a model and knowledge of the quasi-static value of the disturbance v_{ss} to compute the optimal values u^*, x^* and J^*. Since no models in practice describe the process exactly, the hereby found optimum will be an estimate of the real optimum. Estimation errors can be caused by several factors as pointed out in Svensson (1994):

- errors in the model structure
- uncertain parameters
- unmeasured disturbances influencing the process
- unknown state variables
- measurement noise

Depending on the accuracy of the model and a priori knowledge of the model parameters the mismatch between the real optimum and the estimated might be minor and no model adaptation is needed. This means the optimization scheme can be implemented in a straight open-loop manner. However in a refrigeration system some of these parameters

are not known a priori and they tend to vary with time. These time variations can be caused simply by replacement of components but also by wear and soiling/cleaning of system parts. To accommodate for these errors, the adaptation layer in Figure 3.1 is a necessity for many systems. Basically two distinct methods can be used for adaptation (Svensson (1994)):

- *Steady state adaptation*, where the parameters and unmeasured states are estimated based on steady state measurements.
- *Dynamic adaptation*, where the parameters and unmeasured states are estimated based on non-steady-state measurements.

The *steady state adaptation* method suffers from the same problem as the direct optimization method does. The measurements have to be gathered at steady state, which for slow dynamical systems result in a slow adaptation. In addition a suitable criterion for detecting the steady state should be determined, which is not straight forward (Jiang *et al.* (2003) and Liavas *et al.* (1998)).
In a *dynamic adaptation* method the measurements are gathered continuously. Therefore the dynamics of the system has to be taken into account; otherwise the estimates will be erroneous. One way of handling the dynamics is simply to use a dynamical system model and then adapt as well the dynamic as the static parameters. This however requires a larger modelling effort in order to capture the dynamical characteristics as well.

3.2 A New Model Based Approach for On-line Set-Point Optimization

In the following an indirect/model based on-line optimizing control scheme with a dynamic adaptation layer is proposed. The method can be seen as an optimization layer on top of an existing distributed control system, that is we try to compute the optimal set-points for the distributed controllers. The proposed method can be divided into three parts namely a steady state optimization, a steady state prediction and a model parameter adaptation, see Figure 3.2. The idea is to utilize knowledge about the current inputs and disturbances for a steady state prediction of the cost function gradient and then drive the system towards a zero gradient adjusting the set-points. To reduce the prediction error, the steady state model parameters are continuously adapted to current point of operation for the real system. Figure 3.3 depicts the general idea. In order to make the scheme work, i.e. track the real optimum with a small error, the static model must capture the overall characteristics well, such that the parameter adaptation does not dramatically change the curvature of the estimated cost function while adjusting the set-points. The parameter adaptation should only remove biases between the real process and the model,

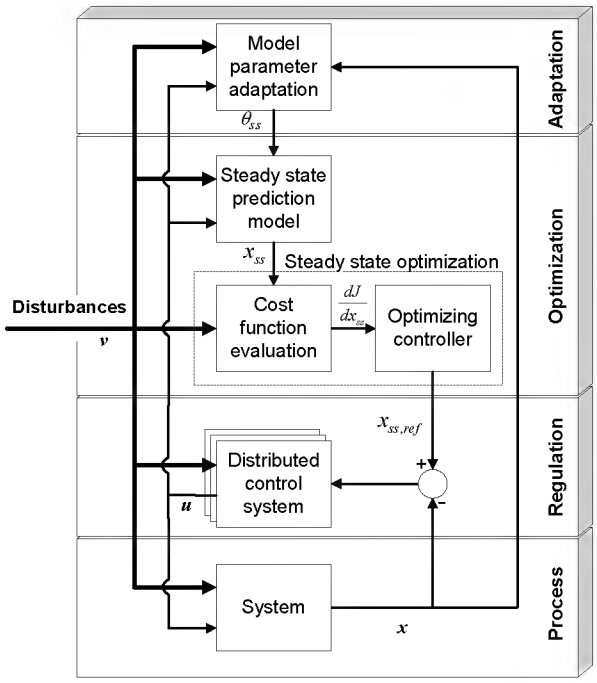

Figure 3.2: The optimizing control structure using the gradient approach.

such that possible model errors can be compensated.
In the following we will start by setting up the steady state cost function and furthermore include systems constrains, such that set-points can be driven towards the optimum, thus without exceeding limitations of the system. Moreover we will analyze feasibility and derive a computational tractable expression for the cost function gradient. Finally the steady state prediction and adaptation layer is went over.

3.2.1 Steady State Optimization Layer

The optimization layer tries to optimize the steady state cost function, given by Eq.(3.1). In the following it is assumed that all of relevant the steady states x_{ss} are controllable and directly or indirectly controlled by a series of distributed controllers. The relevant steady states x_{ss} are the ones that has an impact on the steady state cost function i.e. they enter in Eq.(3.1). Since the control signals are generated by output feedback, it is possible to manipulate the steady states instead of the control signals and therefore use x_{ss} as optimizing variable instead of u_{ss} ($x_{ss} \in \mathbb{R}^n, u_{ss} \in \mathbb{R}^m$). The controlled steady states x_{ss} equals the set-points in the distributed controllers (if using integral

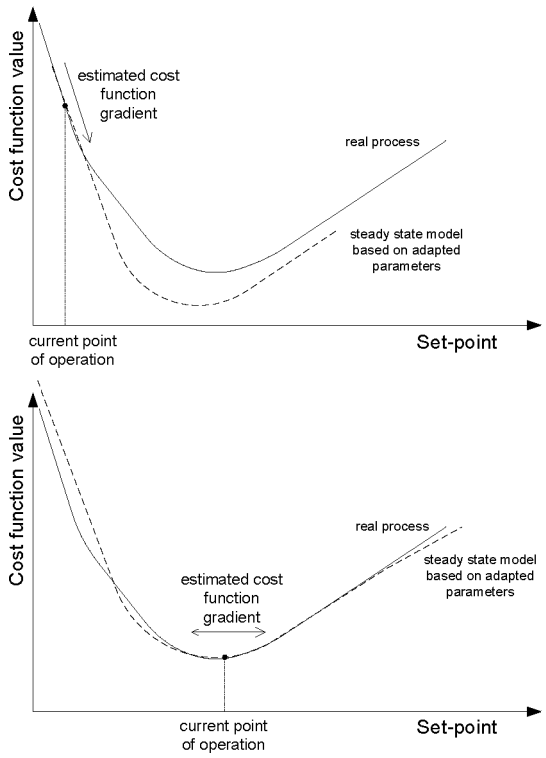

Figure 3.3: The idea behind the proposed set-point optimizing method. The upper part shows a situation where the set-points are driven towards the optimum of the modelled system. In the lower part the optimum is reached and the adaptation has removed possible biases between the real plant and the model.

control), therefore the optimizer x_{ss}^* to Eq.(3.1) can be used as the optimal reference for the distributed controllers. This approach will be adopted in the following. However the optimization problem Eq.(3.1) is further relaxed by the following assumptions.

- The inequality constraints, determined by the operational limitations, can be divided into two subsets namely q constraints on the control signals u_{ss} and p constraints on the set-points x_{ss}. In most practical applications these constraints are linear, hence here they are assumed linear.
- The equality constraints can be divided into a part describing fundamental dependencies between the variables, i.e. the steady state process model $f(u_{ss}, v_{ss}) = x_{ss}$ and a part describing the overall steady state control objectives $o_{ss}(x_{ss}, v_{ss}) = 0$ ($o_{ss} \in \mathbb{R}^l$ is assumed independent of control signal u_{ss}).

- u_{ss} can be separated from the steady state model (f) and inserted in the cost function thus eliminating f from the sets of constraints.

Taking all these assumption in to account, Eq.(3.1) can be rewritten as the following optimization problem:

$$\begin{aligned} & \min_{x_{ss}} J(x_{ss}, u_{ss}(x_{ss}, v_{ss}), v_{ss}) \\ \text{Subject to:} \quad & o_{ss}(x_{ss}, v_{ss}) = 0 \\ & Ex_{ss} + b_x \preceq 0 \\ & Fu_{ss}(x_{ss}, v_{ss}) + b_u \preceq 0, \end{aligned} \tag{3.2}$$

where $E \in \mathbb{R}^{p \times n}$ and $F \in \mathbb{R}^{q \times m}$ are linear matrixes and $b_x \in \mathbb{R}^p$ and $b_u \in \mathbb{R}^q$ are constant vectors. The optimal set-points are given by the optimizer x^*_{ss} to Eq.(3.2) (note that the optimizer $x^*_{ss}(v_{ss})$ depends on v_{ss}).

3.2.1.1 Feasibility

According to the assumptions above the inequality constraints can be divided into two subsets, limitations on the control signal ($u \in \mathcal{U}$) and on the steady states ($x \in \mathcal{X}$). By using the steady state model f, the constraints on u can be mapped in to the x_{ss}-space for a given constant disturbance v_{ss}, $f : (\mathcal{U}, v_{ss}) \curvearrowright \tilde{\mathcal{U}}$. $\tilde{\mathcal{U}}$ is the set of steady states (x_{ss}), that for a given v_{ss} ensures $u_{ss} \in \mathcal{U}$. Now the feasible set $\mathcal{F}$ is given by $\mathcal{F} : \tilde{\mathcal{U}} \cap \mathcal{X} \cap \mathcal{O}$, where $\mathcal{O}$ is the set of solutions to $o_{ss} = 0$ for a given constant v_{ss}. If the feasible set $\mathcal{F}$ is non-empty an optimal solution can be found, but if there exists $v_{ss} \in \mathcal{V}$ (where $\mathcal{V}$ is the set of possible disturbances) that makes $\mathcal{F} = \emptyset$ then the system limitations can not be met and the plant operation becomes infeasible.
The sets $\tilde{\mathcal{U}}$ and $\mathcal{X}$ are in general hard constrained since the boundaries comprises operational limitations which cannot be crossed without endangering the plant. However the objectives (o_{ss}) can be soften without endangering the system, thus reducing the system performance and regaining feasibility. In many cases this is an acceptable price to pay in order to regain feasibility and thus avoid an emergency shutdown. A simple way to relax the objectives is simply to weigh e.g. the 2-norm of o_{ss}. By choosing the 2-norm, the smoothness of the cost function is preserved. Hereby Eq.(3.2) can be rewritten:

$$\begin{aligned} & \min_{x_{ss}} J(x_{ss}, u_{ss}(x_{ss}, v_{ss}), v_{ss}) + \|o_{ss}(x_{ss}, v_{ss})\|^2_R \\ \text{Subject to:} \quad & Ex_{ss} + b_x \preceq 0 \\ & Fu_{ss}(x_{ss}, v_{ss}) + b_u \preceq 0, \end{aligned} \tag{3.3}$$

By choosing a large penalty R for disobeying the objectives (o_{ss}) it can be assured that they are fulfilled as long as $\mathcal{F} \neq \emptyset$, i.e. $\|o_{ss}(x_{ss}, v_{ss})\| < \gamma$, where $\gamma > 0$ can be chosen arbitrarily small, depending on the weight R.

3.2.1.2 Solving the constrained optimization.

By adopting an interior point method or more specifically a barrier method the constraints can be replaced by barrier functions (functions whose value tends to infinity as the constrained variable approaches the boundary). A normal choice for a barrier function is a logarithmic function i.e. $\phi(x) = -log(-g)$ where $g \leq 0$ is an arbitrary inequality constraint, (Boyd and Vandenberghe (n.d.)). Inserting the two sets of inequalities in logarithmic barrier functions following is obtained:

$$\begin{aligned} \phi_1(x_{ss}) &= \begin{cases} -\sum_{i=1}^{p} log(-(e_i x_{ss} + b_{x,i})) & x_{ss} \in \mathcal{X} \\ +\infty & \text{otherwise} \end{cases} \\ \phi_2(x_{ss}, v_{ss}) &= \begin{cases} -\sum_{j=1}^{q} log(-(f_j u_{ss}(x_{ss}, v_{ss}) + b_{u,j})) & x_{ss} \in \tilde{\mathcal{U}} \\ +\infty & \text{otherwise} \end{cases} \end{aligned} \tag{3.4}$$

where e_i is the i'th row of E and f_j the j'th row of F.
By using the barrier functions and introducing a scalar $t \geq 0$ as a relative weight between the barrier and the cost function, Eq.(3.3) can be rewritten as an unconstrained optimization problem.

$$\min_{x_{ss}} t(J(x_{ss}, v_{ss}) + \|o_{ss}(x_{ss}, v_{ss})\|_R^2) + \phi_1(x_{ss}) + \phi_2(x_{ss}, v_{ss}) \tag{3.5}$$

Assuming the optimization problem Eq.(3.5) is convex the optimizer $x_{ss}^*(t, v_{ss})$ should zero the Jacobian:

$$\begin{aligned} &t(\nabla J(x_{ss}^*, v_{ss}) + 2Ro_{ss}(x_{ss}^*, v_{ss})\nabla o_{ss}(x_{ss}^*, v_{ss})) + \sum_{i=1}^{p} \frac{1}{-(e_i x_{ss}^* + b_{x,i})} e_i^T \\ &+ \sum_{j=1}^{q} \frac{1}{-(f_j u_{ss}(x_{ss}^*, v_{ss}) + b_{u,j})} \nabla u_{ss}(x_{ss}^*, v_{ss})^T f_j^T = 0 \end{aligned} \tag{3.6}$$

$x_{ss}^*(t, v_{ss})$ is known as the central path. By letting $t \to +\infty$, $x_{ss}^*(t, v_{ss})$ converges to the true optimizer $x_{ss}^*(v_{ss})$ for the constrained optimization problem Eq.(3.2), that is in the convex case (Boyd and Vandenberghe (n.d.)). Here t will be used as a safety parameter. By adjusting t it can be assured that the optimizer $x_{ss}^*(t, v_{ss})$ stays well inside the interior of the feasible set. Figure 3.4 illustrates how the level sets are affected when increasing t from 0 and towards $+\infty$.

In some cases, e.g. as seen later for energy minimization in refrigeration systems, the steady state objective (o_{ss}) may enter as a part of the system of equations. The use of o_{ss} in the system of equations reduces the modelling effort, as it makes out a part of the required system of equations that uniquely determines J for a given x_{ss} and v_{ss}. When this is the case it is beneficial to augment the optimizing variables (x_{ss}) in Eq.(3.5) with o_{ss}:

$$\min_{[x_{ss}, o_{ss}]} t(J(x_{ss}, o_{ss}, v_{ss}) + \|o_{ss}\|_R^2) + \phi_1(x_{ss}) + \phi_2(x_{ss}, v_{ss}) \tag{3.7}$$

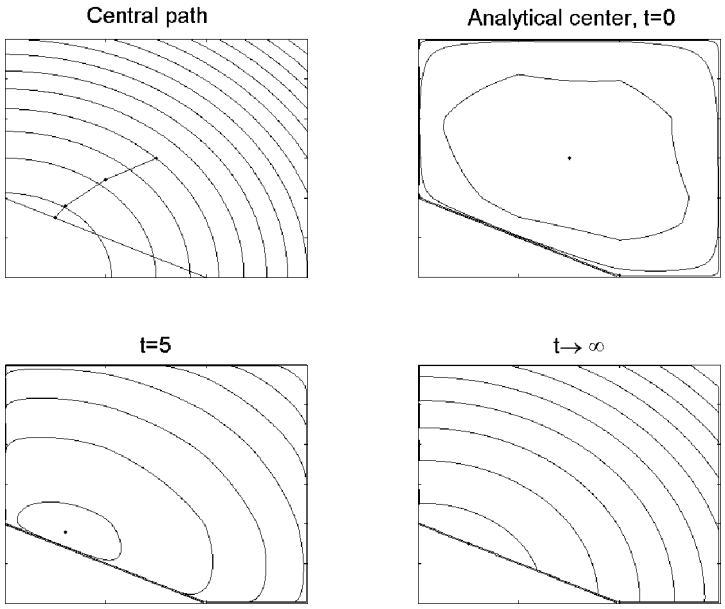

Figure 3.4: The effect of weighting the barrier function.

It is obvious that the optimal value of Eq.(3.5) and Eq.(3.7) is the same, but the Jacobian becomes slightly different:

$$\begin{bmatrix} t\frac{\partial J}{\partial x_{ss}}\Big|_{o_{ss}} + \sum_{i=1}^{p} \frac{1}{-(e_i x_{ss}+b_{x,i})} e_i^T + \sum_{j=1}^{q} \frac{1}{-(f_j u_{ss}+b_{u,j})} \frac{\partial u_{ss}}{\partial x_{ss}}\Big|_{o_{ss}} f_j^T \\ t\left(\frac{\partial J}{\partial o_{ss}}\Big|_{x_{ss}} + 2Ro_{ss}\right) + \sum_{j=1}^{q} \frac{1}{-(f_j u_{ss}+b_{u,j})} \frac{\partial u_{ss}}{\partial o_{ss}}\Big|_{x_{ss}} f_j^T \end{bmatrix} = \begin{bmatrix} 0 \\ 0 \end{bmatrix} \quad (3.8)$$

In this expression the first term is the gradient when moving along the objective (o_{ss}), the second term determines the cost of moving (orthogonal) away from the objective. It can be seen that the second term only becomes "active", when the control signal saturates and the controllability is lost.

Instead of implementing an algorithm that directly calculates the optimal set-point (x_{ss}^*) for every time sample, the Jacobian (left-hand side of Eq.(3.8)) can be used as a control error in a outer loop, as depicted in Figure 3.2. This results in a cascaded control structure, where the distributed controllers are the inner "fast" loops and the optimizing controller using the Jacobian as feedback is the "slow" outer loop. Hereby the computational effort can be reduced as the system "solves" the problem itself in a steepest decent fashion, this idea has previously been published in Larsen *et al.* (2003) and Larsen *et al.* (2004). The idea is then to combine models and measurements to obtain an estimate of the Jacobian Eq.(3.8). To obtain a computationally inexpensive expression of the Jacobian following steps are taken:

- The gradient $\frac{\partial J}{\partial x_{ss}}\big|_{o_{ss}}$ is determined using a model and a steady state prediction of x_{ss}.
- $\frac{1}{-(e_i x_{ss}+b_{x,j})}$ and $\frac{1}{-(f_j u_{ss}+b_{u,j})}$ are determined assuming that $x_{ss} \approx x_f$ and $u_{ss} \approx u_f$, where the subindex f refers to a lowpass filtered version of the measured signal.
- By choosing R sufficiently large it can be assumed that: $\frac{\partial J}{\partial o_{ss}}\big|_{x_{ss}} + 2Ro_{ss} \approx 2Ro_{ss}$.
- The terms $\frac{\partial u_{ss}}{\partial x_{ss}}\big|_{o_{ss}} f_j^T$ and $\frac{\partial u_{ss}}{\partial o_{ss}}\big|_{x_{ss}} f_j^T$ only becomes "active" when the j'th constrain is approached. It is therefore only necessary to have a fairly good approximation of these two gradients when the constrains are active, that is when $x_{ss} \in \partial\tilde{\mathcal{U}}$ ($\partial\tilde{\mathcal{U}}$ denotes the edge of $\tilde{\mathcal{U}}$). Assuming that $\frac{\partial u_{ss}}{\partial x_{ss}}\big|_{o_{ss}}$ and $\frac{\partial u_{ss}}{\partial o_{ss}}\big|_{x_{ss}}$ are approximately constant for all $x_{ss} \in \partial_j\tilde{\mathcal{U}}(v_{ss})$ and $v_{ss} \in \mathcal{V}$, where $\partial_j\tilde{\mathcal{U}}(v_{ss})$ is the j'th edge of $\tilde{\mathcal{U}}(v_{ss})$ created by the j'th constraint of u_{ss}, then $\frac{\partial u_{ss}}{\partial x_{ss}}\big|_{o_{ss}, x_{ss}\in\partial_j\tilde{\mathcal{U}}} f_j^T \approx c_{x,j}$ and $\frac{\partial u_{ss}}{\partial o_{ss}}\big|_{x_{ss}\in\partial_j\tilde{\mathcal{U}}} f_j^T \approx c_{o,j}$ where $c_{x,j} \in \mathbb{R}^n$ and $c_{o,j} \in \mathbb{R}^l$ are the j'th rows of respectively $C_x \in \mathbb{R}^{q\times n}$ and $C_o \in \mathbb{R}^{q\times l}$.

The last point simply means that when a constrain on the control signal is active ($x \in \partial\tilde{\mathcal{U}}$), then a constant vector ($c_{x,j}$) is a fairly good approximation of $\frac{\partial u_{ss}}{\partial x_{ss}}\big|_{o_{ss}} f_j^T$, if it points into the interior of $\tilde{\mathcal{U}}\ \forall\ v_{ss} \in \mathcal{V}$. A fairly good approximation of $\frac{\partial u_{ss}}{\partial o_{ss}}\big|_{x_{ss}\in\partial_j\tilde{\mathcal{U}}} f_j^T$ is one that points in a direction where $\mathcal{F}$ expands.
By taking all of the above points in to account following simplified expression for the Jacobian (Eq. 3.8) is obtained:

$$\nabla\tilde{J} = \begin{bmatrix} t\frac{\partial J}{\partial x_{ss}}\big|_{o_{ss}} + \sum_{i=1}^{p} \frac{1}{-(e_i x_f + b_{x,i})} e_i^T + \sum_{j=1}^{q} \frac{1}{-(f_j u_f + b_{u,j})} c_{x,j} \\ t2Ro_{ss} + \sum_{j=1}^{q} \frac{1}{-(f_j u_f + b_{u,j})} c_{o,j} \end{bmatrix} \tag{3.9}$$

At each time step it is therefore only the value of $\frac{\partial J}{\partial x_{ss}}\big|_{o_{ss}}$ that is somewhat time-consuming to compute.

This methodology of course only gives the global optimum if Eq.(3.5) or Eq.(3.7) is strictly convex or if the cost function declines globally towards the optimum. If this is not the case, there are no guarantees that the method will converge to the global optimum; it could be stuck in a saddle point or a local minima. However the barrier functions at least ensure that the set-points are kept inside the feasible set despite non-convexity. Regaining feasibility does not either rely on convexity but locally whether the feasible set increases when the objectives are relaxed. Later it shall be shown, that for a refrigeration system the minimization of the energy consumption in fact leads to a convex optimization problem.

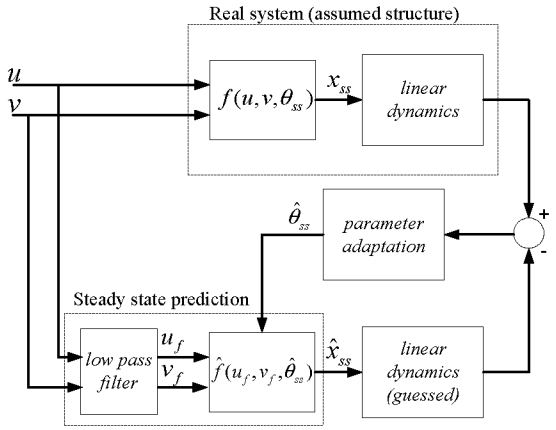

Figure 3.5: The structure of the adaptation layer.

3.2.2 Steady State Prediction and Adaptation Layer

Computation of the Jacobian (Eq.(3.6) or Eq.(3.8)) requires access to the steady values of x_{ss}. Since a steady state cannot be measured continuously it has to be estimated. This is done by assuming that the present low pass filtered version of the control signals (u_f) and disturbances (v_f) are constant until a steady state is reached, that is $u_f \approx u_{ss}$ and $v_f \approx v_{ss}$. Hereby an estimate of x_{ss} can be derived using a steady model of the system (f), see Figure 3.5.
The last layer adapts the steady state model parameters (θ_{ss}) fitting the real system. In this layer the dynamics of the system has to be considered, otherwise the parameter adaptation will be inaccurate in the transients. However the only purpose of the included dynamics in this layer is to filter out the dynamic behavior from the system in the parameter adaptation. Therefore the parameters determining the dynamics are not really of interest. These parameters are therefore left out of the adaptation and guesses used instead. It is assumed that the system can be estimated by an input non-linearity (the steady state model (f)) and a linear dynamic part, similar to the Hammerstein model approach (Edgar and Himmelblau (2001) and Duwaish and Naeem (2001)). Various methods such the MIT-rule or recursive least square methods (Åström and Wittenmark (1989)) can be used for the parameter adaptation, depending on whether the steady state model (f) is linear in the parameter (θ_{ss}). The structure of adaptation and prediction layer is depicted in Figure 3.5. A setup like this will be sufficient for adapting slowly varying parameters (θ_{ss}), as it shall be experimentally proven by the results in Chapter 4.
Summing up a method for on-line set-point optimization has been proposed. The method provides a structure for a simple set-point optimization scheme for a strictly convex cost

function or a cost function that declines globally towards the global optimum. However the method is also applicable where the above mentioned conditions are not fulfilled, in these cases there are however no guarantees that the set-points will converge towards the global optimum. The method provide an optimizing set-point control scheme that can be applied on top of an existing distributed control system.
The framework of the method can furthermore tackle system limitations. By introducing logarithmic barrier functions and a scalar weight it is possible to keep the operation of the plant within the system limitation with an adjustable safety margin. Finally by relaxing the steady state control objective it is possible to maintain operational feasibility in extreme situations, thus with a reduced system performance.

Chapter 4

Energy Minimizing Set-point Control of Refrigeration Systems

Advances in component technology, such as the speed control of compressors, fans etc., has enlarge the degree freedom in the control of refrigeration system. Hereby it has become possible to implement more advanced control schemes that achieve a better performance and furthermore a better energy efficiency. Example of that are given in Gruhle and Isermann (1985) and Parkum and Wagner (1994). The power consumption of a refrigeration system consists of contributions from a number of individual components. The energy optimal control scheme operates at the minimum of the overall power consumption, using the available degrees of freedom in the system to drive the process to the energy optimal steady state (Jakobsen *et al.* (2001)).

Traditionally refrigeration systems are operated at constant set-points. Not much effort has been put into optimizing the set-points according to varying operating conditions, though the potential energy savings are substantial (Jakobsen and Rasmussen (1998), Jakobsen *et al.* (2001) and Larsen and Thybo (2004*b*)). Part of the reason is that many of the refrigeration systems compared to other process systems are relatively small and therefore the cost of implementing a sophisticated optimizing control scheme exceeds the economical benefit of the potential energy savings. It would therefore be interesting to develop a practically feasible and economically tractable control scheme that minimizes the power consumption in refrigeration systems. Motivated by this we will in the following apply the in Chapter 3 proposed method for minimizing the energy consumption in a refrigeration system.

The chapter is structured as follows. At first we will state the energy minimization in refrigeration systems as an unconstraint set-point optimizing problem and subsequently the operational limitations will be taken into account formulating a constraint optimization problem. Next we will derive a general static model for a refrigeration system.

Based on the constraint optimization problem and the static model we will derive the set-point optimizing control scheme for a refrigeration system by applying the proposed method (Chapter 3). Next we will elaborate on the potential energy savings using energy optimal set-points in refrigeration systems. Finally in the last part of the chapter the optimization scheme will be tested on the test refrigeration system and the experimental results will be presented.

4.1 Optimal Set-Points in Refrigeration Systems

An energy optimal control scheme for a refrigeration system must minimize the overall power consumption ($\sum_{\dot{W}}$) while upholding the reference temperature e.g. the cold storage room temperature $T_{cr,ref}$. For exemplification we will in the following use a simple system layout like depicted in Figure 4.1. By using the same terminology as in

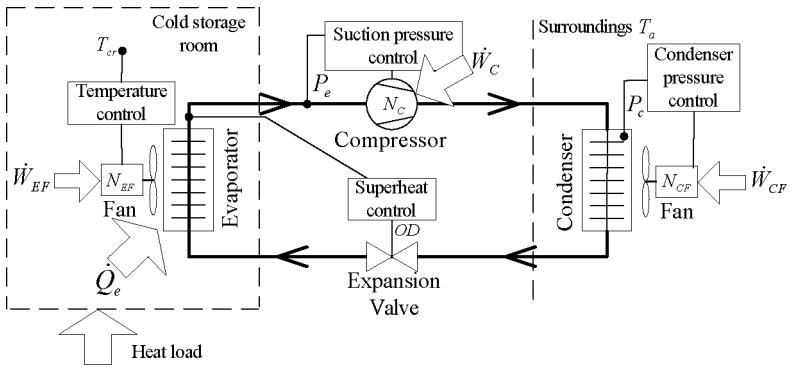

Figure 4.1: Layout of a basic refrigeration system

the figure and adopting the depicted distributed control structure with the 4 independent control loops, the energy minimization can be posed as following minimization problem:

$$\begin{aligned} &\min_{[P_c,P_e,T_{cr}]} \quad (\dot{W}_C + \dot{W}_{CF} + \dot{W}_{EF}) \\ \text{Subject to:} \quad &T_{cr} = T_{cr,ref}, \end{aligned} \tag{4.1}$$

where $\dot{W}$ denotes the power consumption and the subindex denotes the individual components; Compressor (C), Condenser Fan (CF) and Evaporator Fan (EF). The set-points to the control loops, P_c, P_e and T_{cr} are used as optimizing variables, thus disregarding the superheat. It is assumed optimal to keep the superheat constantly small as previously argued in Section 2.2.1. The optimization problem therefore has 3 variables and 1 equality constraint, giving 2 degrees of freedom. The two free variables are respectively the evaporation (P_e) and condensation pressure (P_c).

The set-point optimizing framework described by Eq.(4.1) can easily be adopted to larger systems like supermarket refrigeration systems. This can be done simply by adding up the contribution from each of the components (see Figure 2.5). For example the power consumption from a compressor rack consisting of n compressors can be written as: $\sum_{i=1}^{n} \dot{W}_{C,i}$. The same procedure can be used for a condenser unit consisting of p condenser fans ($\sum_{i=1}^{p} \dot{W}_{CF,i}$), and the display cases in the sales area consisting q evaporator fans ($\sum_{i=1}^{q} \dot{W}_{EF,i}$). However the temperature requirement for the individual or groupings of display cases might be different. Assuming that the display cases can be divide into l groups ($l \leq q$) with the same temperature requirement, then l equality constraints should be introduced. By assuming a distributed control layout with l temperature controllers, one condensing pressure controller and one evaporating pressure controller, following set-point optimization problem can be obtained.

$$\begin{aligned} & \min_{[P_c, P_e, T_{cr,1} .. T_{cr,l}]} \left(\sum_{i=1}^{n} \dot{W}_{C,i} + \sum_{i=1}^{p} \dot{W}_{CF,i} + \sum_{i=1}^{q} \dot{W}_{EF,i} \right) \\ \text{Subject to:} \quad & T_{cr,1} = T_{cr,ref,1} \\ & \vdots \\ & T_{cr,l} = T_{cr,ref,l} \end{aligned} \tag{4.2}$$

Despite the huge number of control loops the optimization has, like Eq.(4.1), 2 free variables, P_c and P_e (2+l variables and l equality constraints = 2 degrees of freedom). Consequently the optimization problem resembles that for a simple system.

Returning to the simple system (Figure 4.1). If the temperature in the cold storage room is kept constant at its reference ($T_{cr,ref}$) and the heat load on the room is constant, then the cooling capacity $\dot{Q}_e$ must be constant as well. Therefore Eq.(4.1) can be reformulated as:

$$\begin{aligned} & \min_{[P_c, P_e]} \left(\dot{W}_C + \dot{W}_{CF} + \dot{W}_{EF} \right) \\ \text{Subject to:} \quad & \dot{Q}_e = \dot{Q}_{e,0} \end{aligned} \tag{4.3}$$

$\dot{Q}_{e,0}$ is the constant required cooling capacity to uphold the temperature ($T_{cr,ref}$), i.e. the steady state control objective is $o_{ss} = \dot{Q}_e - \dot{Q}_{e,0} = 0$. The condenser exchanges heat with the surroundings, therefore the optimization problem does not entirely depend on the refrigeration cycle itself, but on the surrounding temperature as well. It is obvious that the condenser fan has to work harder to exchange heat when the temperature difference between the condenser (the condensation temperature (T_c)) and the surroundings (T_a) is small. To achieve an unambiguous solution, information about the ambient temperature therefore must be included. Changes in the ambient temperature (T_a) is here seen as a "steady state" disturbance, that is $v_{ss} \approx T_a$.
In the following Eq.(4.3) is referred to as the unconstraint optimization problem. Equality constraints can in general be removed from the set of constraints, by insertion in the cost function, hence resulting in an unconstraint optimization problem.

4.1.1 The Constrained Set-Point Optimization

In the previous the operational limitations was not taken into account, in the unconstraint optimization problem (Eq.(4.3)) only the overall steady state control objective was taken into account ($o_{ss} = \dot{Q}_e - \dot{Q}_{e,0}$). In the following we will deal with the system limitations and the constrains they pose to the optimization. As previously argued can the constraints posed by the system limitations be divided into two sets, namely constraints on the set-points ($\mathcal{X}$) and on the control signals ($\mathcal{U}$). We will start by looking at the set-points ($x_{ss} = [P_c, P_e]$). Here the following operational constrains, determining the bounds of $\mathcal{X}$, can be identified:

$P_c \leq P_{c,max}$; ensuring that the maximal allowed pressure in the condenser is respected.

$P_e \geq P_{e,min}$; ensuring that the evaporation temperature does not get too low. A low evaporation temperature can cause damage to the goods close to the evaporator.

$P_c \geq P_e$; ensuring that the refrigerant flows in the right direction making the vapour compression cycle work.

By using the same notation as in Eq.(3.2) the constraints can be collected and written in a matrix form:

$$E = \begin{bmatrix} 1 & 0 \\ 0 & -1 \\ -1 & 1 \end{bmatrix}, \qquad b_x = \begin{bmatrix} -P_{c,max} \\ P_{e,min} \\ 0 \end{bmatrix} \tag{4.4}$$

The system of course also has constrained inputs $u_{ss} = [N_C, N_{CF}, N_{EF}]$, that is the actuator limitations. The opening degree of the expansion valve (OD) is disregarded as it is assumed that the capacity of the valve is so large that it is not posing any real constraints on the system (it will be redundant at all times). The constraint set $\mathcal{U}$ is determined by the saturations of the control signals ($0 \leq N \leq N_{max}$). Written in a matrix form following is obtained:

$$F = \begin{bmatrix} -1 & 0 & 0 \\ 1 & 0 & 0 \\ 0 & -1 & 0 \\ 0 & 1 & 0 \\ 0 & 0 & -1 \\ 0 & 0 & 1 \end{bmatrix}, \qquad b_u = \begin{bmatrix} 0 \\ -N_{C,max} \\ 0 \\ -N_{CF,max} \\ 0 \\ -N_{EF,max} \end{bmatrix} \tag{4.5}$$

The constraint optimization problem can then be written as:

$$\begin{aligned} & \min_{[P_c, P_e]} (\dot{W}_C + \dot{W}_{CF} + \dot{W}_{EF}) \\ \text{Subject to:} \quad & \dot{Q}_e - \dot{Q}_{e,0} = 0 \\ & Ex_{ss} + b_x \preceq 0 \\ & Fu_{ss}(x_{ss}, v_{ss}) + b_u \preceq 0, \end{aligned} \tag{4.6}$$

By relaxing the constraints using barrier functions and softening the steady state control objective ($o_{ss} = \dot{Q}_e - \dot{Q}_{e,0}$) in accordance with Eq.(3.7), the constraint optimization problem can be relaxed and posed as an unconstraint optimization problem:

$$\min_{[x_{ss},\dot{Q}_e-\dot{Q}_{e,0}]} \big[t(\dot{W}_C + \dot{W}_{CF} + \dot{W}_{EF} + \|\dot{Q}_e - \dot{Q}_{e,0}\|_R^2) + \phi_1(x_{ss}) + \phi_2(x_{ss}, v_{ss})\big] \tag{4.7}$$

where $\phi_1(x_{ss})$ and $\phi_2(x_{ss}, v_{ss})$ are given by Eq.(3.4), Eq.(4.4) and Eq.(4.5).
Before we continue with applying the proposed set-point optimization method, a static model has to be derived.

4.2 Static Model of a Refrigeration System

As in the previous we will use the simple system, Figure 4.1 for exemplification. For each of the components, the compressor, the condenser, and the evaporator, a static model will be derived. These models are all tied together by the flow of refrigerant between them. By assuming a steady state, steady flow (see Eq.(2.4)) and neglecting losses in the piping, the state of the refrigerant at the outlet of one component equals the state at the inlet of the next. By applying this, a static model of the *entire* system can be constructed by combining the individual component models.
Much of the details in the derivation of the model is left out here, as most of it can be found in standard textbooks concerning refrigeration (Stoecker (1985)) and heat transfer (Incropera and DeWitt (1985)). In the models below the notation introduced in Chapter 2 will used. The models are written as functions of P_e and P_c, that is the two optimizing variables, see Section 4.1. Whenever the specific enthalpy (h) is used, it will be indicated of which pressure it depends, that is in terms of the refrigeration process. For example the isentropic enthalpy at the outlet of the compressor, h_{is} is in a thermodynamical sense only dependent on the outlet pressure (P_c) and the outlet temperature. However in the refrigeration process, the outlet temperature depends on the inlet pressure (P_e) and the inlet temperature ($T_e + T_{sh}$, where the superheat T_{sh} is a constant controlled variable). This means that h_{is} can be written as a function of P_c and P_e, hence $h_{is}(P_c, P_e)$.

Compressor:
The power consumption in the compressor ($\dot{W}_C$) assuming a constant heat loss coefficient f_q and applying Eq.(2.9) and Eq.(2.13) can be written as:

$$\dot{W}_C = \frac{\dot{Q}_e}{1 - f_q} \cdot \frac{h_{ic}(P_e, P_c) - h_{oe}(P_e)}{h_{oe}(P_e) - h_{oc}(P_c)} \tag{4.8}$$

The enthalpy at the inlet of the condenser (h_{ic}) assuming a constant isentropic efficiency (η_{is}), according to Eq.(2.10):

$$h_{ic} = \frac{1 - f_q}{\eta_{is}} \cdot (h_{is}(P_e, P_c) - h_{oe}(P_e)) + h_{oe}(P_e) \tag{4.9}$$

The mass flow of refrigerant through the compressor ($\dot{m}_{ref}$), where the volumetric displacement is given by V_d, the volumetric efficiency is given by η_{vol} and the density of the refrigerant at the inlet by ρ_{ref} (Stoecker (1985)).

$$\dot{m}_{ref} = N_C \cdot V_d \cdot \eta_{vol} \cdot \rho_{ref}(P_e) \tag{4.10}$$

Condenser:
The power consumption in the condenser fan (axial fan), assuming that the torque is a quadratic function of the rotational speed ($\tau_{CF} = K_{1,CF} \cdot (N_{CF})^2$) (Dixon (1998)).

$$\dot{W}_{CF} = \tau_{CF} \cdot N_{CF} = K_{1,CF} \cdot (N_{CF})^3 \tag{4.11}$$

The mass flow of air ($\dot{m}_{air,C}$) across the condenser is assumed proportional with the rotational speed (Dixon (1998)).

$$\dot{m}_{air,C} = K_{2,CF} \cdot N_{CF} \tag{4.12}$$

The outlet temperature of the air from the condenser (T_{aoc}) can be derived by assuming that the lumped temperature of the condenser wall equals the condensing temperature (T_c). The wall temperature ($= T_c$) is assumed constant across the condenser . The overall heat transfer coefficient is assumed to be given by : $UA = \alpha \cdot \dot{m}_{air}^m$, where α is a constant depending on the characteristic of the air, $\dot{m}_{air}$ (Prandtl, Nusselt and Reynolds number) and the heat transmitting area. The exponent $m = 0.4 \ldots 0.84$ is a constant that depends on the alignment of the tubes in the cross airflow trough the condenser (Incropera and DeWitt (1985)). Based on these assumptions and moreover noting that the inlet temperature to the condenser is T_a, the outlet temperature can be found as (Carabogdan *et al.* (1983)):

$$T_{aoc} = T_c + (T_a - T_c) \cdot \exp\left(-\frac{\alpha_C \cdot \dot{m}_{air,C}^{m_C}}{\dot{m}_{air,C} \cdot C_{p,air}}\right) \tag{4.13}$$

The conservation of energy across the condenser gives (Carabogdan *et al.* (1983)).

$$0 = \dot{m}_{ref}(h_{ic}(P_e, P_c) - h_{oc}(P_c)) - \dot{m}_{air,C} \cdot C_{p,air}(T_{aoc} - T_a) \tag{4.14}$$

Evaporator:
The description for the evaporator is equivalent to that of the condenser, however the heat transfer runs in the opposite direction.
Power consumption in the evaporator fan ($\dot{W}_{EF}$)

$$\dot{W}_{EF} = K_{1,EF} \cdot (N_{EF})^3 \tag{4.15}$$

Mass flow of air across the evaporator ($\dot{m}_{air,E}$)

$$\dot{m}_{air,E} = K_{2,EF} \cdot N_{EF} \tag{4.16}$$

Outlet temperature of air from the evaporator (T_{aoe})

$$T_{aoe} = T_e + (T_{cr} - T_e) \cdot \exp\left(-\frac{\alpha_E \cdot \dot{m}_{air,E}^{m_E}}{\dot{m}_{air,E} \cdot C_{p,air}}\right) \tag{4.17}$$

Conservation of energy across the evaporator.

$$0 = \dot{Q}_e - \dot{m}_{air,E} \cdot C_{p,air}(T_{cr} - T_{aoe}) \tag{4.18}$$

The model above can with ease be extended to include supermarket refrigeration systems. If we briefly look at Figure 2.5 (the layout of a supermarket refrigeration system) then it can be seen that in terms of modelling, the condenser unit and the compressor rack can be perceived as one big condenser and one big compressor. The display cases (or evaporators) can however not be covered by one big evaporator model, because of the different temperature requirements in each of the say l display cases. Therefore l parallel evaporator models has to be included in the system model. This however requires a description of the split of mass flow into the l display cases, which is given by: $\dot{m}_{ref} = \sum_{i=1}^{l} \dot{m}_{ref,i}$. In addition a description of "energy" flow out of the display cases and into the compressor is given by: $\dot{m} \cdot h_{ic} = \sum_{i=1}^{l} \dot{m}_{ref,i} \cdot h_{oe,i}$. These two additional equations is all that is needed for extending the model to larger systems, like supermarket refrigeration systems.
To briefly summarize; we found that a static system model of the refrigeration system can be constructed by a number of component models connected by descriptions of mass and energy flow in between. The component models are in principle so general that they are independent of the specific type of compressor, condenser and evaporator, however the parameters might be different. In the model the following parameters are assumed to be constant, however dependent on the specific type of component: $V_d, \eta_{vol}, f_q, \eta_{is}, K_{1,EF}, K_{2,EF}, \alpha_E, m_E, K_{1,CF}, K_{2,CF}, \alpha_C, m_C$ and $C_{p,air}$.

4.3 Applying the Set-Point Optimizing Scheme for Refrigeration Systems

To illustrate the nature of the optimization problem the unconstraint cost function (Eq.(4.3)) has been computed and plotted in Figure 4.2. This has been done by using the parameter values listed in the Table 4.1, and the static model Eq.(4.8) to Eq.(4.18). As it can be seen, the unconstraint optimization problem Eq.(4.1) is convex with an unambiguous global optimum.
In Figure 4.3 the contour plot of the cost function along with the constraints is depicted, that is the constraint optimization problem given by Eq.(4.6), (note that the constrain $P_e - P_c \leq 0$ is outside the window of the plot).
From Figure 4.3(a) it can be seen that not alone the set $\mathcal{X}$ is convex in x_{ss} ($Ex_{ss} + b_x \preceq$

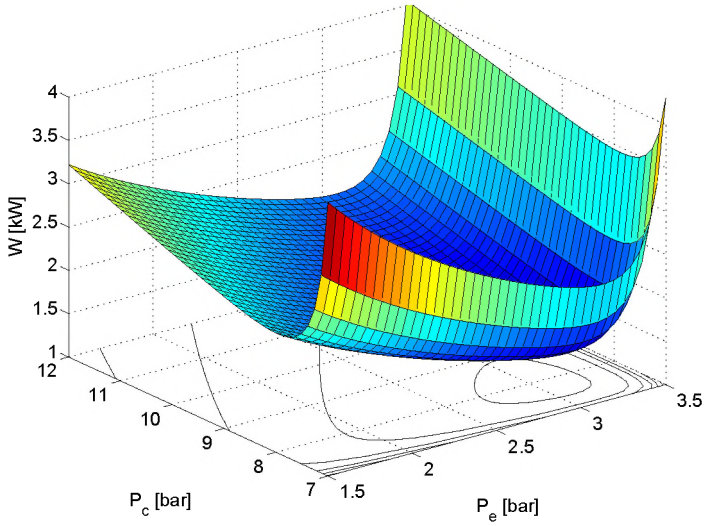

Figure 4.2: The unconstraint cost function, Eq.(4.3), for a constant cooling capacity ($\dot{Q}_e = 4.5$ kW) with the set-points P_c and P_e as optimizing variables.

0 is linear hence convex) but also $\tilde{\mathcal{U}}$ is convex, which means that the feasible set $\mathcal{F}$ is convex. This means that an interior point method using barrier functions and a steepest decent algorithm will converge towards the global optimum (for $t \rightarrow \infty$) (Boyd and Vandenberghe (n.d.)). Therefore if the Jacobian of Eq.(4.7) is computed and used in a feedback as suggested in Section 3.2, the set-points will be driven towards the global optimum.

In Section 3.2.1.1 it was indicated that the set $\tilde{\mathcal{U}}$ was dependent on the steady state disturbance ($v_{ss} = T_a$) and therefore also $\mathcal{F}$. When the ambient temperature increases ($T_a = 25^oC \rightarrow 37.5^oC$) the size of $\mathcal{F}$ decreases see Figure 4.3(b). If T_a increases further ($T_a = 37.5^oC \rightarrow 38.5^oC$) $\mathcal{F}$ will be reduced until it diminishes completely, see Figure 4.3(c). If this happens the system becomes operational infeasible. In other words this means that the condensation pressure can not be kept below $P_{c,max}$ even when the condenser fan is operated at full speed ($N_{CF,max}$). This will with the present control scheme used in supermarket refrigeration systems result in an emergency shutdown. However if the cooling capacity is reduced ($\dot{Q}_e = 4.5kW \rightarrow 4.3kW$) causing a slightly higher room temperature ($T_{cr} = 8.0^oC \rightarrow 8.8^oC$), then feasibility can be regained thus avoiding an emergency shutdown, see Figure 4.3(d).

However in order to make the optimization scheme work the Jacobian Eq.(3.8) has to be computed. By using the static model Eq.(4.8)-(4.18) and that $J = \dot{W}_C + \dot{W}_{CF} + \dot{W}_{EF}$ following expression for $\frac{\partial J}{\partial x_{ss}}|_{o_{ss}}$ can be obtained (in Appendix B details about the

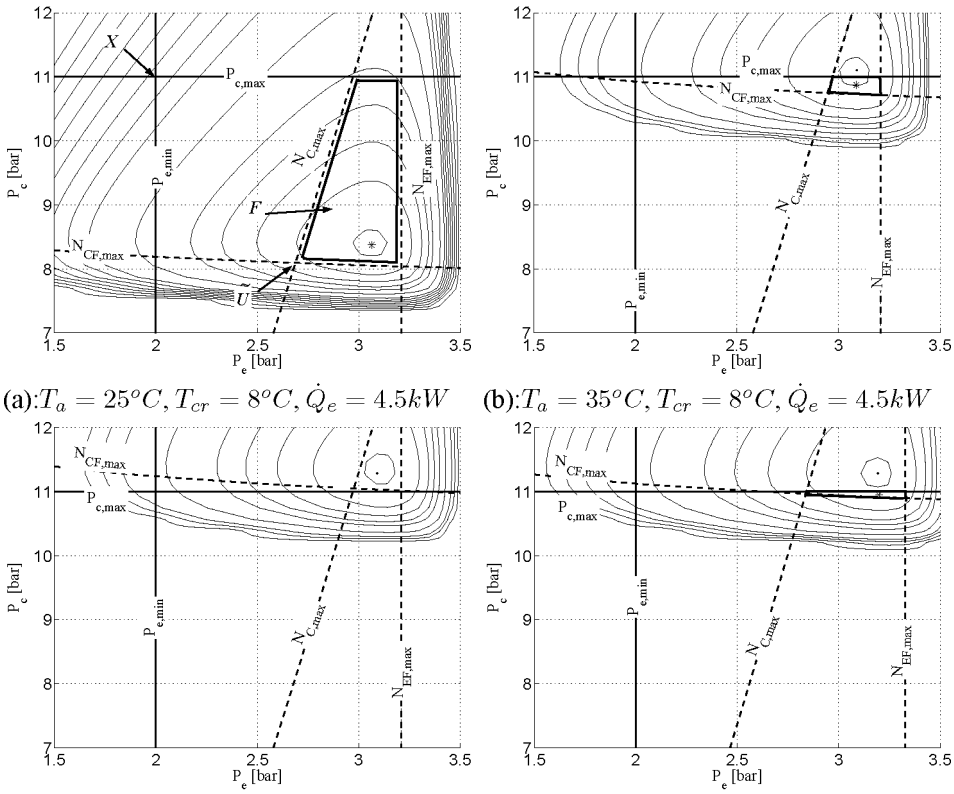

(a):$T_a = 25^oC, T_{cr} = 8^oC, \dot{Q}_e = 4.5kW$ (b):$T_a = 35^oC, T_{cr} = 8^oC, \dot{Q}_e = 4.5kW$

(c):$T_a = 36^oC, T_{cr} = 8^oC, \dot{Q}_e = 4.5kW$ (d):$T_a = 36^oC, T_{cr} = 8.8^oC, \dot{Q}_e = 4.3kW$

Figure 4.3: Contour plots of the cost function plotted along with the system constraints. The $(*)$ denotes the optimum of the cost function with barrier function, Eq.(4.7). (a) The intersection of $\tilde{\mathcal{U}}$ and $\mathcal{X}$ constitutes $\mathcal{F}$. (b) $\mathcal{F}$ decreases as the ambient temperature T_a increases. (c) T_a has increased so much that $\mathcal{F}$ has vanished. (d) By accepting a decreased cooling capacity $\dot{Q}_e$ feasibility is regained.

derivation of the gradients can be found):

$$\begin{bmatrix} \frac{d\dot{W}_C}{dP_c} \\ \frac{d\dot{W}_C}{dP_e} \end{bmatrix} = \dot{W}_C \begin{bmatrix} \frac{\partial his}{\partial P_c}\frac{1}{his-hoe} + \frac{\partial hoc}{\partial P_c}\frac{1}{hoe-hoc} \\ (\frac{\partial his}{\partial P_e} - \frac{\partial hoe}{\partial P_e})\frac{1}{his-hoe} - \frac{\partial hoe}{\partial P_e}\frac{1}{hoe-hoc} \end{bmatrix} \tag{4.19}$$

$$\begin{bmatrix} \frac{d\dot{W}_{CF}}{dP_c} \\ \frac{d\dot{W}_{CF}}{dP_e} \end{bmatrix} = \frac{3\dot{W}_{CF}}{\dot{Q}_c - UA_C(1-m_C)(T_c - T_{aoc})} \begin{bmatrix} \frac{d\dot{W}_C}{dP_c}\frac{\dot{Q}_e}{\dot{W}_C}\frac{h_{ic}-h_{oc}}{h_{oe}-h_{oc}} - \frac{\dot{Q}_c}{T_c-T_a}\frac{\partial T_c}{\partial P_c} \\ \frac{d\dot{W}_C}{dP_e}\frac{\dot{Q}_e}{\dot{W}_C}\frac{h_{ic}-h_{oc}}{h_{oe}-h_{oc}} \end{bmatrix} \tag{4.20}$$

$$\begin{bmatrix} \frac{d\dot{W}_{EF}}{dP_c} \\ \frac{d\dot{W}_{EF}}{dP_e} \end{bmatrix} = \frac{3\dot{W}_{EF}}{\dot{Q}_e + UA_E(1-m_E)(T_e - T_{aoe})} \begin{bmatrix} 0 \\ \frac{\dot{Q}_e}{T_{cr}-T_e}\frac{\partial T_e}{\partial P_e} \end{bmatrix} \tag{4.21}$$

Notice that if $\dot{W}_C$ is measured at steady state, then the gradient Eq.(4.19) only depends on refrigerant properties, i.e. independent of f_q and η_{is} (Eq.(4.19) was derived under the assumption that f_q and η_{is} are constant, independent of P_c and P_e).
The matrices C_x and C_o are approximated by following:

$$C_x^T \approx sign\left(\begin{bmatrix} \frac{dN_C}{dP_c} & \frac{dN_{CF}}{dP_c} & \frac{dN_{EF}}{dP_c} \\ \frac{dN_C}{dP_e} & \frac{dN_{CF}}{dP_e} & \frac{dN_{EF}}{dP_e} \end{bmatrix}\right) \cdot F^T = \begin{bmatrix} -1 & 1 & 1 & -1 & 0 & 0 \\ 1 & -1 & 1 & -1 & -1 & 1 \end{bmatrix} \tag{4.22}$$

$$C_o^T \approx sign\left(\begin{bmatrix} \frac{dN_C}{d\dot{Q}_e} & \frac{dN_{EF}}{d\dot{Q}_e} & \frac{dN_{CF}}{d\dot{Q}_e} \end{bmatrix}\right) \cdot F^T = \begin{bmatrix} -1 & 1 & -1 & 1 & -1 & 1 \end{bmatrix} \tag{4.23}$$

As it can be seen from Eq.(4.22) and Eq.(4.23) very rough estimates of $\frac{\partial u_{ss}}{\partial o_{ss}}\big|_{x_{ss}}$ and $\frac{\partial u_{ss}}{\partial x_{ss}}\big|_{o_{ss}}$ are used namely only the sign. This gives a fairly good approximation[1] that can be computed from only having qualitative knowledge of the system behavior. Inserting Eq.(4.19)-(4.23) in Eq.(3.9) the simplified expression for the Jacobian ($\nabla\tilde{J}$), can be computed. Using $\nabla\tilde{J}$ in a feedback to a set-point controller, the set-points P_c, P_e and $\dot{Q}_e$ can be controlled[2] such that $\nabla\tilde{J}$ is driven towards zero in a steepest decent fashion, that is to the optimum of the relaxed constraint optimization problem Eq.(4.7). Using a steepest decent method, the optimal set-points P_c^*, P_e^* and $\dot{Q}_e^*$ can be found. The feasible set ($\mathcal{F}$) depicted in Figure 4.3 has been computed using the optimal value $\dot{Q}_e^*$. The optimal values of P_c^* and P_e^* are plotted and indicated by the star (*) in Figure 4.3(a),(b) and (d). In Figure 4.3(a) the optimum is in the interior of $\mathcal{F}$, why the optimum of the constrained and unconstrained optimization coincides. In Figure 4.3(b) the optimum of the unconstrained optimization falls outside $\mathcal{F}$, why the true optimum of the constrained optimization lies on the bound of $\mathcal{F}$. However the weight t has been chosen to $t = 0.5$ such that a certain safety margin to the constraints is upheld, why the obtained optimum

[1] A fairly good approximation points to the interior of $\mathcal{F}$, according to Section 3.2.1

[2] $\dot{Q}_e$ is indirectly controlled by changing the temperature reference $T_{cr,ref}$

falls in the interior of $\mathcal{F}$. In Figure 4.3(d) the constraint optimization problem is infeasible, however the relaxation of the steady state control objective ($o_{ss} = \dot{Q}_e - 4.5kW$) allows the cooling capacity to decrease ($\dot{Q}_e = 4.5kW \rightarrow 4.3kW$, such that the operational feasibility can be maintained.

The numerical example above proved that by using the simplified expression of the gradient Eq.(3.9) in a steepest decent algorithm it was possible to compute the optimum. Furthermore it showed that by using the weight t as a safety parameter it is possible to keep the operation of the plant well inside the feasible set. Finally it was proved, that by relaxing the steady state control objective (to uphold the cooling capacity) it was possible to regain feasibility, this by lowering the cooling capacity and allowing the cold storage room temperature (T_{cr}) to increase.

4.4 Potential Energy Savings

The objective of the following section is to give a feeling of the optimization problem and to indicate the amount of energy that it is possible to save by using energy optimal set-points.

Component	Parameter	Value		Parameter	Value	
Compressor	V_d	53.86	$[cm^3]$	f_q	0.20	
	η_{vol}	0.70		η_{is}	0.50	
	$N_{C,max}$	60.00	$[s^{-1}]$			
Evaporator	$K_{1,EF}$	$1.2 \cdot 10^{-3}$	$[Js^2]$	$K_{2,EF}$	0.02	$[kg]$
	α_E	1170.00		m_E	0.50	
	$N_{EF,max}$	60.00	$[s^{-1}]$	$P_{e,min}$	2.00	[bar]
Condenser	$K_{1,CF}$	$1.2 \cdot 10^{-3}$	$[Js^2]$	$K_{2,CF}$	0.02	$[kg]$
	α_C	1170.00		m_C	0.50	
	$N_{CF,max}$	60.00	$[s^{-1}]$	$P_{c,max}$	11.00	[bar]
Air	$C_{p,air}$	1000.00	$[\frac{J}{kg \cdot K}]$			
Refrigerant	Thermodynamical properties of $R134a$ Skovrup (2000)					

Table 4.1: Parameter values. The parameters concerning the compressor and condenser have been obtained from the test refrigeration system.

By using the static model and the parameter values from Table 4.1 the power consumption in various operational conditions has been computed. Figure 4.4(a) depicts the power consumption in the compressor as a function of the condensing pressure (P_c), for a constant cooling capacity ($\dot{Q}_e = 4.5$ kW) and a constant evaporating pressure ($P_e = 2$ bar). It can be seen that by reducing the condensing pressure from for example 12 bar to 8 bar one can reduce the power consumption in the compressor with roughly 30 %.

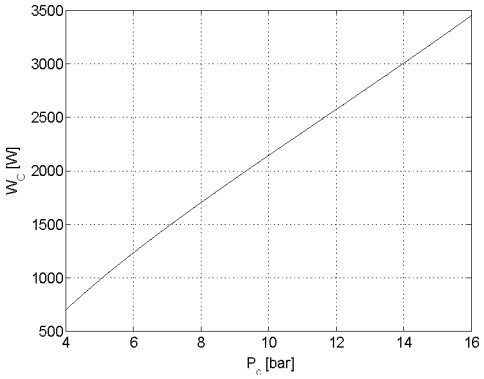

(a) $P_e = 2$ bar and $T_{cr,ref} = 10\ ^oC$

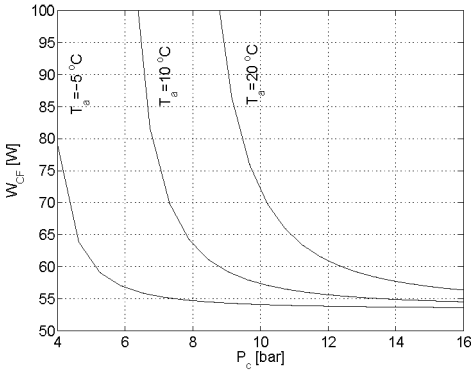

(b) $P_e = 2$ bar and $T_{cr,ref} = 10\ ^oC$

Figure 4.4: The power consumption respectively in the compressor and the condenser fan at varying condensing pressure but constant evaporating pressure

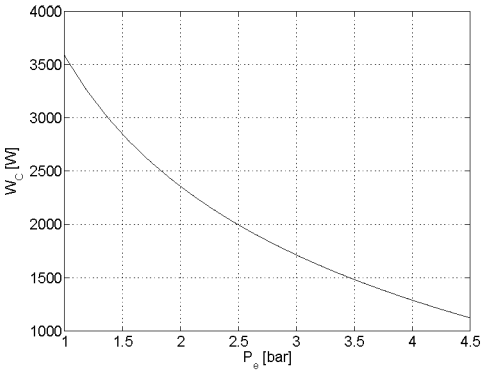

(a) $P_c = 11$ bar and $T_a = 20\ ^oC$

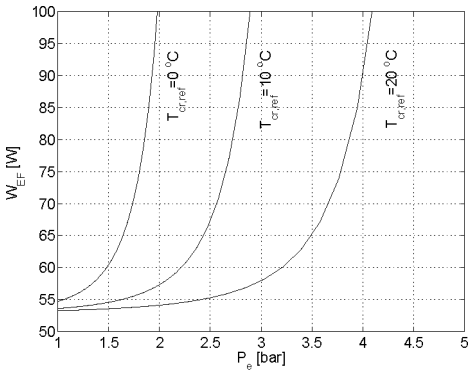

(b) $P_c = 11$ bar and $T_a = 20\ ^oC$

Figure 4.5: The power consumption respectively in the compressor and the evaporator fan at varying evaporating pressure but constant condensing pressure

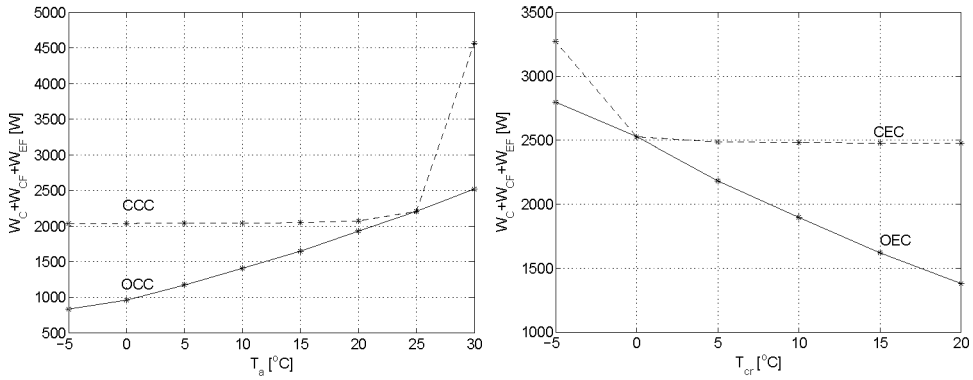

(a) OCC vs. CCC at varying T_a

(b) OEC vs. CEC.at varying T_{cr}

Figure 4.6: Power consumption using optimal set-points compared to traditional control strategies.

This reduced condenser pressure (P_c) can be obtained by increasing the condenser fan speed, while upholding the evaporating pressure (P_e). This of course results in an increased power consumption in the condenser fan as it is illustrated in Figure 4.4(b). It can however be seen that when the ambient temperature (T_a) is low, it requires less energy to obtain this reduced condenser pressure. This indicates that especially in the cold season it is possible to save energy by reducing the condenser pressure (recall that the condenser unit is placed outside on the supermarkets rooftop).
The power consumption in the compressor can however also be reduced by increasing the evaporating pressure, thus increasing the power consumption in the evaporator fan, see Figure 4.5(a) and (b). It can further be seen that if the temperature reference to the cold storage room ($T_{cr,ref}$) is high it requires less energy to obtain this increased evaporation pressure, i.e. the same picture as for the condensing pressure. Therefore if the temperature reference ($T_{cr,ref}$) and/or the ambient temperature (T_a) varies, it pays off continuously to optimize the two pressures, P_c and P_e.
To give an impression of the potential energy savings, a comparison between an optimal condenser pressure set-point control (OCC) and the traditional constant condensing pressure set-point control (CCC) has been performed. The OCC scheme optimizes the condensing pressure (P_c) while keeping the evaporating pressure constant. The power consumption using these two control schemes are shown in Figure 4.6(a). It is assumed that the CCC controlled system runs optimally at $T_a = 25^oC$. As the figure shows, increases the potential energy savings for the CCC controlled system as T_a changes from 25^oC. At an ambient temperature of $T_a = 15^oC$ it is possible to reduce the total power consumption with about 20%, at $T_a = 10^oC$ with 30% and so forth.
In Figure 4.6(b) an optimal evaporating pressure set-point control (OEC) is compared with the traditional constant evaporating pressure set-point control (CEC). The OEC

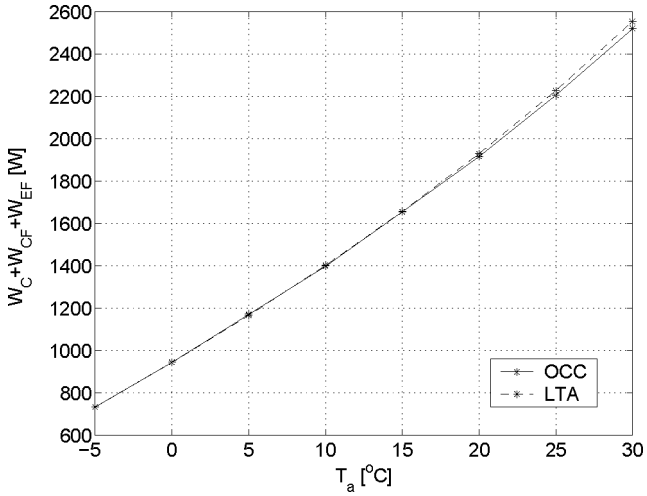

Figure 4.7: Power consumption of OCC compared with the LTA control, $T_c = T_a + 9.5$.

scheme optimizes the evaporating pressure (P_e) while keeping the condensing pressure constant. It is assumed that the CEC controlled system runs optimally when $T_{cr} = 0^oC$. The same picture as for the condenser pressure can be observed, when the cold storage room temperature is changed from the optimal ($T_{cr} = 0^oC$) then the potential energy savings increases. For example, if T_{cr} is changed from 0^oC to 10^oC the potential energy saving is roughly 25% and so forth.

Another control strategy that has been proposed by Jakobsen and Skovrup (2001) is to control the condensing temperature as linear function of the ambient temperature (LTA) (actually the wetbulb temperature but we assume the air is dry), i.e. $T_c = a \cdot T_a + b$. Figure 4.7 depicts the OCC compared with the LTA control strategy. Making a best fit of the parameters it is found that $a \approx 1$ and $b \approx 9.5$. As it can be seen an astonishingly good approximation of the optimal condenser pressure can be obtained using the LTA strategy, this was however for a constant cooling capacity. In a supermarkets refrigeration system daily changes in the required cooling capacity occurs, e.g. between night a day. During the night the display cases are normally covered with insulation to minimize the load from the surroundings hence reducing required cooling capacity. In Figure 4.8(a) is depicted the effect of a 20% increase in cooling capacity on the energy consumption of the LTA compared to the OCC. As it can be seen the LTA is quite robust to a change in Q_e, it can however be seen that the loss in optimality seems to increase with the ambient temperature, hence at $T_a = 25\ ^oC$ the loss is approximately 5% and at $T_a = 30\ ^oC$ it is approximately 6%.
A condenser unit in a supermarket's refrigeration system is as mentioned earlier placed outside and therefore exposed to dirt. A commonly arising problem is that dirt tends to

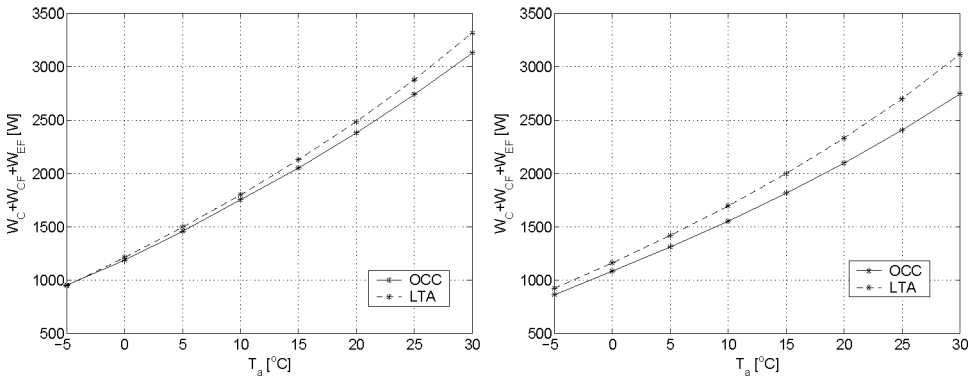

(a) 20% increase of $\dot{Q}_e$ (b) 30% decrease in $K_{2,CF}$

Figure 4.8: Sensitivity in the power consumption using LTA compared to OCC, with respect to changes in the cooling capacity and a reduced mass flow of air lowering the overall heat transfer in the condenser, caused by dirt build up.

builds up on the fins of the condenser, hence reducing the airflow and lowering the over all heat transfer (Thybo and Zamanabadi (2003*a*)). Now Figure 4.8(b) depicts the loss in optimality in the LTA assuming that dirt on the condenser has reduced the mass flow of air by 30%, i.e. $K_{2,CF}$ is reduced by 30%. In Figure 4.8(b) it can be seen that this causes an increased power consumption of the LTA compared to the optimal (OCC), which at $T_a = 25\ ^oC$ amounts to approximately 11%. As the cooling capacity changes during the day and the dirt slowly builds up during weeks or months it is not unrealistic that a supermarkets refrigeration system is operated at an increased cooling capacity while dirt is on the condenser. In Figure 4.9 is plotted the effect of a 20% increase of the cooling capacity (Q_e) and simultaneously a 30% reduction in air flow ($K_{2,CF}$) . In this case it can be seen from Figure 4.9 that the loss of optimality becomes quite significant, at $T_a = 25\ ^oC$ the loss is around 22%.

All in all the LTA strategy is a simple strategy that gives a close estimate of the optimal condenser pressure and is a huge improvement compared to the commonly used CCC strategy. Though the LTA strategy proved to be quite robust towards individual changes in respectively operating conditions and system characteristics, simultaneous changes though caused a considerable loss in optimality. Therefore in refrigeration systems where the cooling capacity varies and dirt builds up on the condenser (after cleaning it regularly) there is still a considerable potential energy saving to be obtained utilizing an OCC compared to the LTA strategy. However the LTA could be improved by including the dependency of Q_e and thus reducing the effect of simultaneous changes in the cooling capacity and mass flow of air.

The exact percentage that it is possible to save depends however on the given characteristics of the compressor and the fans in the individual refrigeration systems. The above

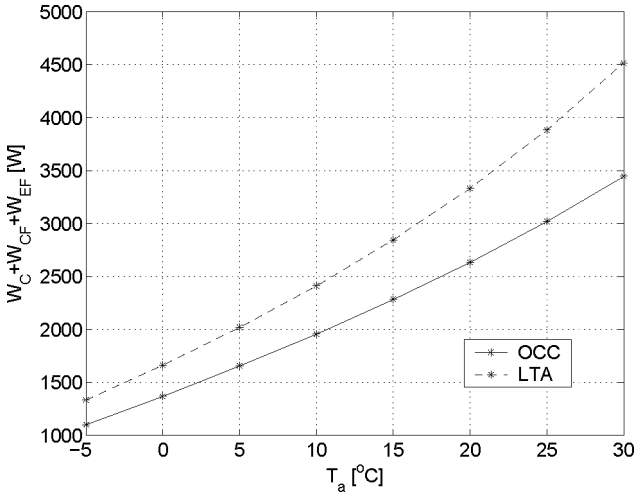

Figure 4.9: Power consumption of OCC compared with the LTA control. The system is exposed to a 20% increase of the cooling capacity (Q_e) and 30% reduction in air flow ($K_{2,CF}$).

made calculations does however indicate, that a substantial reduction in the power consumption can be achieved using respectively a LTA or OCC strategy.

4.5 Experimental Test Results

The proposed set-point optimization control scheme has been tested on the test refrigeration system. However the optimization problem is simplified by disregarding the constrains and keeping the evaporation pressure (P_e) constant. When the evaporation pressure is constant, then the workload of evaporator fan controlling the temperature in the cold storage room is constant as well. This reduces the complexity of the optimization problem as the work of the evaporator fan can be disregarded and the optimizing variables can be reduced to $x_{ss} = P_c$. The optimization problem can then be written as:

$$\begin{aligned} & \min_{[P_c]} (\dot{W}_C + \dot{W}_{CF}) \\ \text{Subject to:} \quad & \dot{Q}_e - \dot{Q}_{e,0} = 0 \\ & P_e - P_{e,0} = 0 \end{aligned} \tag{4.24}$$

That is an OCC scheme. The objective of the OCC scheme is as previously mentioned in Section 4.4 to continually adapt the condensing pressure to the optimal, under the

influence of varying ambient temperatures ($v_{ss} = T_a$). That is the OCC scheme should be able to follow daily/yearly changes in the ambient temperature.
Though the optimization problem is constrained by equalities (the control objectives), then the optimization problem Eq.(4.24) can be solved in the steepest decent fashion as an unconstraint optimization problem. This can be done simply by computing the Jacobian keeping $P_e = P_{e,0}$ and $Q_e = Q_{e,0}$ constant, i.e.

$$\nabla J = \frac{d\dot{W}_C}{dP_c}|_{P_e=P_{e,0},Q_e=Q_{e,0}} + \frac{d\dot{W}_{CF}}{dP_c}|_{P_e=P_{e,0},Q_e=Q_{e,0}} \tag{4.25}$$

$\frac{d\dot{W}_C}{dP_c}$ and $\frac{d\dot{W}_{CF}}{dP_c}$ can be found from Eq.(4.19) and Eq.(4.20).
Before we move on to implement the set-point optimizing control scheme on the test refrigeration system, we will describe the experimental setup and verify the static model on the test system.

4.5.1 The Experimental Setup

The test system described in Chapter 2 has been used for the experiments with the proposed set-point optimizing control scheme. Figure 4.10 depicts the basic system layout of the test system. There is however a slight difference between the test system and the simple system that has been used in the calculation above, instead of air the evaporator cools water, see Figure 4.10. The water is circulated by a pump through a water-heater that delivers a constant heat ($\dot{Q}_{load}$) to the water. This is removed again in the evaporator, i.e. at steady state $\dot{Q}_{load} = \dot{Q}_e$. Conceptually there is no difference whether the evaporator cools water or air in a cold storage room. To avoid a change in notation T_{cr} will therefore in the following denote the water temperature.
The test system Figure 4.10 is equipped with the depicted control system and sensors measuring the indicated entities. The control system comprises two local PI-controllers controlling respectively the suction pressure (=P_e) and the condensing pressure (P_c). The ambient temperature (T_a) is controlled by a HVAC system, that controls the temperature of the room wherein the test system is located. The power to the water-heater ($\dot{Q}_{load}$) is manually adjusted thus controlling the cooling capacity $\dot{Q}_e$ (at steady state $\dot{Q}_{load} = \dot{Q}_e$).

4.5.2 Verification of the Static Model.

In the following we will verify the static model Eq.(4.8)-(4.14), however the evaporator model is disregarded as it is not required for the optimization problem, Eq.(4.25).
To verify the static model of the compressor and the condenser, the test system has been operated at different steady states. The steady states have been obtained at various condensing pressures. The condensing pressure P_c has been stepwise increased from P_c=7

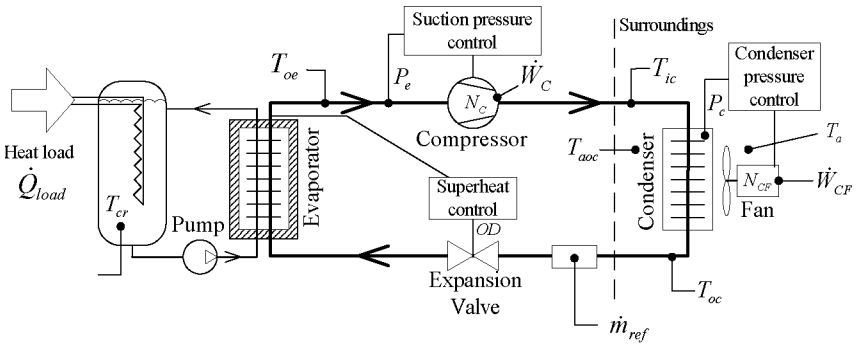

Figure 4.10: The test system

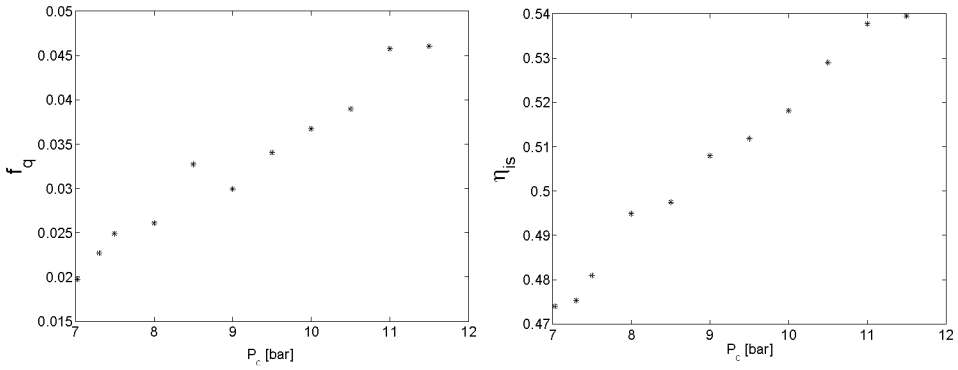

(a) The heat loss coefficient f_q (b) The isentropic efficiency η_{is}

Figure 4.11: Computed compressor parameters at varying condensing pressures.

bar with 0.5 bar up to 11.5 bar. The ambient temperature T_a, the evaporation pressure P_e and the cooling capacity $\dot{Q}_e$ have been kept constant at all time at following values: $T_a = 22\ ^oC$, $P_e = 3$ bar and $Q_e = 3800$ Watt.

The measurements have been gathered, when a steady state has been reached. A steady state was assumed obtained when the water temperature (T_{cr}) (see Figure 4.10) had been settled within $\pm 0.2\ ^oC$ for 1 hour.

Compressor

The compressor model builds on the assumption that the heat loss coefficient f_q and the isentropic efficiency η_{is} can be considered to be constant according to Eq.(4.8) and Eq.(4.9). In Figure 4.11 is the mean of the computed f_q and η_{is} depicted for each of the steady states. As it can be seen from Figure 4.11 the values of f_q and η_{is} however depends on the condensation pressure. These dependencies are however negligible,

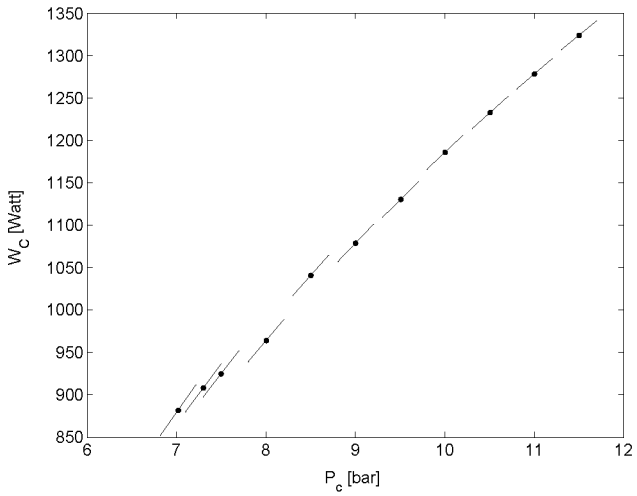

Figure 4.12: Verification of the compressor model. The dots indicate the measured $\dot{W}_C$, and the line segments the computed gradient ($\frac{d\dot{W}_C}{dP_c}$) using Eq.(4.19)

when computing the gradient Eq.(4.19). By using the measured $\dot{W}_C$ and inserting in Eq.(4.19) the gradient ($\frac{d\dot{W}_C}{dP_c}$) at each steady state has been computed and plotted, see Figure 4.12. Recall that Eq.(4.19) was derived based on the assumption that f_q and η_{is} where constant. Though this turned out to be a quite rough assumption it can be seen that the estimated gradient is quite accurate.

Condenser

According to Eq.(4.11) the power consumption in the condenser is a cubic function of the rotational speed. In Figure 4.13(a) the dependency between $\dot{W}_{CF}$ and N_{CF} is depicted. As is can be seen an offset term (k_{offset}) has to be introduced to Eq.(4.11) as $\dot{W}_{CF}(N_{CF} = 0) \neq 0$:

$$W_{CF} = k_{offset} + K_{1,CF} \cdot (N_{CF})^3 \tag{4.26}$$

The offset is arising because the condenser fan speed is controlled by a frequency converter. At low frequencies there are relatively high losses in the converter, therefore at $N_{CF} < 12\ s^{-1}$ the model becomes inaccurate. At higher rotational speeds $N_{CF} > 12\ s^{-1}$ the model Eq.(4.11) seems to fit quite good (see Figure 4.13(a)).

In Figure 4.13(b) the "measured" air flow ($\dot{m}_{air,C}$) has been depicted as function as the rotational speed N_{CF} together with the model Eq.(4.12). The "measured" air flow has been determined based on measurements of $\dot{Q}_c$ and using Eq.(4.14). As it appears from the figure, Eq.(4.12) models the air flow across the condenser quite good.

Figure 4.14(a) depicts the measured temperatures around the condenser. It can be seen that the outlet temperature of the air from the condenser (T_{aoc}) is *higher* than the

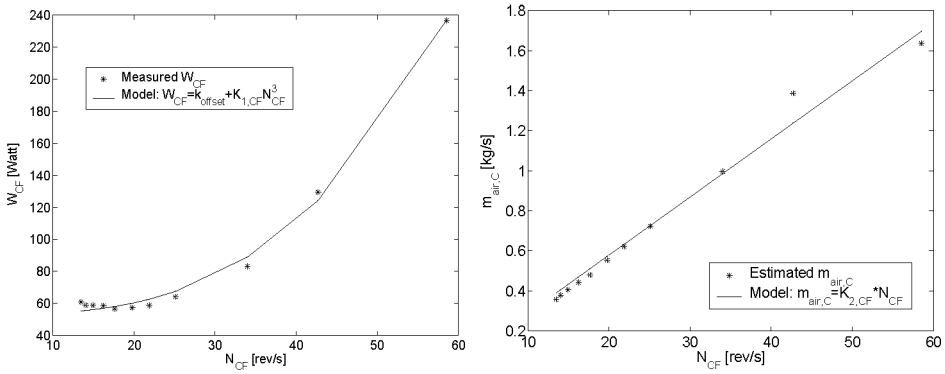

(a) $\dot{W}_{CF}$ as function of N_{CF}. $k_{offset} = 53\,Watt$, $K_{1,CF} = 1.2 \cdot 10^{-3}\,Js^2$
(b) The estimated air flow $m_{air,C}$ as function of N_{CF}. $K_{2,CF} = 0.028\,kg$.

Figure 4.13: Computed condenser fan parameters at varying fan speeds.

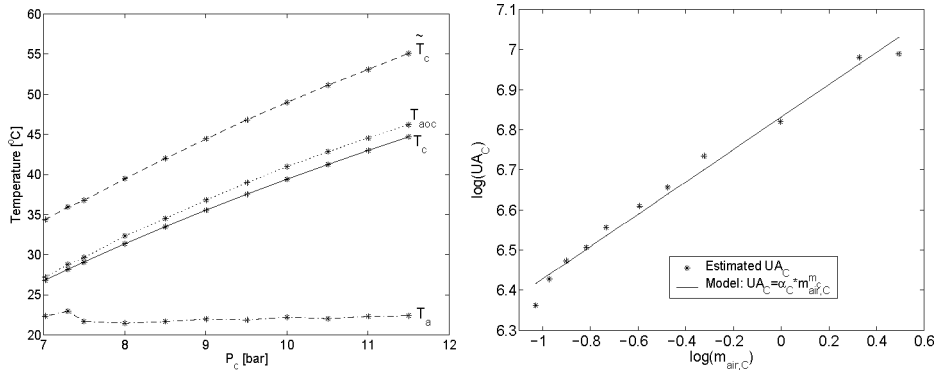

(a) Measured temperatures on primary and secondary side of condenser
(b)The estimated UA_C value as function of the mass flow of air ($m_{air,C}$). $\alpha_C = 926$, $m_C = 0.40$

Figure 4.14: Computed condenser parameters at varying operational conditions

condensing temperature (T_c). This does however not follow the assumption made in Eq.(4.13) where it was assumed that the condenser wall temperature was equal to the condensing temperature (T_c), which would cause T_{aoc} to be *less* than T_c. The reason for this mismatch is that the inlet temperature of the refrigerant to the condenser (T_{ic}) is superheated ($T_{ic} > T_{aoc} > T_c$), i.e. the sensible heat of the refrigerant is not negligible. The condensing temperature (T_c) in Eq.(4.13) is therefore adjusted as follows:

$$\tilde{T}_c = \frac{T_c \cdot h_{lat} + \frac{T_c+T_{ic}}{2} h_{sen}}{h_{ic} - h_{oc}}, \tag{4.27}$$

where h_{sen} and h_{lat} is respectively the sensible heat and latent heat of the refrigerant. That is, $\tilde{T}$ is a weighted mean of the temperature that the air experience on its way through the condenser.
By using Eq.(4.27) and Eq.(4.13) the UA_C-value has been estimated. Figure 4.14(b) depicts $log(UA_C)$ as function of $log(m_{air})$, as it can be seen $UA_C = \alpha_C \cdot m_{air,C}^{m_C} (\Rightarrow log(UA_C) = m_C \cdot log(m_{air}) + log(\alpha_C))$ models the heat transfer quite well.
Assuming that $\frac{\partial \tilde{T}_c}{\partial P_c} \approx \frac{\partial T_c}{\partial P_c}$ and applying Eq.(4.26) the gradient Eq.(4.20) can be rewritten as:

$$\begin{aligned} \frac{d\dot{W}_{CF}}{dP_c} =& \frac{3(\dot{W}_{CF} - k_{offset})}{\dot{Q}_c - UA_C(1-m_C)(\tilde{T}_c - T_{aoc})} \\ & \cdot \left(\frac{d\dot{W}_C}{dP_c} \frac{\dot{Q}_e}{\dot{W}_C} \frac{h_{ic} - h_{oc}}{h_{oe} - h_{oc}} - \frac{\dot{Q}_c}{\tilde{T}_c - T_a} \frac{\partial T_c}{\partial P_c} \right) \end{aligned} \tag{4.28}$$

In Figure 4.15 the computed gradient using Eq.(4.28) has been depicted. The gradient has been computed for each of the steady states. Except for the high pressures ($P_c > 9.5$ bar), where the condenser fan speed (N_{CF}) is low and the fan model Eq.(4.11) becomes inaccurate, the gradient fits the measurements quite well.

We now look at the total system, that is the fan condenser and the compressor. Figure 4.16 depicts the sum of the measured power consumed by the condenser fan and the compressor ($\dot{W}_{CF} + \dot{W}_C$), furthermore the computed gradient ($\frac{d\dot{W}_C}{P_c} + \frac{d\dot{W}_{CF}}{P_c}$) is depicted. The measurements indicate that the optimal condensation pressure resulting in the minimal power consumption lies in the interval $7.25 < P_c < 8.0$ bar close to 7.5 bar. The computed gradients all unambiguously points towards the interval $7.25 < P_C < 7.5$ bar, which is in the interior of the previous mentioned interval. This means the optimization scheme, for the given steady state, no matter where it is started ($7 < P_c < 12$ bar) would drive the condensation pressure into the interval $7.25 < P_C < 7.5$ bar. This results in a worst case error of the estimated optimum P_c^* on 0.75 bar.
This shows that though the static model is quite simple and some rough assumptions have been made, it is still sufficient for driving the set-point quite close to the true optimum.

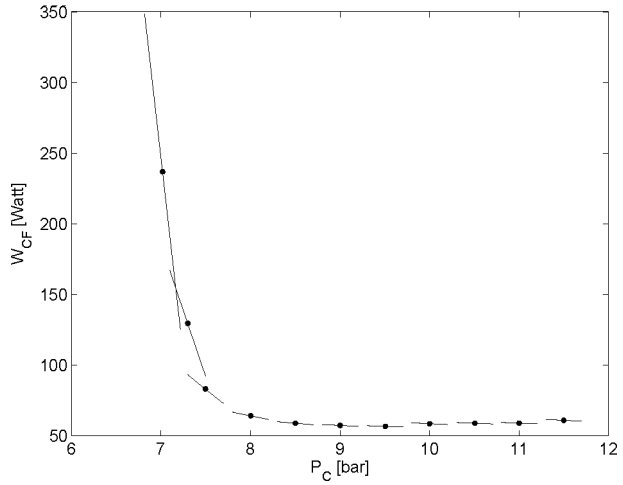

Figure 4.15: Verification of condenser model. The dots indicate the measured $\dot{W}_{CF}$, and the line segments the computed gradient ($\frac{d\dot{W}_{CF}}{dP_c}$) using Eq.(4.28)

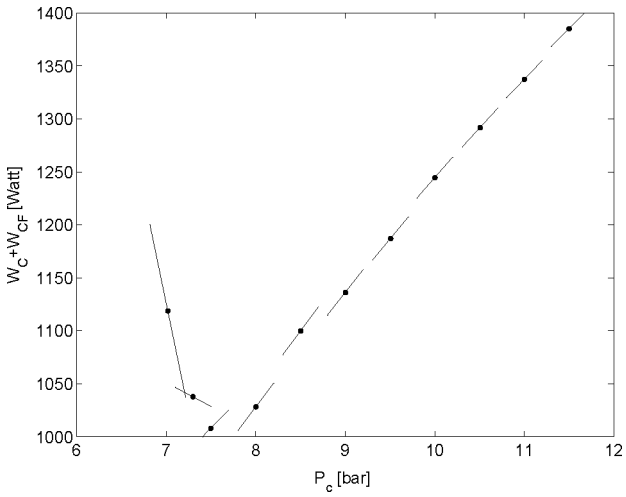

Figure 4.16: Verification of total model including condenser and compressor. The dots indicate the measured $\dot{W}_{CF} + \dot{W}_C$, and the line segments the computed gradient

4.5.3 Implementation and Experimental Results

In the previous section the static model was verified and minor adjustment to models was incorporated. To briefly recall, we wanted to implement the proposed set-point optimization to optimize the condenser pressure (the OCC scheme) according to Eq.(4.24) by zeroing the Jacobian Eq.(4.25):

$$\begin{aligned}\nabla J =& \frac{d\dot{W}_C}{dP_c}\Big|_{P_e=P_{e,0},Q_e=Q_{e,0}} + \frac{d\dot{W}_{CF}}{dP_c}\Big|_{P_e=P_{e,0},Q_e=Q_{e,0}} \\ =& \dot{W}_C\left(\frac{\partial his}{\partial P_c}\frac{1}{h_{is}-h_{oe}} + \frac{\partial h_{oc}}{\partial P_c}\frac{1}{h_{oe}-h_{oc}}\right) \\ &+ \frac{3(\dot{W}_{CF}-k_{offset})}{\dot{Q}_c - UA_C(1-m_C)(\tilde{T}_c - T_{aoc})}\cdot\left(\frac{d\dot{W}_C}{dP_c}\frac{\dot{Q}_e}{\dot{W}_C}\frac{h_{ic}-h_{oc}}{h_{oe}-h_{oc}} - \frac{\dot{Q}_c}{\tilde{T}_c - T_a}\frac{\partial T_c}{\partial P_c}\right),\end{aligned} \tag{4.29}$$

where $UA_C = \alpha_C \cdot m_{air,C}^{m_C}$ and $\tilde{T}_c$ is determined by Eq.(4.27). The optimizing control structure consist of three parts a steady state parameter adaptation, a steady state prediction and a steady state optimization. In the following we will go over the implementation of each part.

Parameter Adaptation

In Table 4.2 the available measurements, estimated variables, adapted parameter, and a priori known the parameters are listed. Note that the mass flow of refrigerant ($\dot{m}_{ref}$), in general, not is measured in commercial refrigeration systems. However if it is assumed that more a priori knowledge of the compressor characteristic is available, the mass flow can be determined quite accurate without needing a direct measurement. The purpose of

Measurement	Estimated variables	Adapted parameters	Parameters known a priori
P_c, P_e	$\dot{m}_{air,C}$	α_C	$k_{offset} = 53$ [Watt]
T_{ic}, T_{oc}, T_{oe}		$K_{CF} = \frac{K_{1,CF}}{(K_{2,CF})^3}$	$m_C = 0.4$ [-]
T_{aoc}, T_a		$\tilde{f}_q = \frac{1}{1-f_q}$	$C_{p,air} = 1000.00\ [\frac{J}{(kg\cdot K)}]$
$\dot{m}_{ref}$, $\dot{W}_C$, $\dot{W}_{CF}$		η_{is}	

Table 4.2: Available measurements, estimated variables, parameters known a priori and adapted parameter in the optimizing control scheme.

the parameter adaptation is two folded. Firstly many of the parameters are not known a priori and only rough initial guesses can be supplied. Secondly some of these parameters are not perfectly constant they might have wake dependencies on operational conditions and furthermore they might be time varying as previously mentioned in Chapter 3.
The parameter adaptation has been carried out by using the so called MIT rule. Using this adaptive parameter adjustment routine, the parameter is adapted by minimizing the

error between the measurements and the model, in accordance to following equation (Åström and Wittenmark (1989)):

$$\frac{d\theta}{dt} = -\gamma e \frac{de}{d\theta}, \tag{4.30}$$

e denotes the model error, θ the parameter estimate and γ determines the adaptation rate. In Section 3.2.2 at Figure 3.5 it was indicated that the parameter adaptation should be performed using the measurement of the controlled variables (x). If however there are more unknown parameters than measured controlled variables such that the number of measurement is insufficient other measurement must be taken into account, this has been done in the following. The model error is determined using following residual equations based on the static model (Eq.(4.8)-(4.14)):

$$e_{\alpha_C} = T_{aoc} - \tilde{T}_c - (T_a - \tilde{T}_c) \cdot \exp\left(-\frac{\alpha_C \cdot \dot{m}_{air,C}^{m_C}}{\dot{m}_{air,C} \cdot C_{p,air}}\right) \tag{4.31}$$

$$e_{K_{CF}} = \dot{W}_{CF} - k_{offset} - K_{CF} \cdot \dot{m}_{air,C}^3 \tag{4.32}$$

$$e_{\tilde{f}_q} = \dot{W}_C - \tilde{f}_q \cdot \dot{m}_{ref}(h_{ic} - h_{oe}) \tag{4.33}$$

$$e_{\eta_{is}} = \dot{m}_{ref}(h_{is} - h_{oe}) - \eta_{is} \cdot \dot{W}_C \tag{4.34}$$

The error gradients can then be written as:

$$\frac{de_{\alpha_C}}{d\alpha_C} = (T_a - \tilde{T}_c) \cdot \frac{m_{air,C}^{m_C}}{m_{air,C} \cdot C_{p,air}} \exp\left(\frac{-\alpha_C \cdot m_{air,C}^{m_C}}{m_{air,C} \cdot C_{p,air}}\right) \tag{4.35}$$

$$\frac{de_{K_{CF}}}{dK_{CF}} = -\dot{m}_{air,C}^3 \tag{4.36}$$

$$\frac{de_{\tilde{f}_q}}{d\tilde{f}_q} = -\dot{m}_{ref}(h_{ic} - h_{oe}) \tag{4.37}$$

$$\frac{de_{\eta_{is}}}{d\eta_{is}} = -\dot{W}_C \tag{4.38}$$

Since all of the model equations are based on steady state conditions, the parameter adaptation only becomes accurate when a steady state is reached. To accommodate for the disturbances related to the dynamics of the system a crude model of the dynamic has been implemented in the adaptation scheme, as described in Section 3.2.2. The most pronounced dynamics is caused by the heat transfer through evaporator wall. This dynamic has simply been copied by using a low pass filter.

An interesting remark can be made to the residual equations Eq.(4.31)-Eq.(4.34) that links the optimizing scheme to fault detection. Assume that the parameters are adapted in a faultless operation and these values afterwards are stored as nominal values. In that case by using the nominal values the Eq.(4.31)-Eq.(4.34) can be used as residual equations for fault detection. In Thybo and Zamanabadi (2003*b*) it is described how energy

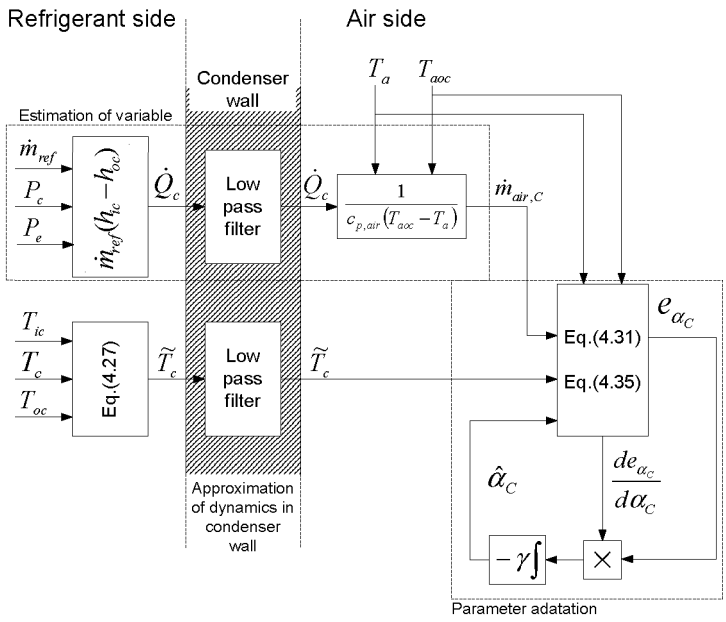

Figure 4.17: Implementation of the computation of $\dot{m}_{air}$ and the adaptation of α_C

balances can be used for generating residuals and how to diagnose fault in commercial refrigeration systems. The residual for the parameter estimation Eq.(4.31)-Eq.(4.34) is exactly derive based on energy balances across the individual components. Actually Eq.(4.31) is used in Thybo and Zamanabadi (2003*a*) for detecting dirt on a condenser and implemented in the latest condenser control system from Danfoss A/S (Danfoss A/S (2005)). However the other residual equations might be helpful in detecting other faults. Nevertheless as the parameters are adapted and used for set-point optimization the steady state effects of the faults are accommodated.

In the following we will only go into details with the implementation and result for the adaptation of the parameter α_C, the fundamental results are the same for the remaining parameters.

Figure 4.17 shows the implementation of the adaptation scheme. As it can be seen from the figure, the variable $\dot{m}_{air}$ is estimated using same rough approximation of the dynamics in the condenser wall as for the parameter adaptation. In the experiment a first order filter with a time constant on 80 sec has been used. In practice the parameter adaptation is only affected little by the exact choice of the time constant why a rough guess is sufficient.

At Figure 4.18(a) the adaptation of α_C is depicted. The adaptation rate has been sat to $\gamma = 1500$ to get a fast adaptation and the sample time is 1 min. The adaptation

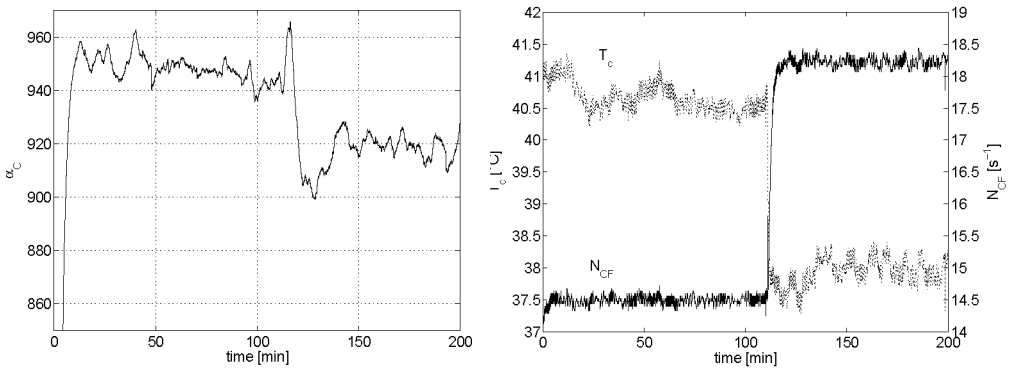

(a) α_C (b) T_c and N_{CF}

Figure 4.18: Adaptation of the parameter α_C. At time=110 min the condensing temperature T_c is changed, $T_c = 40.5 \rightarrow 38^oC$.

was started at time=0 min from the steady state; $T_c = 40.5^oC$ ($\sim P_c = 10.5$ bar) and $N_{CF} = 37.5s^{-1}$. From Figure 4.18(a) it can be seen that the adaptation settles at $\alpha_C \approx 950$ after about 10 min. At time=110 min the condensing temperature T_c has been changed, $T_c = 40.5 \rightarrow 38^oC$ (see Figure 4.18(b)). It can be seen from Figure 4.18(a) that there are some small dynamical interactions on the parameter adaptation, which depends on choice of time constant for the evaporator wall. However the adaptation settles quite fast at $\alpha_C \approx 920$, that is at least fast enough for the set-point optimization.

Steady State Prediction

In order to compute the steady state value of the Jacobian Eq.(4.25) the steady state value of $x_{ss} = P_c$ has to be predicted. As described in Section 3.2.2 the steady state prediction of $x_{ss} = P_c$ is computed based on the current values of the control signal ($u = [N_C, N_{CF}] \approx u_{ss}$) and disturbance ($T_a \approx v_{ss}$). Furthermore we will assume that the current value of the control objectives i.e. the cooling capacity ($\dot{Q}_e$) and the evaporating pressure (P_e) equals their steady state value.

By assuming the dynamic in the condenser fan is negligible and $K_{2,CF}$ is constant, then the current workload in the condenser fan (W_{CF}) is equals the steady state value, according to Eq.(4.26). Hereby the mass flow of air can be found as:

$$\dot{m}_{air,C} = \sqrt[3]{\frac{\dot{W}_{CF} - k_{offset}}{K_{CF}}} \tag{4.39}$$

Finally by using insertion of $\dot{m}_{air,C}$, Eq.(4.8), Eq.(4.13),and Eq.(4.27) in Eq.(4.14) and using the adapted parameters the steady state value of P_c can be found by iteration. For the practical implementation a Newton iteration method was used. At each time step, the solution from the previous time step has been used as initial guess for the next.

Steady State Optimization

By using the adapted value of α_C and the predicted steady state, the Jacobian (Eq.(4.29)) has been computed and used in a feedback for controlling the set-point for P_c, see Figure 4.19. The optimizing set-point controller is simply an integrator with the gain

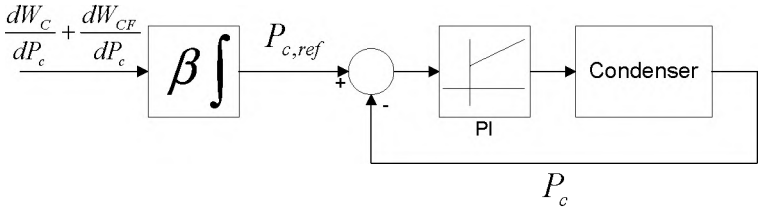

Figure 4.19: Set-point controller for condensing pressure

$\beta = -3 \cdot 10^{-4}$ and a sample time of 1 min. For the tests a rather fast sampling time has been chosen. In real life application a much slower sample time can be chosen, as it should just be able to follow the daily and yearly temperature changes. Using the set-up depicted in Figure 4.19, the condensing pressure set-point optimization has been tested. Figure 4.20(b) shows the value of the computed Jacobian according to Eq.(4.29), before and after the condensing pressure set-point optimizing scheme has been switched on. It can be seen that when the optimization scheme is turned on at time=50 min the Jacobian is driven towards zero, after approximately 70 min the Jacobian reaches zero with a little undershoot. Figure 4.20(a) shows the summed energy consumption in the condenser fan and the compressor. After the optimizing scheme is turned on at time=50, it can be seen (from the filtered signal) that the energy consumption decreases from around 1400 Watt down to 1100 Watt in about 60 min. That is a reduction in the energy consumption in the condenser fan and the compressor at around 20%. This has been obtained by reducing the condenser pressure from 11.5 bar down to around 7.5 bar, while keeping the cooling capacity ($\dot{Q}_e$) approximately constant, see Figure 4.21(a) and (b).

According to the optimizing control, the optimal condenser pressure P_c^* is around 7.5 bar (Figure 4.21(a)), if we compare to the steady state measurements in Figure 4.16, we can see that P_c^* is very close to the result obtained there. That is P_c^* falls in the interval $7.25 < P_c < 8$ bar. The steady state measurements in Figure 4.16 and experimental results Figure 4.21 where both obtained at a ambient temperatures close to $T_a = 22\ ^oC$ (see Figure 4.14(a)). All in all it seems like the condensing pressure set-point optimizing scheme drives condensing pressure quite close to the true optimum.

One of the main objectives with the condenser pressure optimizing scheme (the OCC scheme), was that it should be able to follow changes in the ambient temperature T_a (the "steady state" disturbance $v_{ss} = T_a$). In the following we will therefore test the optimizing schemes ability to adapt to changes in T_a. Figure 4.23(a) depicts the ambient temperature, which has been kept constant at $T_a = 21.5\ ^oC$ until time=21 min, hereafter it has been changed quite abruptly from 21.5 till 26.5 ^oC within approximately

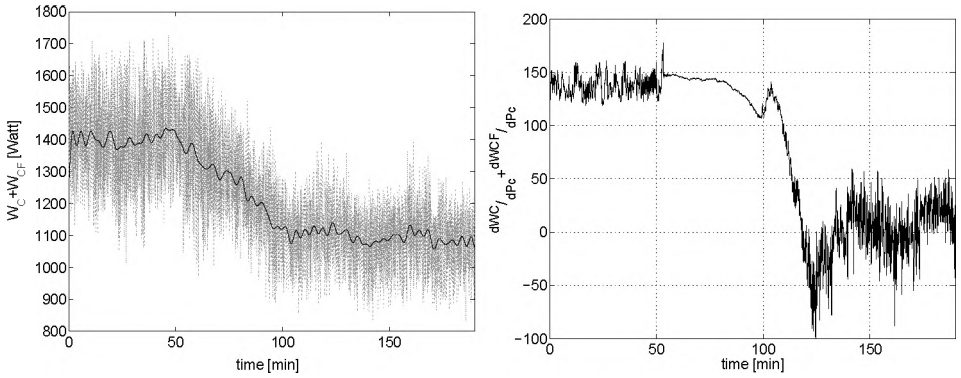

(a) Power consumption in condenser fan and compressor.
(b) The Jacobian of the cost function, Eq.(4.29)

Figure 4.20: Test result utilizing the set-point optimizing control scheme. The optimization scheme is started after 50 min

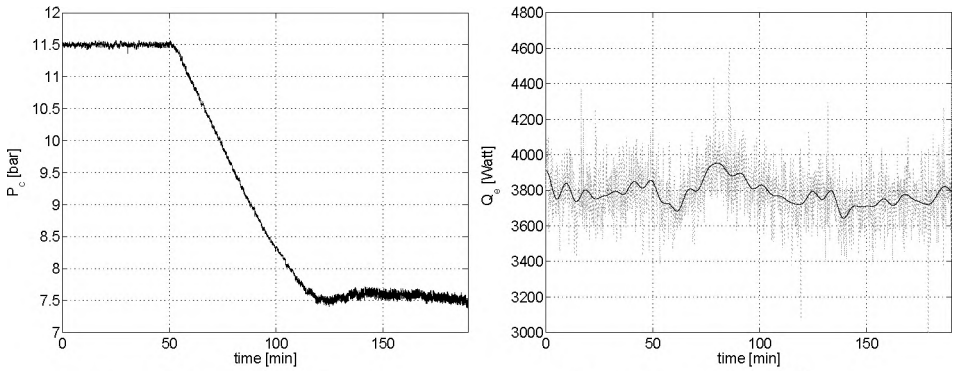

(a) Condenser pressure P_c (b) Cooling capacity $\dot{Q}_e$

Figure 4.21: P_c and $\dot{Q}_e$ before and after the set-point optimizing scheme has been turned on. The set-point optimizing control was started after 50 min.

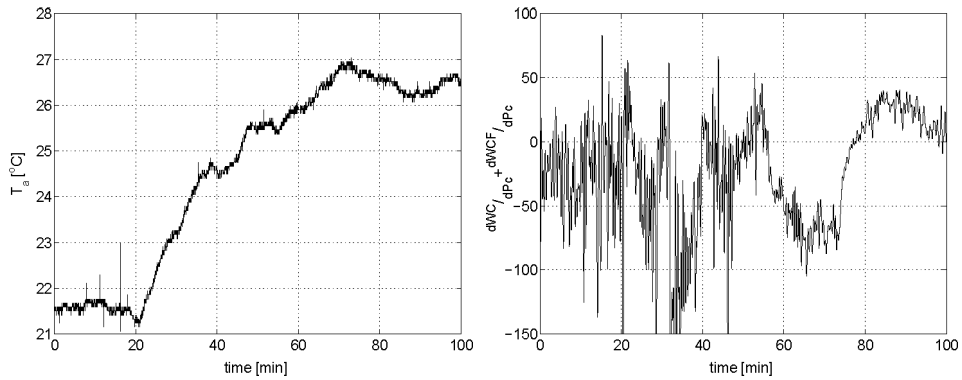

(a) The ambient temperature T_a (b) The Jacobian Eq.(4.29)

Figure 4.22: Change in the ambient temperature, T_a and the influence on the Jacobian. At time=21 min T_a is changed from 21.5 till 26.5 ^oC.

45 min. This courses the Jacobian to drop below zero (see Figure 4.23(b)) meaning that condenser pressure should be increased. Figure 4.23(a) depicts the condensing pressure. It can be seen that the pressure is increased until it reaches around 8.3 bar where it settles at time = 80 min. At this time the Jacobian is driven back close to zero (Figure 4.23(b)). It can be seen pressure settles approximately 20 min after the ambient temperature has settled at 26^oC. This proves that the optimizing scheme is able to follow even quite abrupt changes in the ambient temperature.

4.6 Conclusion Part I

In the first part of the thesis, set-point optimizing control for refrigeration systems was considered. The main emphasis was on deriving a practical feasible and economical tractable optimization scheme for small and mass produced plants such as refrigeration systems. In the following the main conclusion are drawn based on the accomplishments and contributions of Part I.

- In Chapter 3 a method for on-line set-point optimization has been proposed. The method provides a structure for a simple set-point optimization scheme for a strictly convex cost function or a cost function that declines globally towards the global optimum. The method is also applicable where the above mentioned conditions are not fulfilled, in these cases there are however no guarantees that the set-points will converge towards the global optimum. The method provides a set-point optimizing control scheme that can be applied on top of an existing distributed control system.

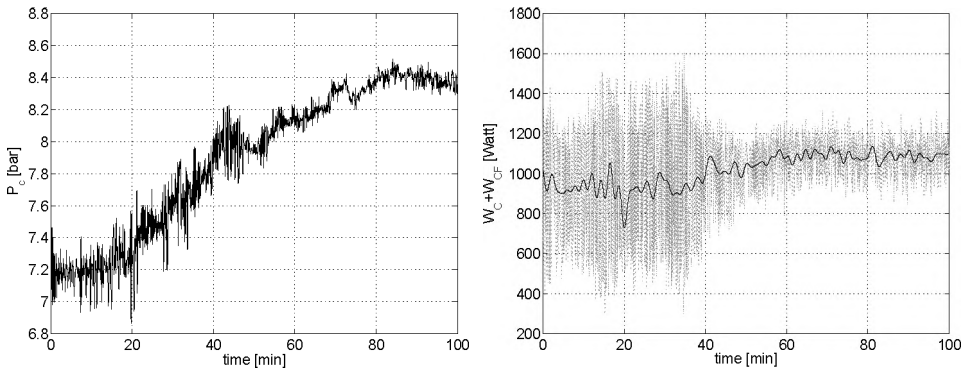

(a) The condensing pressure P_c (b) The power consumption $W_C + W_{CF}$

Figure 4.23: Change in the ambient temperature and the influence on the condensing pressure and the power consumption. At time=21 min T_a is changed from 21.5 till 26.5 ^oC.

The framework of the method can furthermore tackle system limitations. By introducing logarithmic barrier functions and a scalar weight it is possible to keep the operation of the plant within the system limitation with an adjustable safety margin. Finally by relaxing the steady state control objective it is possible to maintain operational feasibility in extreme situations, thus with a reduced system performance. This latter issue was in Chapter 4 demonstrated by a numerical example based on a static model of a simple refrigeration system. Here it was shown that the set-point optimization was able to keep the set-points and the control inputs (the rotational speed of the fans and the compressor) within their limitations while upholding the steady state control objective, that is the cooling capacity should be constant. Furthermore it was shown that in the extreme case where the ambient temperature is high (a hot summers day) and the condensing pressure reaches the maximal limit, while the condenser fan runs at maximal speed it is possible to proceed the operation, thus at a lowered cooling capacity. This would in the present distributed control setup result in an emergency shut down in order to protect the system.

- In Chapter 4 the minimization of the energy consumption in a simple refrigeration system was formulated in the set-point optimizing framework introduced in Chapter 3. It was shown how this set-point optimization easily can be adopted to larger systems like supermarket refrigeration systems. Despite the huge number of control loops in such systems the resulting optimization was shown to resemble that for a simple system.
  It was furthermore shown that a static system model of the refrigeration system can be constructed by a number of general component models connected by de-

scriptions of mass and energy flow in between. The component models are in principle so general that they are independent of the specific type of compressor, condenser and evaporator, however the parameters might be different. By using the same component models though various compositions of these, different system models can be builded such as e.g. a supermarket refrigeration systems.
Utilizing the static models and the proposed set-point optimizing framework for a set-point optimizing control scheme, makes it fairly easy to mass produce the solution for use in various compositions of refrigeration systems.

- To give an idea of the potential energy saving using an energy optimal control scheme. The potential energy savings using the conventional constant set-point control was compared to two versions of optimal set-point control. Namely optimal condenser pressure control (OCC) and optimal evaporating pressure control (OEC) here was found that the energy savings for both controls is in the area of 20-30% depending on the operational conditions.
  The OCC scheme was furthermore compared with a control scheme that approximates the optimal condensing temperature linearly as a function of the ambient temperature (LTA). The LTA scheme proved to give a close estimation of the optimal condenser set-point and moreover displayed a good robustness towards individual changes in the cooling capacity and the overall heat transfer coefficient in the condenser. However following points differentiate the proposed OCC scheme from the LTA.

  - In systems where the cooling capacity continuously varies and dirt builds up on the condenser, considerable losses in optimality can be anticipated using a LTA scheme compared to the OCC scheme.
  - The parameters in the LTA scheme needs to be determined a priori, hence data of the optimal operation for the specific plant must be recorded.
  - The LTA lacks the ability to take system constraints into consideration.

  The exact percentage that it is possible to save using a LTA or OCC scheme however depends on the characteristics of the specific systems. The calculations that was made does however indicate, that a substantial reduction in the power consumption can be achieved by introducing a set-point optimizing control scheme.

- As a part of the project a test refrigeration system that enables the possibility of testing various control structures was designed and built. On this test system an optimal condenser pressure control (OCC) was tested. This was done by applying the in Chapter 3 proposed set-point optimizing control scheme.
  Experimental results proved that the optimizing scheme was able to drive the condensing set-point very close to the true optimum. Within a time frame of approximately 1 hour after enabling the set-point optimizing control scheme, the energy consumption in the condenser fan and the compressor was lowered by 20%. This

was obtained by letting the optimization scheme reduce the condensing pressure from 11.5 bar down to the optimal condensing pressure at around 7.5 bar, while keeping the cooling capacity constant. Moreover this was done using no a priori knowledge of the optimality for the system and only little a priory knowledge of the system characteristics, thus demonstrating the flexibility of the method that enables a mass production of the solution to a variety of systems requiring only little installation time (i.e. feeding the needed a priori knowledge).

Part II

Dynamical Optimizing Control

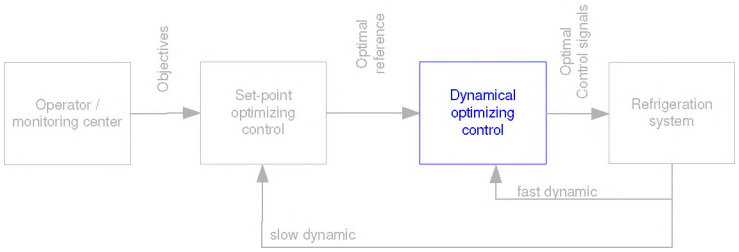

Chapter 5

Dynamical Optimizing Control

In the set-point optimizing control we looked at the control of the refrigeration system from a system oriented point of view. That is by coordinating the operation of the subsystems, we tried to optimize the steady state operation of the *entire* refrigeration system. However the steady state optimizing layer relies on the underlying distributed control system to ensure stability and a reasonable low variance on the controlled variables. In the set-point optimizing layer it was described how to take the system limitations into account such that the operation of the refrigeration system stayed feasible, that is however at steady state. Dynamically we were not able to give any guaranties, therefore a certain safety margin had to be introduced in order to lower the risk of violating system constraints. It is often so that the optimum is close to an operational constraint, therefore a control that dynamically handles constraints and minimizes variance will allow a closer operation to constraints. These are concerns that should be handled in the dynamical optimization layer, along of course with other demands to the dynamic performance, such as fast settling time, minimal control actions etc. The idea in the dynamical optimization layer is not that the whole distributed control system necessarily should be replaced by a centralized optimizing controller. The dynamical optimizing control should only be applied in the subsystems or the groupings of subsystems that limits the obtainable system performance. Parts of the conventional control system will therefore still be present where it performs satisfactorily.

The present control structure in a supermarket refrigeration system is distributed. The distributed control structure does not take into account the cross-couplings in the system. These cross-couplings are naturally inherited from the cyclic structure of the refrigeration process (the vapour compression cycle). Though most of these cross-coupling are relatively weak and do not cause any large disturbance to the individual control loops isolated seen, it turns out that they pose a major problem when hysteresis controllers are used in the local control loops. It can namely cause synchronization of the distributed

hysteresis controllers, thus accumulating the effects of the cross-couplings resulting in large disturbances. The reason for using hysteresis control is caused by the fact that of the control inputs to the display cases are restricted to binary values, i.e. *off/on*.
In the following we will investigate the causes for synchronization by studying a simple example, furthermore we will look at related theoretical work and try to extract some general rules for when synchronization arises in coupled hysteresis controlled systems. The main result is novel approach for desynchronization, which is given in Section 5.3.

5.1 Synchronization of Interconnected Subsystems

Synchronization, or the more general term state agreement, arises in dynamical systems that are interconnections of subsystems (Lin *et al.* (2005*c*)). State agreement means that the states of the subsystems are all equal. The state agreement problem is known from all sorts of systems, e.g. biochemical systems (Gunawardena (2003)), rendezvous in multi-agent systems (Lin *et al.* (2005*a*)), consensus in computer science (Moases and Rajsbaum (2002)) and synchronization (Pogromsky *et al.* (2002)). The description of the synchronization of coupled hysteresis controlled systems is however novel. Milosevic *et al.* (2004) studies cross-interactions between hysteresis controlled converters, but does not describe synchronization. Especially in systems with discrete valued control inputs, it is common to use hysteresis controllers e.g. in power systems (Meyer and Sonnenmoser (1993)), room temperature control in heating systems, and in supermarket refrigeration systems (Larsen *et al.* (2005)).
In the following we will look at the synchronization of hysteresis controlled subsystems. By studying a simple example of two interconnected subsystems both controlled by hysteresis controllers, we will try experimentally to investigate some of the courses for synchronization. Next we will briefly look at some of the recent results obtained for the state agreement problem for multiple nonlinear dynamical systems. Finally we will suggest a model predictive control strategy for desynchronization.

5.1.1 Synchronization of Coupled Hysteresis Controlled Subsystems

In the following we will study some of the causes for synchronization in a simple coupled hysteresis controlled system, namely an interconnection of two hysteresis controlled integrators. Though it is a very simple system, it does illustrate the main causes for synchronization.
Consider the following two subsystems (two integrators):

$$\begin{aligned} \dot{x}_1 &= 1 - 2u_{sub}\delta_1 \\ \dot{x}_2 &= 1 - 2u_{sub}\delta_2, \end{aligned} \tag{5.1}$$

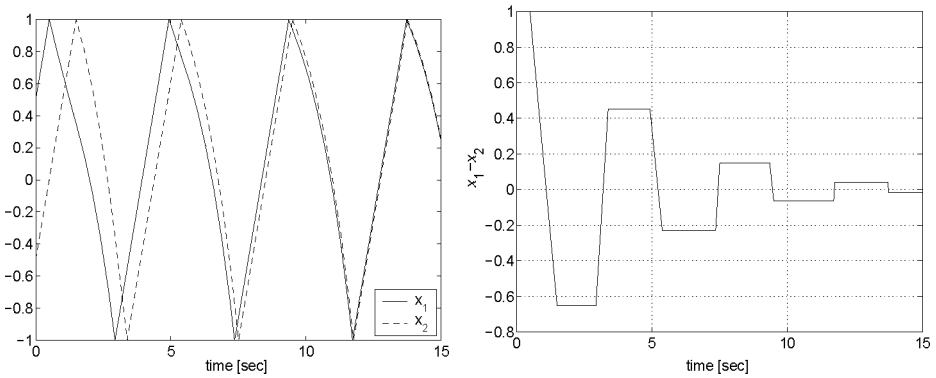

Figure 5.1: Synchronization of the two interacting hysteresis controlled systems (negative feedback)

where $\delta_1, \delta_2 \in \{0, 1\}$ are integer values that switches the common the input to the subsystems u_{sub} *on* and *off*.
If these two systems both are controlled by hysteresis controllers with an upper bound equal 1 and a lower bound equal -1, then the δ's follow the switching law given by:

$$\delta_i = \begin{cases} 1 & \text{if} \quad x_i \geq 1 \\ 0 & \text{if} \quad x_i \leq -1 \\ \delta & \text{if} \quad -1 < x_i < 1, \end{cases} \tag{5.2}$$

where $i \in \{1, 2\}$. Now if we set $u_{sub} = 1$ and start the system, x_1 and x_2 will move up and down between the upper and lower bound. In this case there are no interconnection, the subsystems are completely independent of each other. However if we introduce the following feedback in the system, the two subsystems will synchronize.

$$u_{sub} = 1 - (\alpha_1 x_1 + \alpha_2 x_2), \tag{5.3}$$

where $\alpha_1 \geq 0$ and $\alpha_2 \geq 0$ are two scalars (coupling strengths) that determine how much the input u_{sub} depends on the states x_1 and x_2. Figure 5.1 depicts a simulation result for $\alpha_1 = \alpha_2 = 0.15$ and the initial states $x_1(0) = 0.5$ and $x_2(0) = -0.5$. The figure clearly shows that the two integrators synchronize and we achieve state agreement ($x_1 = x_2$) as the difference $x_1 - x_2$ tends to zero. The larger we choose the coupling strengths α_1 and α_2 the faster the subsystems will synchronize. Even very small values of the coupling strengths make the subsystems synchronize eventually. However if the system is started perfectly desynchronized e.g. at $x_1(0) = 1$ and $x_2(0) = -1$, then synchronization will not occur. If however the initial value deviates even slightly from exact desynchronization, the system will synchronize. In other words there are two equilibriums, an unstable; where the system is perfectly desynchronized and a stable; where the

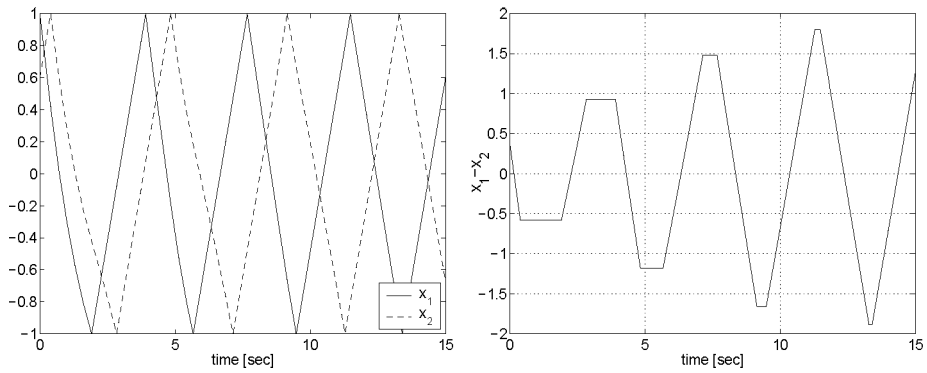

Figure 5.2: Desynchronization of the two interacting hysteresis controlled systems (positive feedback).

system is perfectly synchronized.
If the sign of the feedback is changed i.e. $u_{sub} = 1 + (\alpha_1 x_1 + \alpha_2 x_2)$, the case is reversed. Then the equilibrium, where the two subsystems are desynchronized, is stable and the equilibrium, where they are synchronized, is unstable. This is shown by the simulation result in Figure 5.2. The simulation is carried out with the coupling strengths $\alpha_1 = \alpha_2 = 0.15$ and the initial states $x_1(0) = 1$ and $x_2(0) = 0.6$. As it can be seen from the figure, the states desynchronize and stay desynchronized.
Now we will return to the case with negative feedback again, that is stable synchronization. In the previous simulations, the subsystems both had the same "natural" switching frequency. Now we will study what will happen, if the switching frequency is not the same. To change the switching frequency the upper bound in the hysteresis control of x_2 has been changed from 1 to 1.2, furthermore the coupling strengths are set at $\alpha_1 = \alpha_2 = 0.01$ and the initial states at $x_1(0) = 1$ and $x_2(0) = -1$. Figure 5.3 depicts the simulation result with these parameters. The difference in frequency between the two systems is too large for the systems to synchronize. It can be seen that the state x_1 has the highest switching frequency and it "overtakes" x_2. If we however increase the coupling strengths to $\alpha_1 = \alpha_2 = 0.2$, the system will synchronize, see Figure 5.4. Complete state agreement at all time can of course not be obtained because of the different hysteresis bounds.
The last point we want to illustrate is the effect of unequal coupling strengths. If we set $\alpha_1 = 0$ and $\alpha_2 > 0$ (or vice versa) the systems will synchronize (negative feedback). The size of α_1 compared with α_2 merely determines whether x_1 is mostly attracted to x_2 or vice versa. If positive feedback is used, then exact desynchronization is only obtained if all the α's are equal, otherwise the systems will desynchronize but not perfectly phase shifted.
The picture for systems consisting of a larger number of interconnected hysteresis con-

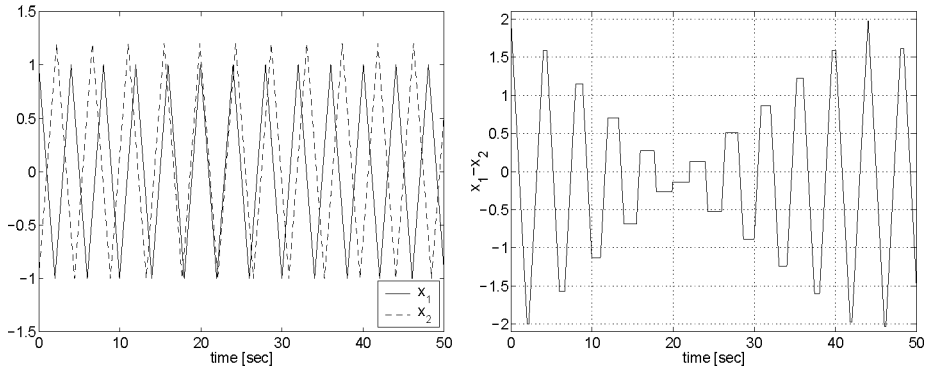

Figure 5.3: Two interacting hysteresis controlled systems with different hysteresis bounds and weak negative feedback.

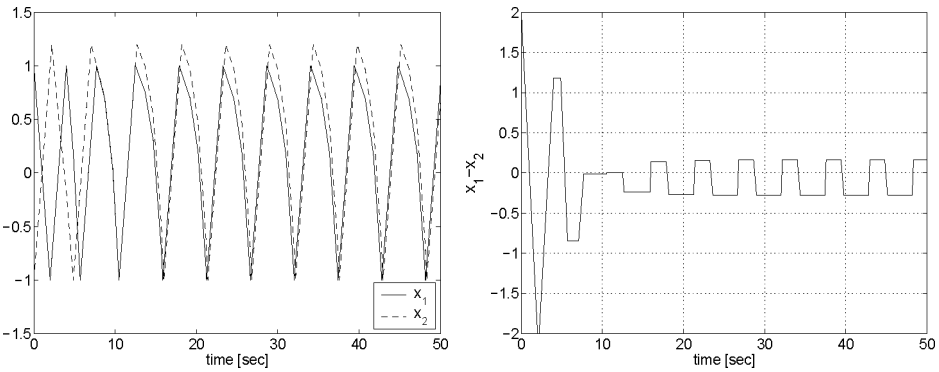

Figure 5.4: Synchronization of two interacting hysteresis controlled systems with different hysteresis bounds and strong negative feedback.

trollers resembles what, was described above for the two hysteresis controllers. If the feedback is negative the subsystems are attracted to synchronization, if the feedback is positive they are attracted to desynchronization. Furthermore by changing the sign of the feedback in the individual subsystems, groups of subsystems can be made to synchronize and others to desynchronize. This is illustrated for a system consisting of 3 subsystems, where following feedback is used $u_{sub} = 1 - \alpha_1 x_1 - \alpha_2 x_2 + \alpha_3 x_3$ and $\alpha_1 = 0.15$, $\alpha_2 = 0.15$ and $\alpha_3 = 0.3$ in this case subsystem 1 and 2 will synchronize and 3 will desynchronize as depicted in Figure 5.5. The number of equilibriums increases with the number of hysteresis controlled subsystems. There are though still only one stable equilibrium i.e. where the hysteresis controllers are all synchronized[desynchronized] if the feedback is negative[positive].

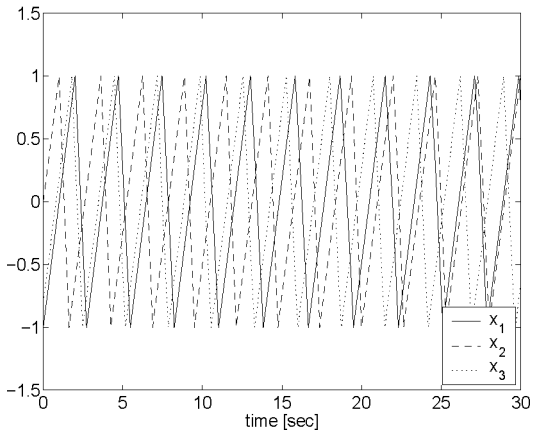

Figure 5.5: Synchronization of subsystem 1 and 2, desynchronization of system 3

5.1.2 The State Agreement Problem for Coupled Nonlinear Systems

A recent result obtained by Lin *et al.* (2005*b*) states a theorem for state agreement for multiple nonlinear dynamical systems. Consider the following interconnection of n subsystems:

$$\begin{aligned} \dot{x}_1 &= f_1(x_1, ..., x_n) \\ &\vdots \\ \dot{x}_n &= f_n(x_1, ..., x_n), \end{aligned} \tag{5.4}$$

where $x_i \in \mathbb{R}^m$ and $i \in \{1, 2, ..., n\}$.
By assuming that the vector fields (f_i) of the subsystems satisfy a certain sub-tangentiality condition, it is proved that the interconnected system reaches state agreement if and only if the interconnection digraph is quasi strongly connected (QSC). Figure 5.6 briefly describes the definition of a digraph being QSC, more details can be found in Lin *et al.* (2005*b*). To give an intuitive example of the theorem, one can imagine a number of agents in the plane. If *every* agent moves towards the interior of the convex hull of its neighbors (meaning that the agents acts according to a QSC interaction digraph and fulfil the sub-tangentiality condition), then according to the theorem, state agreement will follow. The last-mentioned is however, assuming that the agents cannot speed up infinitely fast (f_i should be continuous).
An application of the theorem in Lin *et al.* (2005*b*) is to prove synchronization of the Kuramoto model of coupled nonlinear oscillators. The time evolution of the phase in the

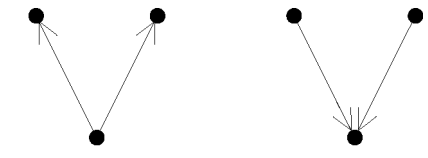

Figure 5.6: A digraph is said to be QSC if for every two nodes v_i and v_j there is a node v from which v_i and v_j is reachable (Lin *et al.* (2005*b*)). The graph (a) is QSC, whereas graph (b) is not.

i'th oscillator is given as:

$$\dot{\theta}_i = \omega_i + K_i \sum_{j \in \mathcal{N}_i} sin(\theta_j - \theta_i), \tag{5.5}$$

where $K_i > 0$ is the coupling strength, ω_i is the natural frequency and $\mathcal{N}_i$ is the set of interacting neighbors. It is proven in Lin *et al.* (2005*b*) that for identical coupled oscillators ($\omega_i = \omega$) synchronization will be achieved if and only if the interaction digraph is QSC and the initial values $\max_{i,j} \|\theta_j(0) - \theta_i(0)\| < \pi$. It turns out that $\max_{i,j} \|\theta_j - \theta_i\| < \pi$ is an invariant set for the systems Eq.(5.5).

If we study an example with two identical oscillators, coupled such that their interaction digraph is QSC, then as long as the initial condition $\|\theta_1(0) - \theta_2(0)\| < \pi$ is satisfied and the coupling strength $K_i > 0$ the oscillators will synchronize. If however the oscillators are started exactly desynchronized $\|\theta_1(0) - \theta_2(0)\| = \pi$ then they will not synchronize. This was the same experience we had with the hysteresis controlled system. If the coupling strength $\alpha_1, \alpha_2 > 0$ and the hysteresis controlled subsystems were started exactly desynchronized, then the subsystems would not synchronize.
Now if we look at the interaction structure in the hysteresis controlled system Eq.(5.1) using the feedback Eq.(5.3) or generally $u_{sub} = 1 - \sum_{i=j}^{n} \alpha_j x_j$ then unless all the α's are zero, the interaction digraph will be QSC, that is however *only* if all of the δ's are simultaneously 1. The structure of the digraph therefore changes depending on the δ's. This means that the interconnection digraph is *state* dependent, this is however an important difference from the Kuramote oscillators, where the interconnection digraph is static. Recent results reported in Lin *et al.* (2005*a*) obtained for systems with *time* dependent interaction digraph, poses a similar theorem as above, thus with slightly harder conditions for the vector fields (f_i) and furthermore requiring that the interconnection digraph should be *uniformly* quasi strongly connected (UQSC). UQSC means that the interacting union digraph in time intervals ($T > 0$) for all $t > 0$ should be QSC. Translated to the hysteresis controlled system this means that there should exist time intervals over which, all of the δ's have been 1. If the switching frequencies of all the δ's are larger than zero, then the interconnection digraph will be UQSC. However an important

precondition for applying the theorem on the hysteresis controlled systems is though still not fulfilled namely that all f_i should be continuous. Though the theorems presented in Lin *et al.* (2005*c*) and Lin *et al.* (2005*b*) were not applicable to hysteresis controlled systems, it though brought the attention to the importance of the coupling structure. Generally we can say that if the coupled hysteresis controlled system is not UQSC then synchronization will not be attained at least not for all subsystems. Furthermore the example of the Kuramoto oscillators exhibited similar behaviors as the hysteresis controlled subsystems, thus accrediting the findings for the hysteresis controlled system.

5.1.3 Desynchronizing Control

In the previous we looked at the simple hysteresis controlled system Eq.(5.1) with the feedback given by Eq.(5.3). Many hysteresis controlled systems has by construction this (negative) feedback, especially systems involving cyclic processes. The negativeness emerges because the subsystem removes "energy" from the system, whenever the subsystems are turned on ($\delta_i = 1$). In supermarket refrigeration systems the negative feedback is a result of the refrigerant returning from the hysteresis controlled display cases to the suction manifold (see Section 2.3). In heating systems it is the water returning from the hysteresis controlled heat elements to a hot water tank, other examples can surely be found. Nevertheless common for both examples are, that besides this *endogenous* feedback, the input to the hysteresis controlled subsystems (u_{sub}) is affected by an *exogenous* control input (u_{exo}). In supermarket refrigeration systems the exogenous input would be the compressor controlling the suction pressure in the suction manifold and in the heating system it would be the water heater trying to uphold a certain temperature in the hot water tank. u_{sub} is therefore normally a controlled variable controlled by u_{exo}. Furthermore do the input to the subsystems (u_{sub}) and the subsystems themselves, in general, contain more complicated dynamics than the simple integrator system described previously. We will therefore consider a more general family of subsystem than integrators.
Consider the following discrete time affine model of n subsystems:

$$\begin{aligned} x_1(k+1) &= A_1 x_1(k) + \delta_1(k) B_1 u_{sub}(k) + c_1, \quad y_1(k) = C_1 x_1(k) + D_1 u_{sub}(k) + d_1 \\ &\vdots \qquad\qquad\qquad\qquad\qquad\qquad\qquad\qquad \vdots \\ x_n(k+1) &= A_n x_n(k) + \delta_n(k) B_n u_{sub}(k) + c_n, \; y_n(k) = C_n x_n(k) + D_n u_{sub}(k) + d_n \end{aligned} \tag{5.6}$$

where $k \in \mathbb{N}_0$ is the discrete time-instant and $x_i \in \mathbb{R}^m$, $y_i \in \mathbb{R}$, $u_{sub} \in \mathbb{R}^p$ are the states, outputs and inputs. $A_i \in \mathbb{R}^{m \times m}$, $B_i \in \mathbb{R}^{m \times p}$, $C_i^T \in \mathbb{R}^m$ and $D_i^T \in \mathbb{R}^p$ are linear discrete time system matrices and $c_i \in \mathbb{R}^m$ and $d_i \in \mathbb{R}$ are constant vectors ($i \in \{1, ..., n\}$).

The subsystems are assumed to have the following input:

$$\begin{aligned} x_u(k+1) &= A_u x_u(k) + B_u u_{exo}(k) - B_\alpha \begin{bmatrix} x_1(k) \\ \vdots \\ x_n(k) \end{bmatrix} \\ u_{sub}(k) &= C_u x_u(k) + d_u \end{aligned} \tag{5.7}$$

where $x_u \in \mathbb{R}^l$, $A_u \in \mathbb{R}^{l \times l}$, $B_u \in \mathbb{R}^{l \times q}$, $B_\alpha \in \mathbb{R}^{l \times nm}$, $C_u \in \mathbb{R}^{p \times l}$, $d_u \in \mathbb{R}^q$ and $u_{exo} \in \mathbb{R}^q$. As it can be seen has u_{sub} been extended with a dynamic part and exogenous input u_{exo} (x_u denotes the states of u_{sub}). The coupling strengths (the α's) have been collected in a matrix B_α.
The interconnected system Eq.(5.6) and Eq.(5.7) is subjected to a hysteresis control law for each of the n subsystem. The switching law for the i'th system is given by:

$$\delta_i(k) = \begin{cases} 1 & \text{if} \quad y_i(k) \geq \bar{y}_i \\ 0 & \text{if} \quad y_i(k) \leq \underline{y}_i \\ \delta_i(k-1) & \text{if} \quad \underline{y}_i < y_i(k) < \bar{y}_i \end{cases} \tag{5.8}$$

where $\bar{y}_i$ and $\underline{y}_i$ are the upper and lower bounds on y_i in the hysteresis control. Note it has been assumed, that the δ's can not switch between samples, only at samples.
Figure 5.7 depicts the interconnected system described by Eq.(5.6) - Eq.(5.8).
In the following we will say that the system Eq.(5.6) - Eq.(5.8) is synchronized if state agreement is attained for all $x_1, ..., x_n$, i.e. exclusive x_u. Now notice that if, for all $i \in \{1, .., n\}$, the controllability matrix of A_i, $B_i C_u$ has $rank \geq 1$ and there exists time intervals where $\delta_i \neq 0$, then the interconnecting digraph is UQSC (if the controllability matrix of A_i, $B_i C_u$ $rank \geq 1$, then x_u will affect all the x_i's hence UQSC). Notice this means that the system can still be UQSC even if $B_\alpha = 0$, obviously the x_i's will not synchronize then, because there is no feedback. Since we are only interested in knowing when $x_1, ..., x_n$ synchronize (exclusive x_u), then the precondition that the system should be UQSC, can be ratified. We will therefore furthermore require, that there exists a feedback from at least one of the states in one of the subsystems. We thus require the following precondition for synchronization; the system Eq.(5.6) - Eq.(5.8) should be UQSC and there should exist at least *one* $i \in 1, ..n$ such that the observability matrix of A_i, $B_{\alpha,i}$ has $rank \geq 1$, where $B_\alpha = [B_{\alpha,1}, ..., B_{\alpha,i}, ...B_{\alpha,n}]$.

Now if we assume all of the subsystems are synchronized, i.e. state agreement is attained, then it means that all states (x) are equal, moving up and down as all of the n hysteresis controllers switches on and off simultaneously. Hereby the interference on u_{sub} from each of the subsystems are accumulated, thus causing periodically large variations at the controlled variable u_{sub}. In the context of refrigeration systems and heating systems, this means that we will get large variations on respectively the suction pressure, and the temperature in the hot water tank. In a traditional distributed control setup the compressor would try to suppress the variations on the suction pressure and

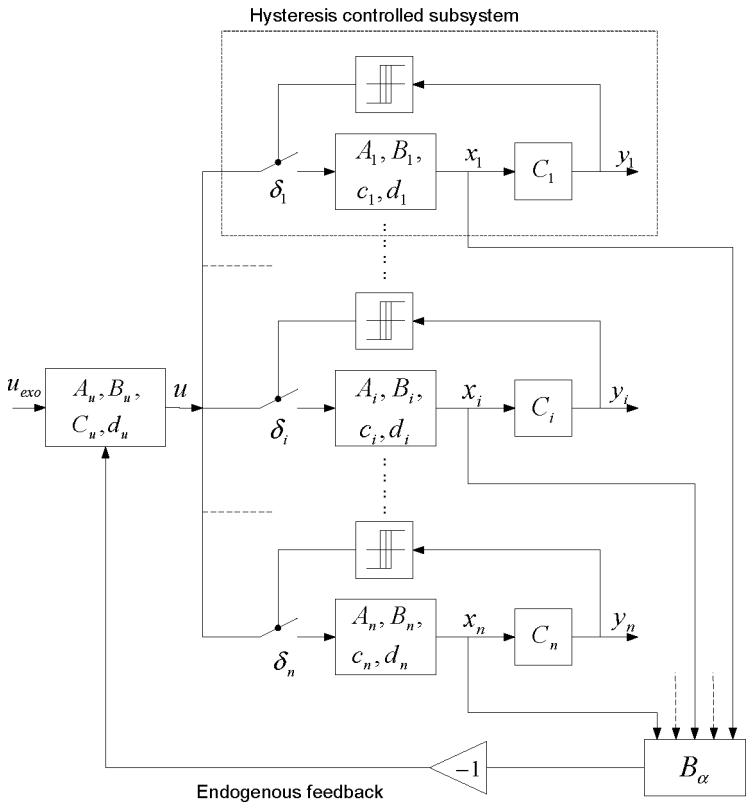

Figure 5.7: The interconnected systems consisting of n hysteresis controlled subsystems

a water heater would try to suppress the variations on water temperature in the tank. This would cause excessive control actions in respectively the compressor and the water heater, however they would never succeed in suppressing these variations. In short the synchronization causes two major problems, namely large variations on the controlled variable (u_{sub}) and excessive control actions on u_{exo}. In Chapter 6 we will discuss more in details the problems related to synchronization in supermarket refrigeration systems.

In the following we will look on how to avoid synchronization and thereby reduce the variation on the controlled variable u_{sub} and reduce the control actions on u_{exo}.
Recall that if we had a positive endogenous feedback in the system, then the subsystems would stabilize desynchronized. Consider the interconnected system Eq.(5.6)-Eq.(5.8). Now assume that the endogenous feedback is negative and the subsystems are synchronized. The idea is now to construct a state feedback that creates a positive endogenous feedback, i.e. we want to construct a state feedback matrix (K), where

$u_{exo} = K[x_1, ..., x_n]^T$ such that $B_u K - B_\alpha = \beta B_\alpha$, where $\beta \geq 0$. Assuming without loss of generality $B_u^T B_u$ has full rank then

$$K = (\beta + 1)(B_u^T B_u)^{-1} B_u^T B_\alpha \tag{5.9}$$

By using this state feedback the sign of the endogenous feedback is changed, thus, according to the previous observations, stabilizing the system at desynchronization. Notice that if $\beta = 0$, in Eq.(5.9), then the state feedback will simply decouple the subsystems. The state feedback only takes care of the desynchronization, i.e. at relatively high frequencies. In order to keep u_{sub} around the desired set-point, a low frequent part has to be introduced to u_{exo}, such as e.g. an output from a PI-controller (u_{PI}). That is the entire control signal becomes $u_{exo} = Kx + u_{PI}$. However one should be aware of the following points before trying to utilizing this feedback scheme in practice:

- It requires that all the states in the subsystems are measured or can be estimated (the pair A_i and C_i is observable).
- In order to make this control scheme work, only small (compared with the switching frequency) time delays in the measurements and in the actuator can be allowed, otherwise it is not possible to generate a positive feedback (i.e. stabilize the unstable equilibrium).
- It would require excessive and fast control actions to desynchronize the hysteresis controllers, if they are close to synchronization.

Now if we assume we had a model of the system available, then we would be able to predict the future values of the states (x). We could thereby allow time delays in the measurements and in the actuators, because we could be pre-active in the control. This would however still leave us with the problem that we would need large and fast control actions. This is a requirement, that it is not possible to fulfill with the compressor in a refrigeration system. It is therefore, in most cases, not possible solely by using the exogenous control input (u_{exo}) to desynchronize the subsystems. We do however have the possibility dynamically to change the bounds in the hysteresis control, that is to manipulate the switching law (Eq.(5.2)). Thybo (2005) proposed a "reversed" control strategy for a supermarket refrigeration system, where the main idea is to utilize the hysteresis bounds in the control of suction pressure, to suppress the fast dynamics. Thereby the control action in the compressor can be reduced as the compressor only maintains the sufficient "mean" pressure.
However, the main objective was that we would like to tailor a control that minimizes the control actions on u_{exo} and minimizes variations on u_{sub}. The idea in the following is that, if we are able to predict future values of the states (x), then we must be able to schedule the operation of the subsystems by manipulating the switches (δ), such that we by using a minimal control effort (u_{exo}) minimizes the variance on u_{sub}. This must furthermore be done such that the outputs from the subsystems (y_i) are kept within the

upper and lower bounds. The idea proposed in the following is to solve this as an optimization problem in a moving horizon fashion, i.e. using Model Predictive Control (MPC). However, this can not be solved as a standard linear MPC problem because of the hybrid nature of the system. Before we carry on we will therefore briefly introduce MPC and hybrid systems.

5.2 Background

This section introduces some of the preliminaries of MPC and hybrid systems that is used later on.
The hysteresis controlled system described by Eq.(5.6) - Eq.(5.8) incorporates discrete valued control actions, namely the δ's. The δ's switches the dynamics in the subsystems between different linear (affine) descriptions, making it a linear hybrid system. We will in the following restrict the introduction of hybrid systems to the discrete-time linear framework of Mixed Logical Dynamical (MLD) systems Bemporad and Morari (1999). The MLD form is a suitable way of representing hybrid systems, when the intention is to use them in connection with MPC. Besides hybrid systems, we will introduce MPC and try to motivate the use of MPC for the problem of scheduling the operation of coupled hysteresis controlled subsystems such that synchronization is avoided.

5.2.1 Discrete Time Hybrid Models

Hybrid systems are complex systems which have discrete event dynamics as well as continuous time dynamics. This broad class of systems includes continuous systems with phased operation (bouncing ball, walking robots, biological cell growth and division), continuous systems controlled by discrete logic (aircraft autopilot modes, thermostats, chemical plants with valves and pumps, automobile automatic transmissions), and coordinating processes (air and ground transportation systems, swarms of air vehicles). In general, hybrid systems switch between different modes of operation. In each of the modes the systems follows different dynamical descriptions. The switch between modes can be triggered by variables crossing certain thresholds, elapse of certain time periods, or by external inputs (HYSCOM (n.d.)). There are a wide range of ways to represent hybrid systems, in the following we will however only introduce the framework of MLD systems, that is we will restrict our models to the discrete-time domain and piecewise affine dynamics.

5.2.1.1 Mixed Logical Dynamical Models

The MLD models are a generalized form of representing linear hybrid systems. Other ways of representing linear hybrid systems are reported, however this class of models

are roughly speaking all equivalent (Heemels *et al.* (2001)).
The general MLD form of a hybrid system introduced in Bemporad and Morari (1999) is

$$x(k+1) = Ax(k) + B_1u(k) + B_2\delta(k) + B_3z(k) \tag{5.10a}$$
$$y(k) = Cx(k) + D_1u(k) + D_2\delta(k) + D_3z(k) \tag{5.10b}$$
$$E_2\delta(k) + E_3z(k) \leq E_4x(k) + E_1u(k) + E_5, \tag{5.10c}$$

where $k \in \mathbb{N}_0$ is the discrete time-instant, and $x \in \mathbb{R}^{n_c} \times \{0,1\}^{n_\ell}$ denotes the states, $u \in \mathbb{R}^{m_c} \times \{0,1\}^{m_\ell}$ the inputs and $y \in \mathbb{R}^{p_c} \times \{0,1\}^{p_\ell}$ the outputs, with both continuous and binary components. Furthermore, $\delta \in \{0,1\}^{r_\ell}$ and $z \in \mathbb{R}^{r_c}$ represent binary and auxiliary continuous variables, respectively. These variables are introduced when translating propositional logic or piecewise affine functions into mixed integer linear inequalities.
All constraints on states, inputs and auxiliary variables are summarized in the inequality Eq.(5.10c). Note that this formulation allows specification of additional linear constraints on as well continuous variables and boolean variables. Note also that the equations Eq.(5.10a) and Eq.(5.10b) are linear; the nonlinearity is hidden in the integrality constraints over the binary variables. Various examples of representing different kinds of systems in the MLD form can be found in Bemporad and Morari (1999).

5.2.1.2 HYSDEL

Representing a hybrid system directly in the MLD form Eq.(5.10a) - Eq.(5.10c) is in general a tedious and non-trivial task. In order to automatize this procedure, the compiler HYSDEL[1] (HYbrid System DEscription Language), that generates the matrices of the MLD model starting from a high level description of the dynamic and logic of the system, has been developed. HYSDEL allows the user to model hybrid systems in a textual basis. The structure of the modelling resembles that of a Discrete Hybrid Automaton (DHA), i.e. a connection of a finite state machine, an event generator, a switched affine system and a mode selector. For a detailed description of HYSDEL and DHA's consult the HYSDEL manual (Torrisi *et al.* (2000)). In the case study, Chapter 6 HYSDEL has been used for building a MLD model of a supermarket refrigeration system. In Appendix C the HYSDEL code can be found.

5.2.2 Model Predictive Control

Many systematic control design techniques are nowadays available to solve stabilization, tracking, robustness, noise reduction problems etc. both for linear (e.g. PID, lead/lag

[1] The HYSDEL compiler is available at `http://control.ee.ethz.ch/~hybrid/hysdel/`

networks, LQG, H_∞) and nonlinear (e.g. sliding mode, feedback linearization, gain scheduling, nonlinear H_∞) systems. However, none of these are able to handle constraints. The first and far most important reason for using MPC is unconditionally its ability to handle constraints on as well inputs, states and outputs. This is the point that parts it from other control techniques. In linear MPC, if no constraints are present, the MPC scheme results in nothing else but a sub-optimal LQR controller. However MPC offers other advantages that makes it convenient to use (Maciejowski (2002) and Camacho and Bordons (2003)) such as:

- It is easy and intuitive to tune. The tuning parameters make sense to a layman.
- Multivariable problems can easily be handled.
- Knowledge of future references and disturbances can easily be taken in to account.
- Feed forward of measurable disturbances is naturally incorporated.

The major drawback is however the required on-line computation that is needed at each time-instance for optimizing an objective function. This makes demands on the available time for computation and on the speed of the hardware. However, the acceleration in the speed and decrease in prize of modern computing hardware along with recent developed of methods for explicit off-line solutions for as well linear systems (Bemporad *et al.* (2002)) and linear hybrid systems (Dua and Pistikopoulos (2000)), has made MPC feasible for a larger variety of systems.

The idea in MPC is to use a model of the given plant to predict the future development of the output (y) for a certain time horizon (N time-steps), see Figure 5.8. These predicted values depends however on the present states (at time-step k) and the future sequence of control signals ($[u(k), ..., u(k+N)]$). The future sequence of the control signals is calculated by optimizing an objective function over the N-step time horizon. The objective function typically penalizes the derivation of the predicted outputs from a reference. Of this *open-loop* optimal control sequence only the first is applied to the plant. At next sampling interval ($k+1$) a new state measurement is obtained (thus providing feedback) and the objective function is optimized once again over the shifted horizon ($k+1, ..., k+N+1$) (moving horizon). Constrains on the input, output and states can be accounted for by optimizing the objective function subjected to these constrains. Figure 5.8 depicts the MPC strategy. If there are no constrains and the objective function is quadratic (i.e. the model is linear and the objective function is based on the 2-norm), then there exist a closed form solution, even for the infinite horizon, namely the LQR. However if constraints are present, there exists no closed form solution and the optimization problem can only be solved by using a finite horizon (however explicit solutions for the infinite horizon can though be computed (Bemporad *et al.* (2002))). Hence linear MPC is closely related to the LQR.

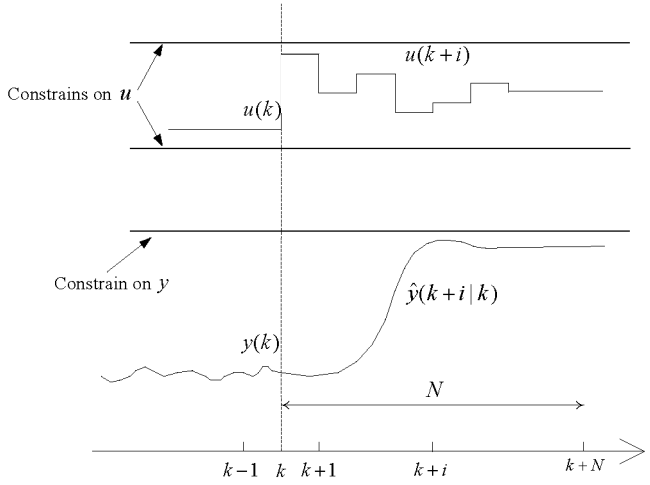

Figure 5.8: The MPC strategy. Constrains on input and output are illustrated by the horizontal solid lines.

This introduced the basic ideas of a moving horizon and MPC. For more insight a number of books (e.g. Maciejowski (2002), Camacho and Bordons (2003) and Rossiter (2000)) and survey papers (e.g. C. E. Garcia and Morari (1989), Mayne *et al.* (2000) and Qin and Badgwell (2003)) can be found.

5.2.3 Predictive Control of MLD Systems

As introduced in Tyler and Morari (1999), MPC is well suited for finding control laws for hybrid systems described in the MLD form.
The predictive control problem for MLD systems can be defined as follows. Let u_{ref}, x_{ref} and y_{ref} be desired steady state values. Consider the following constrained finite time optimal control (CFTOC) problem

$$\begin{aligned}\min_{U(k)} J(U(k), x(k)) = \sum_{i=0}^{N-1} \Big(&\|Q_1(u(k+i) - u_{ref})\|_{\{1,\infty\}} \\ &+\|Q_2(x(k+i|k) - x_{ref})\|_{\{1,\infty\}} + \|Q_3(y(k+i|k) - y_{ref})\|_{\{1,\infty\}} \Big)\end{aligned} \tag{5.11}$$

subjected to the MLD model Eq.(5.10a)-Eq.(5.10c) at $i = k, ..., k+N-1$,

where $U(k) = [u(k)^T, ..., u(k+N-1)^T]$ and Q_1, Q_2 and Q_3 are assumed to be full column rank matrices. It can be seen that the cost function penalize the predicted evolution of the state, control input and output over the finite horizon N. The optimal

control sequence at time-instant k is obtained by minimizing the cost function subjected the evolution of the MLD model including its mixed integer linear inequalities plus possibly additional constraints. As we are using linear norms (either 1 or ∞-norm) and the MLD model contains binary variables, the CFTOC problem amounts to solving a Mixed Integer Linear Program (MI-LP). Because of the binary variables the MI-LP is not convex (a local minima is not necessarily a global minima), in fact it is in general NP-hard. NP-hard means that by using the algorithms available, the solution time grows in worst case exponentially with the number of binary variables (Raman and Grossmann (1991)). As the number of binary variables grows linearly with the length of the horizon (Morari (2002)), this clearly indicates why it is convenient to use a finite time horizon. Though solving the CFTOC problem is hard, efficient algorithms and solvers, that can handle large size problems exists, such as ILOG (2003).
To summarize, MPC of MLD systems requires solving of a MI-LP problem at each time instance. By modelling the systems directly in HYSDEL the MLD model can automatically be generated, thereby converting the CFTOC problem into a standard MI-LP form that can be exported and solved by existing solvers.

5.3 A Novel Approach for Desynchronization

To briefly recall; the objective was to formulate a CFTOC problem, where the optimal control sequence minimizes the variance on u_{sub} using a minimal control effort, thus desynchronizing the subsystems. Since the hysteresis controlled system Eq.(5.6) - Eq.(5.8) is hybrid, we want to formulate it in the MLD framework such that the CFTOC problem can be solved as a standard MI-LP.
In the following we will transform the hysteresis controlled system Eq.(5.6) - Eq.(5.8) in to a MLD-form. We will construct two different MLD models, a full version taking all dynamics in to account (version 1) and a reduced version (version 2), which is computational more tractable, however still sufficient for dealing with the problems of synchronization.

Version 1
The interconnected system Eq.(5.6) and Eq.(5.7) can be written in a more compact form:

$$\begin{aligned} \tilde{x}(k+1) &= \tilde{A}\tilde{x}(k) + [\tilde{B}_1, c]\tilde{u}(k) + \tilde{B}_2\tilde{\delta}(k) + \tilde{B}_3 z(k) \\ \tilde{y}(k) &= \tilde{C}\tilde{x}(k) + d, \\ \tilde{E}_2\tilde{\delta}(k) + \tilde{E}_3 z(k) &\leq \tilde{E}_4 x(k) + \tilde{E}_5, \end{aligned} \tag{5.12}$$

where $\tilde{x} = [x_1, ..., x_n, x_u]^T$, $\tilde{y} = [y_1, ..., y_n, u_{sub}]^T$, $\tilde{u} = [u_{exo}, 1]^T$,$\tilde{\delta} = [\delta_1, ..., \delta_n]$ and z is an auxiliary variable defined as: $z = [x_u\delta_1, ..., x_u\delta_n]^T$ and system matrixes is given

by:

$$\tilde{A} = \begin{bmatrix} A_1 & & 0 & 0 \\ & \ddots & & \vdots \\ 0 & & A_n & 0 \\ & -B_\alpha & & A_u \end{bmatrix} \quad \tilde{B}_2 = \begin{bmatrix} B_1 d_u & & 0 \\ & \ddots & \\ 0 & & B_n d_u \\ 0 & \dots & 0 \end{bmatrix} \quad \tilde{B}_1 = \begin{bmatrix} 0 \\ \vdots \\ 0 \\ B_u \end{bmatrix} \quad c = \begin{bmatrix} c_1 \\ \vdots \\ c_n \\ 0 \end{bmatrix}$$

$$\tilde{B}_3 = \begin{bmatrix} B_1 C_u & & 0 \\ & \ddots & \\ 0 & & B_n C_u \\ 0 & \dots & 0 \end{bmatrix} \quad \tilde{C} = \begin{bmatrix} C_1 & & 0 & D_1 C_u \\ & \ddots & & \vdots \\ 0 & & C_n & D_n C_u \\ 0 & \dots & 0 & C_u \end{bmatrix} \quad d = \begin{bmatrix} d_1 \\ \vdots \\ d_n \\ d_u \end{bmatrix} \tag{5.13}$$

The new variable z is defined by the nonlinear term $z_i = x_u \delta_i$, however this can be replaced by the following mixed integer(MI)-inequalities, assuming $x_u \in [m, M]$.

$$\begin{aligned} z_i(k) &\leq M\delta_i(k) \\ z_i(k) &\geq m\delta_i(k) \\ z_i(k) &\leq x_u(k) - m(1 - \delta_i(k)) \\ z_i(k) &\geq x_u(k) - M(1 - \delta_i(k)) \end{aligned}$$

Writing these MI-inequalities in a matrix form the matrices $\tilde{E}_2$, $\tilde{E}_3$, $\tilde{E}_4$ and $\tilde{E}_5$ are obtained.

One of the objectives was to minimize the control actions on u_{exo}, that is to minimize $\Delta u_{exo}(k) = u_{exo}(k) - u_{exo}(k-1)$. It is therefore convenient to rewrite the system Eq.(5.12) by augmenting the state vector $\tilde{x}(k)$ with $u_{exo}(k-1)$ ($x(k) = [\tilde{x}(k), u_{exo}(k-1)]^T$) such that Δu_{exo} can be written as an output.

The upper ($\bar{y}$) and lower ($\underline{y}$) bounds, maintained by the hysteresis control, has not yet been considered. Recall that the idea was to use the upper and lower bounds (along with Δu_{exo}) as control inputs. Now if we look at the switching law Eq.(5.8) then the logic determining whether δ_i is *on* or *off*, has to be incorporated in Eq.(5.12) as MI-inequalities.

Let $\bar{u}_i$ and $\underline{u}_i$ be controllable upper and lower bounds for the i'th subsystem. Let $\delta_{\bar{u}_i}$ and $\delta_{\underline{u}_i}$ be two sets of binary variables determined by $[\delta_{\bar{u}_i}(k) = 1] \leftrightarrow [\bar{u}_i(k) - y_i(k) \leq 0]$ and $[\delta_{\underline{u}_i}(k) = 1] \leftrightarrow [y_i(k) - \underline{u}_i(k) \leq 0]$. Let furthermore $x_{\ell,i}(k+1) = \delta_i(k)$ be a logic state keeping track of the old values of δ_i. By assuming that δ_i should switch *on* when the upper bound is reached and vice versa when the lower bound is reached, the logic determining the hysteresis control law can be set up. In the Table 5.3 the logic and the matching MI-inequalities can be found. More details on transforming logic rules into MI-inequalities can be found in Christiansen (1997), Hayes (1993) and Bemporad and Morari (1999).

Now updating the system, Eq.(5.12), with the new input, state and binary vectors and

Logic	MI-inequalities
Initialization of $\delta_{\bar{u}_i}$ and $\delta_{\underline{u}_i}$	
$[\delta_{\bar{u}_i}(k)=1] \leftrightarrow [\bar{u}_i(k)-y_i(k) \leq 0]$	$\bar{u}_i(k)-y_i(k) \leq \overline{M}_i(1-\delta_{\bar{u}_i}(k))$ $\bar{u}_i(k)-y_i(k) \leq \varepsilon+(\overline{m}_i-\varepsilon)\delta_{\bar{u}_i}(k)$
$[\delta_{\underline{u}_i}(k)=1] \leftrightarrow [y_i(k)-\underline{u}_i(k) \leq 0]$	$y_i(k)-\underline{u}_i(k) \leq \underline{M}_i(1-\delta_{\underline{u}_i}(k))$ $y_i(k)-\underline{u}_i(k) \leq \varepsilon+(\underline{m}_i-\varepsilon)\delta_{\underline{u}_i}(k)$
Hysteresis control of the i'th subsystem	
$[\delta_i(k)=1] \leftrightarrow [\delta_{\bar{u}_i}(k)=1]$ $\vee([\delta_{\underline{u}_i}(k)=0] \wedge [x_{\ell,i}(k)=1])$	$\delta_{\bar{u}_i}(k)-\delta_i(k) \leq 0$ $\delta_{\underline{u}_i}(k)-(1-\delta_i(k)) \leq 0$ $(1-\delta_{\underline{u}_i}(k))+x_{\ell,i}-\delta_i(k)) \leq 1$ $(1-\delta_{\bar{u}_i}(k))+(1-x_{\ell,i}(k))-(1-\delta_i(k)) \leq 1$
State update (binary states)	
	$x_{\ell,i}(k+1)=\delta_i(k)$

Table 5.1: Logic determining the switching law of the i'th hysteresis controller. $\overline{M}_i$ [$\overline{m}_i$] are over [under] estimates of $\bar{u}_i(k)-y_i(k)$, $\underline{M}_i$ [$\underline{m}_i$] are over[under] estimates of $y_i(k)-\underline{u}_i(k)$ and ε is a small tolerance (typically the machine precision).

including the MI-inequalities (Table 5.3):

$$\begin{aligned} x(k+1) =& Ax(k)+B_1u(k)+B_2\delta(k)+B_3z(k) \\ y(k) =& Cx(k)+D_1u \\ E_2\delta(k)+E_3z(k) \leq& E_4x(k)+E_1u(k)+E_5, \end{aligned} \tag{5.14}$$

where
$x(k)=[\tilde{x}(k), u_{exo}(k-1), [x_{\ell,1}(k), ..., x_{\ell,n}(k)]]^T$,
$y(k)=[\tilde{y}, \Delta u_{exo}(k)]$
$u(k)=[u_{exo}(k), 1, [\underline{u}_1(k), ..., \underline{u}_n(k)], [\bar{u}_1(k), ..., \bar{u}_n(k)]]^T$,
$\delta(k)=[[\delta_{\underline{u}_1}(k), ..., \delta_{\underline{u}_n}(k)], [\delta_{\bar{u}_1}(k), ..., \delta_{\bar{u}_n}(k)], [\delta_1(k), ..., \delta_n(k)]]^T$
$z(k)=[x_u(k)\delta_1(k), ..., x_u(k)\delta_n(k)]^T$.
The system matrices are given by:

$$A=\begin{bmatrix} \tilde{A} & \tilde{B}_1 & 0 \\ 0 & 0 & 0 \\ 0 & 0 & 0 \end{bmatrix}, B_1=\begin{bmatrix} \tilde{B}_1 & c & 0 & 0 \\ I & 0 & 0 & 0 \\ 0 & 0 & 0 & 0 \end{bmatrix}, B_2=\begin{bmatrix} 0 & 0 & 0 \\ 0 & 0 & 0 \\ 0 & 0 & I+\tilde{B}_2 \end{bmatrix} B_3=\begin{bmatrix} \tilde{B}_3 \\ 0 \\ 0 \end{bmatrix},$$

$$C=\begin{bmatrix} \tilde{C} & 0 & 0 \\ 0 & -I & 0 \end{bmatrix} \text{ and } D_1=\begin{bmatrix} 0 & d & 0 & 0 \\ I & 0 & 0 & 0 \end{bmatrix}$$

The matrices concerning the inequalities E_1, E_2, E_3, E_4 and E_5 define the upper and lower bounds on x, u and the auxiliary variable z, plus incorporating the MI-inequalities in stated in Table 5.3. These are rather large and trivial matrices, that along with A, B_1, B_2, B_3 and C can be automatically generated using HYSDEL.
We have shown the system Eq.(5.6) - Eq.(5.8) can be transformed into a MLD form. By

Variable	Size	
	real	binary
x	$n \cdot m + q + l$	n
u	$2n + q{+}1$	0
z	$n \cdot l$	0
δ	0	$3n$

Table 5.2: Size of the MLD model, version 1, Eq.(5.14)

subjecting the objective function (Eq.(5.11)) to the MLD model Eq.(5.14) and choosing appropriate weight matrices (Q_1, Q_2, and Q_3) the objectives can be met.
Let $Q_1 = diag(Q_{u_{exo}}, q, Q_{\underline{u}}, Q_{\bar{u}})$, $Q_2 = diag(Q_{\tilde{x}}, Q_{u_{exo}}, Q_{x_\ell})$ and $Q_3 = diag(Q_y, Q_{u_{sub}}, Q_{\Delta u_{exo}})$. By choosing $Q_{\Delta u_{exo}} > 0$ and $Q_{u_{sub}} > 0$ to be diagonal matrices with large values in the diagonal, it is possible to minimize the variations on u_{sub} and simultaneously minimize the control actions Δu_{exo}, thus fulfilling the objectives and desynchronizing the subsystem.
It can however be seen from Table 5.2 that the resulting MI-LP contains quite a lot of binary variables, namely 4 times the number of subsystems plus as many z variables as there are subsystems. Recall that the computation time is strongly dependent on the number of binary variables, it therefore pays off to reduce the size of the problem, i.e. reduce the number of binary variables.

Version 2
Motivated by the huge number of binary variables in the previous representation of the interconnected systems (version 1), we will in the following try to construct a simpler MLD model.
We will now use the δ's as input instead of the upper and lower bounds in the hysteresis control. The system can then be written as:

$$\begin{aligned} \tilde{x}(k+1) &= \tilde{A}\tilde{x}(k) + [\tilde{B}_1, c, \tilde{B}_2]u(k) + \tilde{B}_3 z(k) \\ \tilde{y}(k) &= \tilde{C}\tilde{x}(k) + d, \\ \tilde{E}_3 z(k) &\leq \tilde{E}_4 x(k) + \tilde{E}_1 u(k) + \tilde{E}_5, \end{aligned} \tag{5.15}$$

where $\tilde{x} = [x_1, ..., x_n, x_u]^T$, $\tilde{y} = [y_1, ..., y_n, u_{sub}]^T$, $u = [u_{exo}, 1, \delta_1, ..., \delta_n]^T$, $z = [x_u\delta_1, ..., x_u\delta_n]^T$ and the system matrices are given by Eq.(5.13).
Now introducing Δu_{exo} in the output, for the same reason and by using the same method as above in version 1, the system Eq.(5.15) can be written as:

$$\begin{aligned} x(k+1) &= Ax(k) + B_1 u(k) + B_3 z(k) \\ y(k) &= Cx(k) + D_1 u \\ E_3 z(k) &\leq E_4 x(k) + E_1 u(k) + E_5, \end{aligned} \tag{5.16}$$

Variable	Size	
	real	binary
x	$n \cdot m + q + l$	0
u	q+1	n
z	$n \cdot l$	0
δ	0	0

Table 5.3: Size of the MLD model, version 2, Eq.(5.16)

where $x(k) = [\tilde{x}(k), u_{exo}(k-1)]^T$, $y = [\tilde{y}, \Delta u_{exo}]^T$, and the system matrices are given by: $A = \begin{bmatrix} \tilde{A} & \tilde{B}_1 \\ 0 & o \end{bmatrix}$, $B_1 = \begin{bmatrix} \tilde{B}_1 & c & \tilde{B}_2 \\ I & 0 & 0 \end{bmatrix}$, $B_3 = \begin{bmatrix} \tilde{B}_3 \\ 0 \end{bmatrix}$, $C = \begin{bmatrix} \tilde{C} & 0 \\ 0 & -I \end{bmatrix}$ and $D_1 = \begin{bmatrix} 0 & d \\ I & 0 \end{bmatrix}$.

The matrices E_1, E_2, E_3, E_4 and E_5 are determined by the bounds on x, u and the MI-inequalities determining z. They further more they incorporates the upper and lower bounds ($\bar{y}_i$ and $\underline{y}_i$) on y_i in the subsystems. Since the switches (δ) are incorporated as control inputs and directly determined by the solving a CFTOC problem, the hysteresis control law does not have to be regarded and formulated as a MI-inequalities.

The CFTOC resembles that for version 2, i.e. consider the objective function (Eq.(5.11)) and submit it to the MLD model Eq.(5.16). The objective (minimizing the variance on u_{sub} by using minimal control action Δu_{exo}, thus avoiding synchronization) can be obtained by choosing the weight matrices in the same way as in version 1. However to avoid excessive switching in the subsystems the δ's has to be weighted as well.

Now if we look at the complexity of the problem, it can be seen by comparing Table 5.2 and 5.3, that the number of binary variables and states are much smaller in the version 2 model than in the version 1, hence much more computational tractable. This clearly shows that the size of the MLD-model and hence the matching CFTOC problem clearly depends on how the control problem is posed. Furthermore one should be aware of the fact that the MLD representation is not unique, the same system therefore has several representations, which are not equally computational tractable.

In Chapter 6 we will demonstrate the use of the desynchronizing control on a supermarkets refrigeration system based on the version 2 representation of the control problem.

Chapter 6

Desynchronizing Control of Supermarket Refrigeration Systems

A typical supermarket refrigeration system consists of a central compressor rack that maintains the required flow of refrigerant to the refrigerated display cases located in the supermarket sales area. Each display case has an inlet valve for refrigerant that needs to be opened and closed such that the air temperature in the display case is kept within tight bounds to ensure a high quality of the goods.

For many years, the control of supermarket refrigeration systems has been based on distributed control systems, which are flexible and simple. In particular, each display case used to be equipped with an independent hysteresis controller that regulates the air temperature in the display case by manipulating the inlet valve.

The major drawback, however, is that the control loops are vulnerable to self-inflicted disturbances caused by the interaction between the distributed control loops. In particular, practice show that the distributed hysteresis controllers have the tendency to synchronize, meaning that the opening and closing actions of the valves coincide. Consequently, the compressor periodically has to work hard to keep up the required flow of refrigerant, which results in low efficiency, inferior control performance and a high wear on the compressor.

The control problem is significantly complicated by the fact that many of the control inputs are restricted to discrete values, such as the opening/closing of the inlet valves and the stepwise control of the compressor. Furthermore, the system features switched dynamics turning the supermarket refrigeration system into a hybrid system.

In the following we will first briefly recall the layout of a supermarket refrigeration system, and provide an overview of the traditional control setup. Next we will derive a nonlinear model of the refrigeration system, and furthermore by linearization, we will transform the model into an interconnection of linear hysteresis controlled subsystems. Next we will analyze the causes for synchronization based on the results provided in Chapter 5. Finally we will based on the linearized model apply the proposed desynchronizing MPC and test it on the nonlinear model.

6.1 System Description

In the following section we will briefly recall the layout of a supermarkets refrigeration system. We will however give a more detailed description of the display cases, as they play an important part, later on, in the model and when we will study synchronization. Furthermore we will briefly recall the traditional control structure and motivate the use of a desynchronizing control.

6.1.1 System Layout

As mentioned earlier the supermarkets refrigeration system can be divided into a high and a low temperature part. We will however only consider the high temperature part here.
Now recall that the system can be divided into three parts namely the compressor rack, the condenser unit and the refrigerated display cases. Figure 2.5 depicts the layout. The compressors maintain the flow of refrigerant in the system, by compressing the low pressure refrigerant from the suction manifold, which is returning from the display cases. The high pressure refrigerant, leaving the compressors, flows to the condenser unit, where it condenses. The condensed refrigerant flows from the condenser unit and into liquid manifold and further on to the display cases, where it evaporates. Hereafter the evaporated refrigerant returns in the suction manifold, whereby the refrigeration cycle is closed.
The Display Cases
A variety of different display cases exist, in the following description we will however focus on open display cases, which are by far the most common type. The basic equations describing the dynamics for open as well as closed display cases or clod storage rooms are similar, however the load for the surroundings though differ. Now figure 6.1 depicts a cross section of an open display case.

The refrigerant is let into the evaporator located at the bottom of the display case, where the refrigerant evaporates under heat absorption from the surrounding air circulated through the evaporator. The resulting air flow creates an air-curtain at the front of the display case. The fact that the air-curtain is colder than the goods enables a

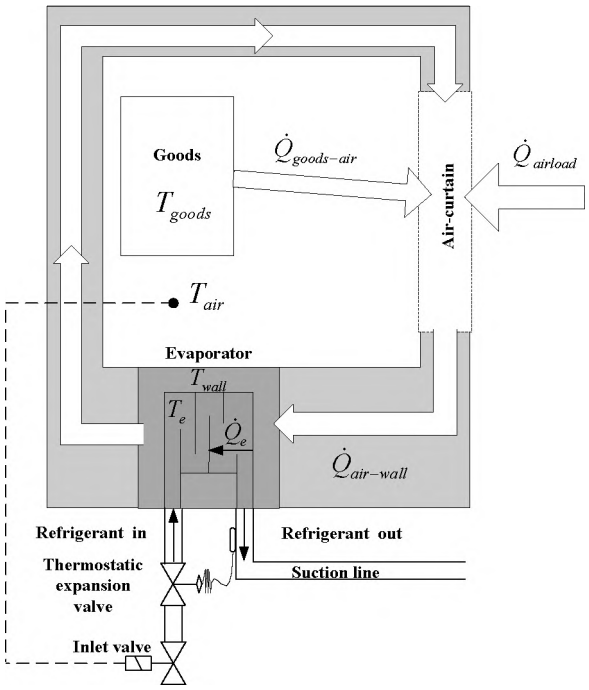

Figure 6.1: Cross section of a refrigerated display case.

heat transfer from the goods ($\dot{Q}_{goods-air}$) and - as a side effect from the surroundings ($\dot{Q}_{airload}$) to the air-curtain. Inside the display case is located a temperature sensor (T_{air}), which measures the temperature next to the goods. This temperature measurement is used in the control loop as an indirect measure of the goods temperature. Furthermore, at the inlet to the evaporator is located an (off/on) inlet valve which is used to control the temperature in the display case. In series with the inlet valve is a thermostatic expansion valve which is used to control the superheat, that is when the inlet valve is open. In some versions there is no extra thermostatic expansion valve, in that case the superheat is regulated by pulse width modulation of the inlet valve.

6.1.2 Traditional Control

The control systems used in today's supermarket refrigeration systems are, as previously mentioned decentralized. Each of the display cases is equipped with a temperature controller and a superheat controller that controls the filling level of the evaporator. The compressor rack is equipped with a suction pressure controller. Furthermore, the con-

denser is equipped with a condensation pressure controller, and on top, various kinds of supervisory controllers may be used that help adjusting the set-points, such as e.g. described in Chapter 3 and 4. Here we will only consider the display case temperature controller and the compressor controller.

The air temperature T_{air} in the display cases are controlled by a hysteresis controller that opens and closes the inlet valve. This means that when T_{air} reaches a certain upper temperature bound the valve is opened and T_{air} decreases until the lower temperature bound is reached and the valve is closed again (Danfoss A/S (2004*a*)). Unfortunately, when the valve is closed, the air temperature continues to decrease below the lower bound creating an "undershoot", this is caused by two things. Firstly, the remaining refrigerant contained in the evaporator evaporates, and secondly, the thermal capacity of the evaporator wall adds an extra order to the system dynamics.

In the supermarket many of the display cases are alike in design and they are working under uniform conditions. As a result, the inlet valves of the display cases are switched with very similar switching frequencies. Therefore, the valves have a tendency to synchronize leading to periodic high and low flow of evaporated refrigerant into the suction manifold thus creating large variations in the suction pressure.

Recall that the compressors controls the suction pressure by turning off and on compressors in the compressor rack (Danfoss A/S (2004*b*)). The suction pressure controller is normally a PI-controller with a dead band around the reference of the suction pressure. The dead band ensures that the integration is stopped as long the suction pressure is within the dead band. When the pressure exceeds the upper bound the integration is started and one or more additional compressors are turned on, eventually, to reduce the pressure, and vice versa when the pressure falls below the lower bound. Hereby moderate changes in the suction pressure and small biases from the reference do not initiate a compressor switching. Nevertheless, pronounced synchronization effects lead to frequent compressor switching causing large fluctuations in the suction pressure and a high wear on the compressors.

All of these problems would however be solved if a continuous control of the air temperature was applied, e.g. a cascaded control with a superheat control in the inner loop and an air temperature control in the outer loop. The inner loop would control the filling level of the evaporator (the superheat is an indirect measure of the filling level) and the outer loop would adjust the filling continuously to maintain the required air temperature.

The reason, however, why hysteresis controllers are used in the display cases, despite the severe side effects, has various reasons. If a mechanical superheat controller (a thermostatic expansion valve) is installed in the display cases, it is of course not possible to apply a cascaded control structure. Furthermore if the evaporator in the display cases is operated with a low degree of filling, then the temperature distribution across the display case will be in-homogenous, thus deteriorating the goods quality. Finally, humid air will cause a frost build up on the coldest areas of the evaporator, thus deteriorating the heat transfer and blocking the air flow through the evaporator. The hysteresis control has the positive side-effect, that in the off periods the frost will melt, perhaps not completely but

enough to create a more dense ice layer that actually improves the heat transfer (Fahlén (1996)), defrosting of the evaporators can therefore be carried out less often using hysteresis control.
In the following we will therefore apply the proposed control scheme for desynchronization, thus accommodating the otherwise deteriorated control performance and furthermore maintaining the desired qualities of the hysteresis controls. Before we turn to the implementation, we will however need an appropriate model of the system. In the following we will derive a model and study more in detail the phenomenon of synchronization in supermarkets refrigeration systems.

6.2 Dynamic Model of a Supermarkets Refrigeration System

In the literature only few dynamic models of refrigeration systems can be found (e.g. Xiang-Dong *et al.* (1997) and Larsen and Holm (2003)) and yet less describing larger systems consisting of a number of evaporators. However in Gordon *et al.* (1999) is a very detailed dynamic model of a multiple evaporator system presented. For describing the effects of synchronization we can settle with a somewhat less detailed model. We will therefore start by summarizing the main features of a nonlinear continuous-time model of a supermarket refrigeration system derived by Jakobsen and Skovrup (2004). The aim of the model is exactly to describe the major dynamic interconnections that might complicate the *system* control. The model is accepted at Danfoss and used for a firsthand verification of new control algorithms.
Afterwards on the nonlinear model is linearized, obtaining an interconnection of linear hysteresis controlled subsystems, according to Eq.(5.6)-Eq.(5.7). The linearized model will be used later on for analysis and implementation of a desynchronizing control.

6.2.1 Nonlinear Continuous-Time Model

The nonlinear model of the supermarket refrigeration system is composed of individual models of the display cases, the suction manifold, the compressor rack and the condensing unit. The main emphasis in the modelling is laid on the suction manifold and the display cases such that the dynamics relevant for controlling the compressor(s) and display cases are captured. Furthermore the model must be able to describe the dynamics whether the inlet valve is closed or opened and it should capture the phenomena of synchronization.
The Display Cases
The dynamics in the display case can be described by three states, namely the goods' temperature T_{goods}, the temperature of the evaporator wall T_{wall} and the mass of liquid refrigerant in the evaporator M_{ref}. The input to the display case model is the suction

pressure (P_{suc}), the state of the inlet valve (closed or opened, $valve \in \{0, 1\}$) and the disturbance $\dot{Q}_{airload}$. The model of the display cases encompasses three parts, namely the goods, the evaporator and the air-curtain in between. The following derivations are based on a layout of a display case similar to the one depicted in Figure 6.1, the notation introduced in the figure will furthermore be used in the following. By setting up the energy balance for the goods and the evaporator, the following two state equations can be derived, assuming a lumped temperature model.

$$\frac{dT_{goods}}{dt} = -\frac{UA_{goods-air}}{M_{goods} \cdot C_{p,goods}} \cdot (T_{goods} - T_{air}) \tag{6.1}$$

$$\begin{aligned} \frac{dT_{wall}}{dt} =& \frac{UA_{air-wall}}{M_{wall} \cdot C_{p,wall}} \cdot (T_{air} - T_{wall}) \\ & - \frac{UA_{wall-ref}(M_{ref})}{M_{wall} \cdot C_{p,wall}} \cdot (T_{wall} - T_e) \end{aligned} \tag{6.2}$$

where UA is the overall heat transfer coefficient with the subscript denoting the media between which the heat is transferred, M denotes the mass, and C_p the heat capacity, where the subscript denotes the media the parameter refers to. Moreover T_e is the evaporation temperature, which is an output from the model of the suction manifold that will be derived later on. The air temperature T_{air} is determined in the following.
As indicated in Eq. (6.2), the heat transfer coefficient between the refrigerant and the evaporator wall $UA_{wall-ref}$ is a function of the mass M_{ref} of the liquified refrigerant in the evaporator. It is assumed here that this relation can be described by the following linear function:

$$UA_{wall-ref}(M_{ref}) = UA_{wall-refrig,max} \cdot \frac{M_{ref}}{M_{ref,max}}, \tag{6.3}$$

where $M_{ref} = M_{ref,max}$, when the evaporator is completely filled with liquid refrigerant, this is also when the maximal overall heat transfer coefficient $UA_{wall-refrig,max}$ is attained.
The accumulation of liquid refrigerant in the evaporator is described by:

$$\frac{dM_{ref}}{dt} = \begin{cases} 0 & \text{if } valve = 1, \\ -\frac{\dot{Q}_e}{\Delta h_{lg}} & \text{if } valve = 0 \text{ and } M_{ref} > 0, \\ 0 & \text{if } valve = 0 \text{ and } M_{ref} = 0. \end{cases} \tag{6.4}$$

where Δh_{lg} is the specific latent heat of the remaining liquid refrigerant in the evaporator (when the valve closes), which is a nonlinear function of the suction pressure. $\dot{Q}_e$ is the cooling capacity of the individual display case, which can be found by setting up the energy balance for the evaporator:

$$\dot{Q}_e = (T_{wall} - T_e) \cdot UA_{wall-ref}(M_{ref}) \tag{6.5}$$

The amount of liquid refrigerant in the evaporator M_{ref} follows a switched nonlinear dynamics governed by Eq. (6.4). It is assumed that the evaporator is filled instantaneously when the inlet valve is opened ($valve = 1 \Rightarrow M_{ref} = M_{ref,max}$). Furthermore, when the valve is closed ($valve = 0$) and all of the enclosed refrigerant has evaporated ($M_{ref} = 0$), then $\frac{dM_{ref}}{dt} = 0$. Figure 6.2 depicts the finite state machine for the state M_{ref}.

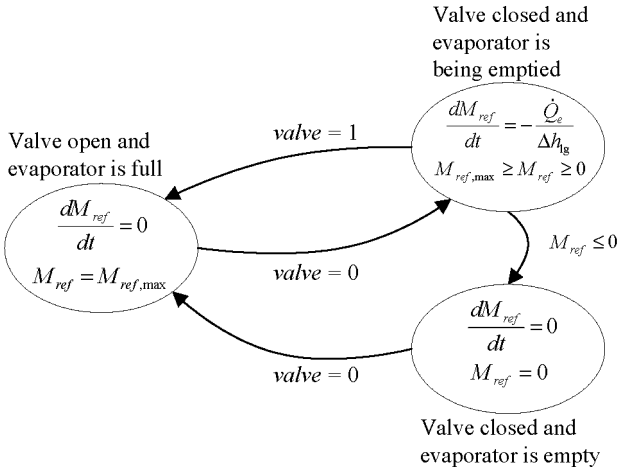

Figure 6.2: Finite state machine, describing the mass of refrigerant in the evaporator (M_{ref}).

When the refrigerant leaves the evaporator it flows on to the suction manifold. The mass flow out of the evaporator is given by:

$$\dot{m} = \begin{cases} \frac{\dot{Q}_e}{h_{oe} - h_{ie}} & \text{if } valve = 1, \\ \frac{\dot{Q}_e}{\Delta h_{ig}} & \text{if } valve = 0, \end{cases} \tag{6.6}$$

where h_{ie} is the inlet enthalpy which is a nonlinear refrigerant specific function of the condensing pressure and the subcooling and h_{oe} is the outlet enthalpy which is a nonlinear function of the suction pressure and the superheat.
Finally, the air temperature T_{air} can be found by setting up the energy balance for the air-curtain ($\dot{Q}_{air-wall} = \dot{Q}_{goods-air} + \dot{Q}_{airload}$). It is assumed that the heat capacity of the air is zero and that the temperature distribution in the air is uniform.

$$T_{air} = \frac{\dot{Q}_{airload} + T_{goods} \cdot UA_{goods-air} + T_{wall} \cdot UA_{air-wall}}{UA_{goods-air} + UA_{goods-air}}, \tag{6.7}$$

where $\dot{Q}_{airload}$ is an external heat load on the air-curtain from the surroundings.

The Suction Manifold
The dynamic in the suction manifold is modelled by two states, namely the density of the refrigerant in the suction manifold ρ_{suc} and the suction pressure P_{suc}. Setting up the mass and energy balance, and assuming an ideal gas, the corresponding state equations are obtained

$$\frac{d\rho_{suc}}{dt} = \frac{\dot{m}_{in-suc} - \dot{V}_{comp} \cdot \rho_{suc}}{V_{suc}}, \tag{6.8}$$

$$\frac{dP_{suc}}{dt} = R\frac{\dot{H}_{in-suc} - h_{out-suc}\dot{V}_{comp} \cdot \rho_{suc}}{C_v \cdot V_{suc}}, \tag{6.9}$$

$\dot{m}_{in-suc} = \sum_{i=1}^{n} \dot{m}_i$ is the total mass flow from the display cases and into the suction manifold, where $\dot{m}_i$ is the mass flow out of the i'th display case determined by Eq.(6.6) and n is the number of display cases. The "energy" flow in to the suction manifold is given by $\dot{H}_{in-suc} = \sum_{i=1}^{n} \dot{m}_i h_{oe,i}$, where $h_{oe,i}$ is the outlet enthalpy from the i'th display case. V_{suc} is the volume of the suction manifold, $\dot{V}_{comp}$ is the volume flow out of the suction manifold determined by the compressor(s), R is the gas constant for the refrigerant and C_v is the specific heat capacity.

The Compressor
In most refrigeration systems, the compressor capacity is discrete-valued, as compressors can be switched only either on or off. Let m denote the total number of compressors. The compressor bank is modelled using a constant volumetric efficiency η_{vol} and the maximal displacement volume V_d. Thus, the volume flow $\dot{V}_{comp,i}$ out of the suction manifold created by the i'th compressor can be determined as follows

$$\dot{V}_{comp,i} = comp_i \cdot \frac{1}{100} \cdot \eta_{vol} \cdot V_d \qquad i = 1, .., m \tag{6.10}$$

where $comp_i$ is the i'th compressor capacity, and $\dot{V}_{comp} = \sum_{i=1}^{p} \dot{V}_{comp,i}$ is the total volume flow.

By disregarding the dynamics of the condenser, a full model of the supermarket refrigeration system has now been attained. Summing up, the model of the suction manifold contains 2 states ($[P_{suc}, \rho_{suc}]$) and 3 inputs ($[\dot{V}_{comp}, m_i, h_{oe,i}]$). Each display case contains 3 states ($[T_{goods,i}, T_{wall,i}, M_{ref,i}]$), 2 inputs ($[P_{suc}, valve_i]$) and 1 disturbance ($[\dot{Q}_{airload,i}]$). To give an overview of the model the flowchart is depicted in Figure 6.3.

6.2.2 Linear Model

In the following we will linearize the nonlinear model derived above, such that display cases and the suction manifold can be described as an interconnection of linear hysteresis controlled subsystems i.e. according to Eq.(5.6)-Eq.(5.7).

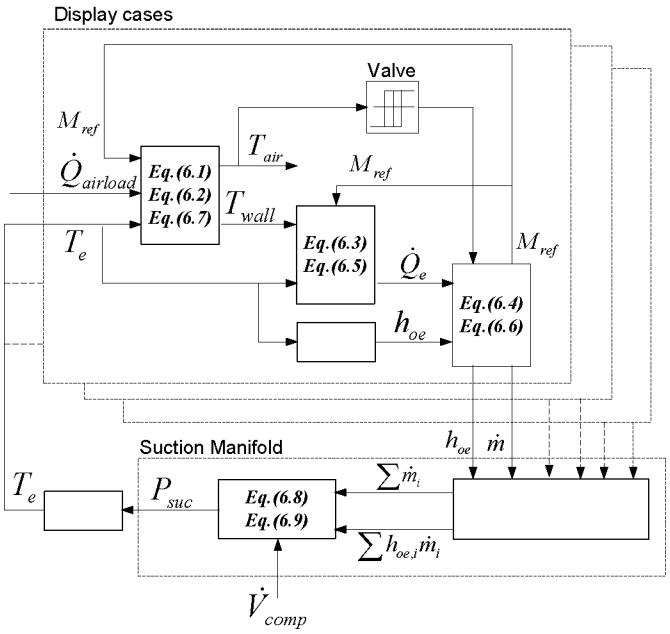

Figure 6.3: Flowchart for the nonlinear model of the supermarkets refrigeration system.

The Display Cases

The term describing the goods temperature (Eq.(6.1)) is linear, it is simply a low-pass filtering of the air temperature (T_{air}), therefore this expression is kept unchanged

$$\frac{dT_{goods}}{dt} = -\frac{UA_{goods-air}}{M_{goods} \cdot C_{p,goods}} \cdot (T_{goods} - T_{air}),$$

The equation describing the wall temperature (Eq.(6.2)) is on the other hand nonlinear, it contains a product of the two states T_{wall} and M_{ref}. By disregarding the cooling capacity of the enclosed refrigerant (when the inlet valve closes), the wall temperature can be described by following linear system:

$$\frac{dT_{wall}}{dt} = \frac{UA_{air-wall}}{M_{wall} \cdot C_{p,wall}} \cdot (T_{air} - T_{wall}) - \frac{\dot{Q}_e}{M_{wall} \cdot C_{p,wall}} \tag{6.11}$$

Disregarding the cooling capacity of the enclosed refrigerant in Eq.(6.11), means that the undershoot in the air temperature is not modelled. This "undershoot" is however important to capture when controlling the air temperature. By introducing $\delta \in \{0, 1\}$ to describe the valve action and a low-pass filtering of $\dot{Q}_e$, the emptying time of the

evaporator can be approximated by the filtering time-constant τ_{fil}:

$$\frac{d\dot{Q}_e}{dt} = \frac{1}{\tau_{fil}}(\delta \cdot (T_{wall,0} - T_e) \cdot UA_{wall-ref,max} - \dot{Q}_e) \tag{6.12}$$

It is assumed that cooling capacity ($\dot{Q}_e$) only depends on T_e, thus disregarding the dynamical influence of T_{wall}. $T_{wall,0}$ is therefore the constant "mean" wall temperature.
Finally by linearizing the evaporation temperature, the display case is transformed to a switched linear system. The dependence between T_e and P_{suc} can be approximated by a linear (affine) function. Linearizing around the normal point of operation ($P_{suc,0}$), the following expression for T_e can be obtained:

$$T_e = \frac{dT_e}{dP_{suc}}\Big|_{P_{suc}=P_{suc,0}} \cdot (P_{suc} - P_{suc,0}) + T_{e,0} \tag{6.13}$$

By inserting in Eq.(6.11) a switched linear model is obtained.
The air temperature is computed using Eq.(6.7), i.e.

$$T_{air} = \frac{\dot{Q}_{airload} + T_{goods} \cdot UA_{goods-air} + T_{wall} \cdot UA_{air-wall}}{UA_{goods-air} + UA_{goods-air}},$$

The Suction Manifold
Now if we study the equation describing the pressure in the suction manifold (P_{suc}) Eq.(6.9), it can be seen that it contains two nonlinear terms namely $\dot{H}_{in-suc}$ and $h_{out-suc} \cdot \dot{V}_{comp} \cdot \rho_{suc}$. Recall that ρ_{suc} is a state, $h_{out-suc}$ is a function of P_{suc} and $\dot{V}_{comp}$ is (indirectly) a control input.
If the outlet and inlet enthalpy are assumed identical and constant for all the display cases, i.e. $h_{oe,i} = h_{oe,0}$ and $h_{ie,i} = h_{ie,0}$, then by insertion of Eq.(6.6) (disregarding the emptying when the valve is closed), $\dot{H}_{in-suc}$ can be written as:

$$\dot{H}_{in-suc,0} = \frac{h_{oe,0}}{h_{oe,0} - h_{ie,0}} \sum_{i=1}^{n} \dot{Q}_{e,i}, \tag{6.14}$$

where T_e is determined by Eq.(6.13).
By assuming that the density of the refrigerant in the suction manifold ($\rho_{suc} = \rho_{suc,0}$) is constant, meaning that the state ρ_{suc} is truncated, and furthermore assuming that $h_{out-suc} = h_{out-suc,0}$ is constant the nonlinearities in Eq.(6.9) can removed.

$$\frac{dP_{suc}}{dt} = R\frac{\dot{H}_{in-suc,0} - h_{out-suc,0}\dot{V}_{comp} \cdot \rho_{suc,0}}{C_v \cdot V_{suc}}, \tag{6.15}$$

where $\dot{V}_{comp}$ is determined by Eq.(6.10).

Now writing the linearized (switched) system in a more compact form, the following can be obtained for a supermarkets refrigeration system consisting of n display cases

$$\begin{aligned} \dot{x}_1(t) &= A_1 x_1(t) + \delta_1(t) B_1 u_{sub}(t) + c_1, \quad y_1(t) = C_1 x_1(t) + d_1 \\ &\vdots \qquad\qquad\qquad\qquad\qquad\qquad \vdots \\ \dot{x}_n(t) &= A_n x_n(t) + \delta_n(t) B_n u_{sub}(t) + c_n, \quad y_n(t) = C_n x_n(t) + d_n, \end{aligned} \tag{6.16}$$

and for the suction manifold

$$\begin{aligned} \dot{x}_u(t) &= B_u u_{exo}(t) - B_\alpha \begin{bmatrix} x_1(t) \\ \vdots \\ x_n(t) \end{bmatrix} \\ u_{sub}(t) &= C_u x_u(t) + d_u \end{aligned} \tag{6.17}$$

where $x_i(t) = [T_{goods,i}, T_{wall,i}, \dot{Q}_{e,i}]^T$, $y_i = T_{air,i}$, $u_{sub} = T_{wall,0} - T_e$, $x_u = P_{suc}$ and $u_{exo} = \dot{V}_{comp}$. The system matrices can be found in Appendix D.
Finally by discretizing Eq.(6.16) - Eq.(6.17), the system is brought in the form of Eq.(5.6) - Eq.(5.7), i.e. an interconnection of linear hysteresis controlled subsystems. The linearized system therefore has a flowchart similar to the one depicted in Figure 5.7. To compare the nonlinear and the linearized model a simulation has been performed.

Component	Parameter	Value		Parameter	Value	
Display case	$UA_{goods-air}$	60	$[W/K]$	M_{goods}	400	$[kg]$
	$UA_{air-wall}$	360	$[W/K]$	M_{wall}	180	$[kg]$
	$UA_{wall-ref,max}$	900	$[W/K]$	$M_{ref,max}$	0.6	$[kg]$
	$C_{p,wall}$	385	$[\frac{J}{kg \cdot K}]$	τ_{fil}	40	$[sec]$
	$C_{p,goods}$	1000	$[\frac{J}{kg \cdot K}]$	$P_{suc,0}$	4	$[bar]$
	$\dot{Q}_{airload}$	900	$[W]$	$\rho_{suc,0}$	25	$[kg/m^3]$
				$T_{wall,0}$	0	$[^oC]$
Suction manifold	V_{suc}	5	$[m^3]$	R	85	$[\frac{J}{kg \cdot K}]$
	C_v	649	$[\frac{J}{kg \cdot K}]$			
Compressor	V_d	10	$[m^3/h]$	η_{vol}	0.8	
Refrigerant	Thermodynamical properties of $R404a$ Skovrup (2000)					

Table 6.1: Parameter values for the linear and nonlinear model. The parameters are approximated to achieve responses similar to real plants.

The air temperatures (T_{air}) has been controlled by hysteresis controllers and the compressor has been operated at a constant capacity (the used parameter values can be found in table 6.1).

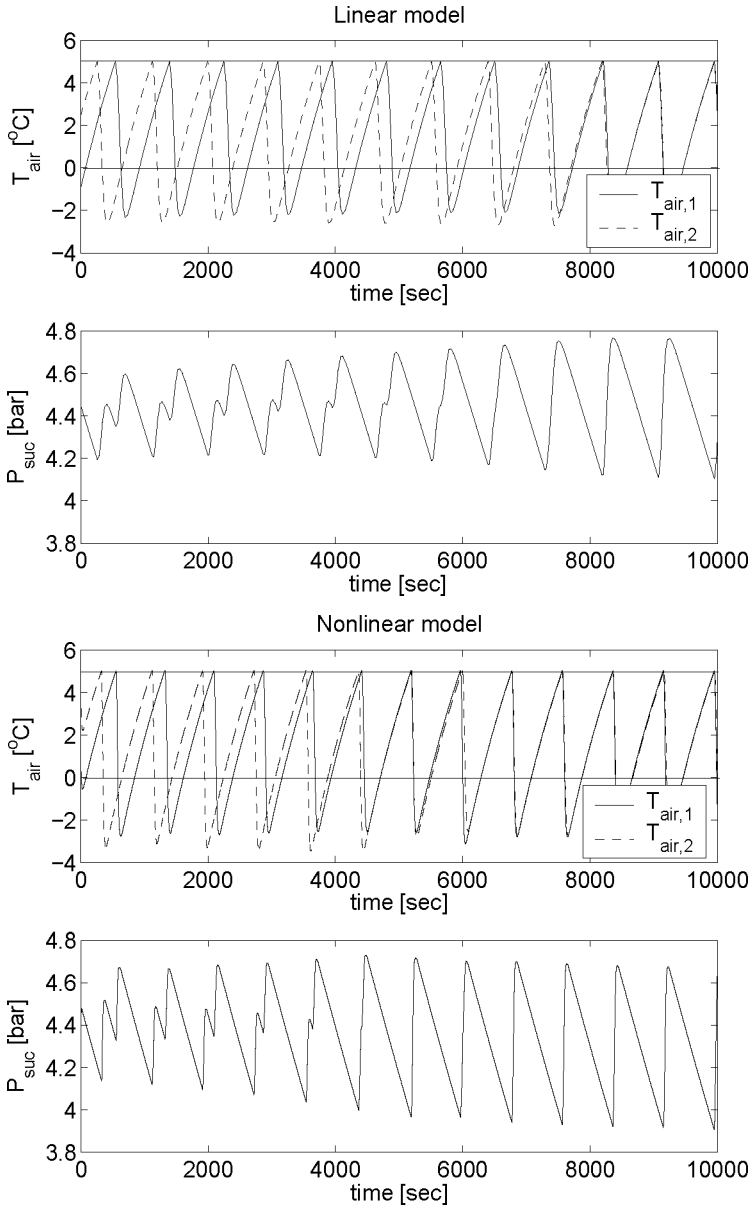

Figure 6.4: Simulation of the linear and nonlinear system with 2 hysteresis controlled display cases. The upper part of the plots depicts the air temperatures, where the horizontal lines illustrate the upper and lower bound in the hysteresis controllers. The lower part of the plots depicts the suction pressures.

As it can be seen the air temperatures have a certain undershoot. Recall this undershoot was caused by the enclosed refrigerant in the evaporator when the valve closes. For the linear system this undershoot is approximated by a low-pass filter. It can however be seen that the filtering also has an effect on the suction pressure as the variations are smoothend as well, thus reducing the tendency to synchronization. This will be discussed more in details below, however it can, in general, be seen that the linear model captures the effects of synchronization and most important, the resulting increased variations on the suction pressure.

6.3 Synchronization in Supermarkets Refrigeration Systems

In this section we will study more in detail the causes for synchronization in supermarkets refrigeration systems. In Chapter 5 we found that, besides the coupling structure, the coupling strength and the "natural" switching frequency is determinative for synchronization. By analyzing the parameters in the derived models we will try to find out, which parameters determines the coupling strength and the switching frequency.
The first precondition that we found should be fulfilled for the subsystems to synchronize, was that the interconnection digraph should be UQSC and that there should exist a feedback from at least one of the subsystems. If we study the flowchart of the nonlinear system, Figure 6.3, and the matching equations it can be seen that, when all the inlet valves are open ($valve = 1$), then the state P_{suc} in the suction manifold affects (via T_e) the states in all of the display cases. Hence, if there exists time intervals, where all of the valves have been open the system is UQSC. Furthermore it can immediately be seen that there exist a feedback from the display cases to the suction manifold ($\dot{m}_i$ and $h_{oe,i}$), i.e. the preconditions for synchronization is fulfilled. If the linearized system Eq.(6.16) - Eq.(6.17) is analyzed it can be found that the controllability matrix of A_i, $B_i C_u$ and the observability matrix of A_i, $B_{\alpha,i}$, both have $rank \geq 1$, i.e., according to findings in Chapter 5, the precondition for synchronization is fulfilled. Figure 6.4 depicts simulation results for two equal sized display cases, simulated on as well the nonlinear as the linearized system. The simulation clearly shows that both systems synchronize.
We found earlier that the coupling strength and the switching frequency where determinative for, whether the subsystems would synchronize. If we start by studying at the switching frequency in the display cases, it is obvious to see, that it is determined by the following:

- The size of $\frac{dT_{air}}{dt}$ when the inlet valve is open and closed respectively.
- The size of the undershoot in T_{air}.
- The range of the hysteresis bounds.

If we look at Eq.(6.1), Eq.(6.2) and Eq.(6.7), it can be seen that $\frac{dT_{air}}{dt}$ is determined by the two variables $\dot{Q}_{airload}$ and T_e, furthermore by parameters determining the heat transfer and heat capacity of the evaporator wall and the goods. These parameters are determined by the design of the display case and the properties of the stored goods. However the heat transfer from the evaporator wall to the air is in general much better, than from the goods to the air ($UA_{air-wall} > UA_{goods-air}$), this means that the dynamics in the display case largely is determined by its design and not by the contents of goods. In a supermarket many of the display cases are alike or designed based on the same guidelines, meaning that the parameters often are homogenous (for equally designed display cases are $UA_{air-wall}/M_{wall}$ and $UA_{wall-refrig}/M_{wall}$ approximately constant). Furthermore the display cases are located in the supermarkets sales area, where they are affected by approximately the same disturbances, i.e. $\dot{Q}_{air-load}$ and they are all operated at the same evaporation temperature T_e (or equivalently P_{suc}). This means that $\frac{dT_{air}}{dt}$ for all the display cases, when the inlet valves are opened and closed respectively, approximately are the same.
The size of the undershoot in T_{air} is determined by the capacity of the enclosed refrigerant in the display case, when the inlet valve is closed, i.e. $M_{ref,max}\Delta h_{lg}$, and the heat capacity of the evaporator wall. The heat capacity of the wall and the mass of the enclosed refrigerant is determined by the design of the evaporator. The latent heat Δh_{lg} is determined by the suction pressure, i.e. the lower P_{suc} the larger Δh_{lg}, which means that the undershoot gets larger when the suction pressure is low. The undershoot is therefore determined by design parameters, which where alike for the majority of display cases, and the current suction pressure, which is common for all the display cases.
In a supermarket the refrigerated goods can normally be divided into a few categories depending on the required storage temperature. This means that there would be various groupings of display cases containing goods that need to be preserved at similar temperatures. The preset hysteresis bounds for these display cases would be similar. The display cases in the supermarket can therefore be divided in a few groups operated with different hysteresis bounds. The display cases within the group are operated with similar bounds.
Summing up this means that a supermarkets system consists of groupings of display cases, where the display cases within the group operates with similar switching frequencies, but different in between the groups. This means that display cases within the groups has an enhanced risk of synchronizing. Furthermore connected to the refrigeration system, would typically be a couple of walk-in storage rooms that exhibits, in general, a much slower switching frequency caused by the lower heat load and much larger capacity of the air in the room.

We will now turn to study the coupling strength. If we look at the coupling matrix B_α in the linear model (see Appendix D), it can be seen that the coupling strengths are identical for all the display cases and independent of the design of the display cases. It

can however be seen that the volume of the suction manifold (V_{suc}) affects the coupling strengths. The smaller V_{suc} the higher coupling strength hence higher attraction to synchronization. However once the size of the suction manifold is given the attraction to synchronization is entirely be determined by the feedback from the display cases, i.e. $\dot{Q}_{e,i}$ (the applied cooling capacity in the display case). The larger $\dot{Q}_{e,i}$ the higher attraction to synchronization, meaning that display cases within a wider range of switching frequencies will synchronize. The size of $\dot{Q}_{e,i}$ depends on the size of the display cases, see Eq.(6.5), ($UA_{wall-ref}$ depends on the surface area of the evaporator), therefore will large display cases contribute more to synchronization than small display cases. However if a number of smaller display cases have synchronized, they will have the same effect as a large and therefore amplify the attraction synchronization.
Now if we study Eq.(6.5) it appears that the size of $\dot{Q}_{e,i}$ also depends on T_e and thereby on the suction pressure. So if the suction pressure is increased, then $\dot{Q}_{e,i}$ will be decreased and the attraction to synchronization will be decreased and vice versa. Figure 6.5 depicts a simulation, on the nonlinear system of the two display cases with slightly different hysteresis bounds, hence different "natural" switching frequencies. It can be seen that when the suction pressure is low ($\dot{Q}_{e,i}$ high), then the attraction to synchronization is high and the display cases synchronizes. After 4000 sec the suction pressure is increased from around 4.2 bar to 5.2 bar, $\dot{Q}_{e,i}$ is thereby lowered meaning that the attraction to synchronization is weakened. When the pressure reaches 5.2 bar the attraction is so weak that the difference in the natural switching frequency causes the display cases to stop synchronizing.

Other effects however turns out to play an important part in the attraction to synchronization for real supermarkets refrigeration systems. If the suction pressure is high then $\dot{Q}_{e,i}$ is low and the time it takes to bring the air temperature down will be longer. A limited positive disturbance in the suction pressure when the pressure is high, might even cause $\dot{Q}_{e,i}$ to be so low such that the air temperature in a group of display cases cannot be dragged down to the lower bound. The temperatures will therefore all coincide within a narrow temperature range in between the upper and lower bounds. Such a pressure disturbance could be caused by either switching a compressor off (if the suction pressure is controlled by discrete compressor capacities) or if a large subsystem such as a cold storage room is turned on. Nevertheless when the suction pressure eventually decreases again the group of displays cases will be synchronized. Furthermore if the suction pressure is controlled by a (discrete) number of compressors that can be turned on and off and the compressors starts to periodically switch on and off (initiated by synchronization of a coupled of display cases) the compressor will cause a periodical variation in the suction pressure, thus increasing the attraction to synchronization. The influence on the suction pressure caused by turning on another compressor in the compressor rack, depends however on the specific suction pressure. At high pressure, turning on another compressor initiates a larger pressure drop in the suction manifold than at low at pressure (at high pressure the density in the suction

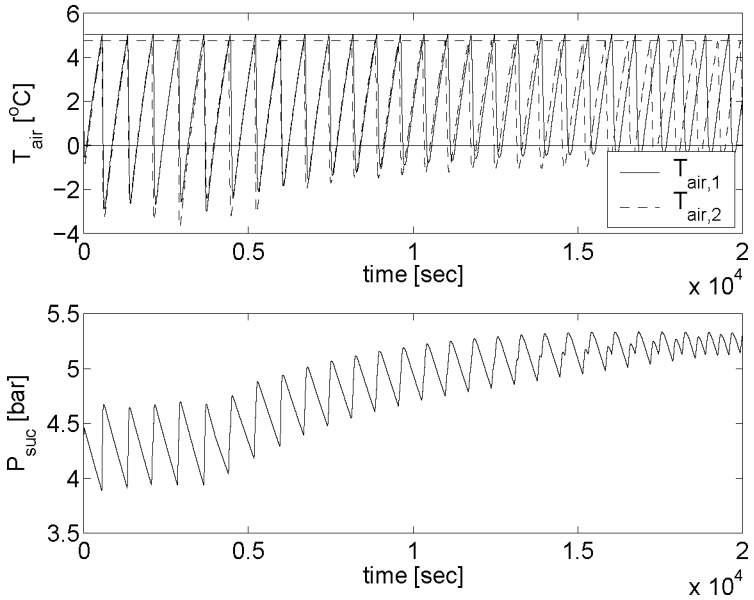

Figure 6.5: Simulation of the nonlinear system with respectively 2 hysteresis controlled display cases with slightly different hysteresis bounds. Increasing the suction pressure decreases the attraction to synchronization.

manifold is high, meaning that an increased volume flow out of the suction manifold caused by turning on an extra compressor, leads to a higher mass flow, hence larger pressure drop). Hence this points towards a lower attraction to synchronization a high pressures.
All in all it is hard to give an unambiguous description of how the *level* of suction pressure effects the attraction to synchronization. However it is clear that the variation on the suction pressure is important for the attraction to synchronization.

Now summing up, we found that the design parameters, the load from the surroundings and the suction pressure are alike for most of the display cases. Furthermore individual groupings of display cases will have similar hysteresis bounds, therefore the switching frequencies for those groups will be alike. We furthermore found that the size of the applied cooing capacity in the display cases ($\dot{Q}_{e,i}$), each time the inlet valve opens, are determinative for the attraction to synchronization. Furthermore we found that the variations on the suction pressure are important for the attraction to synchronization. All in all this substantiates that the conditions for synchronization are present in a supermarket system and the controllable parameters affecting synchronization is the suction pressure

and the hysteresis bounds.

6.4 Desynchronizing Control

In this section we will apply the, in Chapter 5, proposed desynchronizing control on the non-linear model of the supermarkets refrigeration system. In Section 6.2 we derived a switched linear model of a supermarkets refrigeration system, which we showed in Section 5.1.3 could be transformed into a MLD model (after discretizing) and applied in a MPC. However the control problem is slightly more complicated than the framework described in Section 5.1.3 as the exogenous control input is discrete-valued. Recall that the compressors in the compressor rack could either be turned on and off, thus creating discrete valued compressor capacities. We will therefore start by extending the MLD-model with these changes, such that it can be applied in the desynchronizing control scheme.

6.4.1 MLD-Model

In the following we transform the linearized model Eq.(6.16) and Eq.(6.17) into a MLD-form, according to the representation given by Eq.(5.16), introduced in Chapter 5. However some changes is incorporated beforehand.
In the framework introduced in Chapter 5, the exogenous input (u_{exo}) to the interconnected systems Eq.(5.6) - Eq.(5.7) was assumed to be continuous. The input to the refrigeration system is however discrete-valued, as the compressor rack consist of m capacities that can switch *on* and *off*. If we study Eq.(6.15) then the nonlinearity $h_{out-suc} \cdot \dot{V}_{comp}$ was removed by assuming that $h_{out-suc}$ was constant ($h_{out-suc}$ is a function P_{suc}). A better approximation of the nonlinear model can be achieved if $h_{out-suc}$ is linearized instead.

$$h_{suc-out} = \left.\frac{dh_{suc-out}}{dP_{suc}}\right|_{P_{suc}=P_{suc,0}} \cdot (P_{suc} - P_{suc,0}) + h_{suc-out,0}, \tag{6.18}$$

This introduces the bilinear term, $P_{suc} \cdot \dot{V}_{comp}$ in Eq.(6.15). However if we let $\delta_{comp,i} \in \{0, 1\}$ denote whether the i'th compressor capacity is turned *on* or *off* then Eq.(6.15) can be rewritten as:

$$\begin{aligned}\frac{dP_{suc}}{dt} =& [b_{u,1}\dot{V}_{comp,1}, ..., b_{u,1}\dot{V}_{comp,m}] \begin{bmatrix} \delta_{comp,1} \\ \vdots \\ \delta_{comp,m} \end{bmatrix} - B_\alpha \begin{bmatrix} x_1 \\ \vdots \\ x_n \end{bmatrix} \\ &+ [b_{u,3}\dot{V}_{comp,1}, ..., b_{u,3}\dot{V}_{comp,m}] \begin{bmatrix} \delta_{comp,1}P_{suc} \\ \vdots \\ \delta_{comp,m}P_{suc} \end{bmatrix}\end{aligned} \tag{6.19}$$

where

$$\begin{aligned} b_{u,1} &= -R\frac{h_{out-suc,0} - \frac{dh_{suc-out}}{dP_{suc}} \cdot P_{suc,0} \cdot \rho_{suc,0}}{C_v \cdot V_{suc}} \\ b_{u,3} &= -R\frac{\frac{dh_{suc-out}}{dP_{suc}} \cdot \rho_{suc,0}}{C_v \cdot V_{suc}}, \end{aligned} \tag{6.20}$$

By discretizing Eq.(6.19) it can be transformed into a MLD-form. Note however that the procedure of replacing the δP_{suc}-value with an auxiliary variable z in continuous-time, causes a change in the model-structure when the system is discretized. To avoid this further complication Eq.(6.19) is assumed to be discretized using a forward Euler approximation, which preserves the structure of the continuous-time model in discrete-time. Choosing a suitable sampling time T_{samp} is however difficult, as the switched dynamic in the display case exhibit greatly differing time constants. Specifically, the decrease of T_{air} when the valve is open is significantly faster than the increase when the valve is closed. To avoid long prediction horizons (in terms of steps) in the MPC, a long sample time needs to be chosen. In general, however, this implies that the valve should be opened for *less* time than the sampling interval in order to bring the temperature down from the upper to the lower temperature bound without excessive undershoot. The necessary additional flexibility is achieved by introducing the intermediate opening time t_{open} as a continuous-valued control input which allows one to vary the opening *time* of the valve within the sampling interval. This behavior is well approximated by introducing t_{open} as a variable that varies the opening *degree* of the valve, i.e. rewriting Eq.(6.12) we get:

$$\frac{d\dot{Q}_e}{dt} = \frac{1}{\tau_{fil}}(\delta\frac{t_{open}}{T_{samp}} \cdot (T_{wall,0} - T_e) \cdot UA_{wall-ref,max} - \dot{Q}_e) \tag{6.21}$$

where T_{samp} is the intended sample time (the system is still in continuous-time). This however introduces the nonlinearity $\delta \cdot t_{open} \cdot (T_{wall,0} - T_e)$. Recall that $T_{wall,0} - T_e$ in the linear model Eq.(6.16), is the input to the subsystems (u_{sub}). If $u_{sub,0} = T_{wall,0} - T_{e,0}$ is assumed constant, then the remaining nonlinearity ($\delta \cdot t_{open}$) can be substituted by a set of MI-inequalities, as follows:

$$\begin{aligned} &\frac{d\dot{Q}_e}{dt} = \frac{1}{\tau_{fil}}(\frac{t_{open}}{T_{samp}} \cdot (T_{wall,0} - T_{e,0}) \cdot UA_{wall-ref,max} - \dot{Q}_e) \\ &\text{subjected to} \\ &\quad t_{open} \leq \delta T_{samp} \\ &\quad t_{open} \geq 0 \end{aligned} \tag{6.22}$$

By applying the changes (Eq.(6.19) and Eq.(6.22)) to the linearized system (Eq.(6.16) and Eq.(6.17)) following is obtained:

$$\begin{aligned}
\dot{x}_1(t) =& A_1 x_1(t) + t_{open_1}(t) B_1 \frac{u_{sub,0}}{T_{samp}} + c_1, \quad y_1(t) = C_1 x_1(t) + d_1 \\
&\vdots \qquad\qquad\qquad\qquad\qquad\qquad \vdots \\
\dot{x}_n(t) =& A_n x_n(t) + t_{open_n}(t) B_n \frac{u_{sub,0}}{T_{samp}} + c_n, \quad y_n(t) = C_n x_n(t) + d_n, \\
\dot{x}_u(t) =& [b_{u,1} V_{comp,1}, ..., b_{u,1} V_{comp,m}] u_{exo}(t) \\
&+ [b_{u,3} V_{comp,1}, ..., b_{u,3} V_{comp,m}] z(t) - B_\alpha \begin{bmatrix} x_1(t) \\ \vdots \\ x_n(t) \end{bmatrix} \\
u_{sub}(t) =& C_u x_u(t) + d_u
\end{aligned} \tag{6.23}$$

subjected to a set of MI-inequalities,

where $x_i(t) = [T_{goods,i}, T_{wall,i}, \dot{Q}_{e,i}]^T$, $y_i = T_{air,i}$, $u_{sub} = T_{wall,0} - T_e$, $x_u = P_{suc}$ and $u_{exo} = [\delta_{comp,1}, ..., \delta_{comp,m}]^T$ and $z = [\delta_{comp,1} P_{suc}, ..., \delta_{comp,m} P_{suc}]^T$. The system matrices are given by Eq.(6.20) and Appendix D. Recall that when the discretization of Eq.(6.23) is performed subsequently, the state x_u is assumed discretized using an Euler approximation, thus maintaining the system structure.

Now if we look at the system Eq.(6.23), then it can be seen that the system is no longer UQSC as the input to the subsystems u_{sub} are assumed constant. The system will therefore not synchronize by itself. At first glance this seems to be a serious problem with the model, however recall that the model is meant to be used in a MPC framework, which means that the initial states are updated with measurements at every time-instance. Furthermore $u_{sub,0}$ will be updated at every time-instance (it will however be constant during the N-step prediction). This means that if the real system synchronizes, then the MLD model will as well. The effects of synchronization *is* captured by the MLD model, which means that if the real system and thereby also the MLD model synchronizes, it will cause large variations on the predicted variable u_{sub}. Therefore if the objective function penalizes variations on u_{sub} from its reference, then it will be optimal to desynchronize the operation of the subsystems.

By discretizing the system Eq.(6.23) it can be transformed into a MLD-form according to Eq.(5.16), where $x_i(t) = [x_1, ..., x_n, x_u, u_{exo}(k-1)]^T$, $y = [y_1, ..., y_i, u_{sub}, \Delta u_{exo}]$, $u = [\delta_1, t_{open,1}, ..., \delta_n, t_{open,n}, u_{exo}]^T$ and $z = [\delta_{comp,1} P_{suc}, ..., \delta_{comp,m} P_{suc}]^T$. Summing up this means that a refrigeration system consisting of n display cases and controlled by m discrete compressor capacities will result in a MLD model of the size indicated in table 6.2

Variable	Size	
	real	binary
x	$3 \cdot n + 1$	m
u	n	$n + m$
z	m	0
δ	0	0

Table 6.2: Size of the MLD model for a refrigeration system consisting of n display cases and controlled by m discrete compressor capacities.

6.4.2 Implementation on a Refrigeration System

In the following we will test the desynchronizing scheme on the nonlinear model of a supermarket refrigeration system. We will focus on a system consisting of two display cases and two equal sized compressors with the discrete capacities $comp_1 \in \{0, 50\}$ and $comp_2 \in \{0, 50\}$. The parameters used in the model can be found in Table 6.1. The input vector is defined as $u = [\delta_{valve,1}, t_{open,1}, \delta_{valve,2}, t_{open,2}, \delta_{comp,1}, \delta_{comp,2}]^T$, the state vector is defined as $x = [T_{goods,1}, T_{wall,1}, \dot{Q}_{e,1}, T_{goods,2}, T_{wall,2}, \dot{Q}_{e,2}, P_{suc}, \delta_{comp}]^T$, where $\delta_{comp} = \delta_{comp,1} + \delta_{comp,2}$. The output vector as $y = [T_{air,1}, T_{air,2}, P_{suc}, \Delta comp]^T$, where $\Delta comp = 50(\Delta\delta_{comp})$. Note that the $\Delta comp$ formulation will be needed in to penalize the switching of the compressor, as described in Section 5.3. Notice furthermore that by adding the summed compressor switches to the state-update instead adding them individually, the number of states can be reduced by $m - 1$ where m is the number of discrete compressor capacities.
The sampling interval is $T_{samp} = 60$ sec. In order to accommodate the fact that, it on a real plant takes a while to fill the evaporator after opening the valve, a lower bound on t_{open} is introduced. It is assumed that it takes 10 sec to ensure that the evaporator is completely filled, i.e. we set $t_{open} \in [10, 60]$.
The procedure in Section 6.4.1 yields an MLD system with 8 states (7 states from the system and 1 additional state for $\delta_{comp}(k-1)$), 2 z-variables, 4 binary-variables and 52 inequality constraints (see also table 6.2). The derivation of the MLD system is performed by the compiler HYSDEL, the code can be found in Appendix C.

6.4.2.1 Control Objectives

The control objectives are to bring the suction pressure P_{suc} close to its reference value at $P_{suc,ref} = 4.2$ bar ($\sim T_e = -10^oC$) with little variance, while fulfilling the soft con-

straints[1] on the air temperatures in the display cases $T_{air} \in [0, 4]$, and while switching the compressors as little as possible in order to minimize wear. Switch transitions in the inlet valves of the display cases are by far less critical concerning wear. Furthermore in some cases, it is desired that the air temperature has the zigzag behavior as experience indicate that this gives a more compact icing on the evaporator improving the heat transfer and giving a uniform temperature distribution across the display case, as mentioned earlier. The air temperature has been constrained softly for two reasons firstly it is not crucial that the temperature stays within the bounds at all time, secondly it improves feasibility of the CFTOC problem (Eq.(6.25)) as it expands the feasible set.
Here, an objective function is used that penalizes with the ∞-norm over a finite horizon the following three terms. (i) the deviation of the suction pressure P_{suc} from its reference, (ii) the switching of the manipulated variables (the compressor and valve control actions) and (iii) the violation of the soft constraints on T_{air}. The control law is then obtained by minimizing the objective function subject to the evolution of the MLD model and the physical constraints on the manipulated variables. As we are using the ∞-norm, this minimization problem amounts to solving a MI-LP.
According to Section 5.3 and the above formulated objectives, the following optimal control problem is considered:

$$\min_{u(0),..,u(N-1)} J = \sum_{k=0}^{N-1} \left(\|u(k)\|_{Q_1}^{\infty} + \|y(k) - y_{ref}(k)\|_{Q_2}^{\infty} \right) \tag{6.24}$$

$$+ p \cdot \sum_{k=1}^{N-1} \left(\underline{S}(k) + \overline{S}(k) \right) \tag{6.25}$$

subject to the evolution of the MLD model computed from Eq.(6.23) over the prediction horizon N and taking into account the discrete-valued nature of some of the manipulated variables ($\delta_{valve,i}$ and $\delta_{comp,j}$).
The deviation of P_{suc} from its reference is weighted by $Q_2 = diag(Q_{Tair}, Q_{Psuc}, Q_{\Delta comp})$. To ensure only small variations in P_{suc} a large weight is chosen, i.e. $Q_{Psuc} = 500$. Recall that step changes in the compressor capacity have a magnitude of 50 ($comp \in \{0, 50, 100\}$). To avoid compressor switching when the suction pressure lies within a reasonable dead band of ± 0.2 bar, we set $Q_{\Delta comp}$ to 2. Thus, switching a compressor on or off costs $2 \cdot 50 = 100$, and the deviation in P_{suc} has to amount to $\frac{100}{500} = 0.2$ bar before a change in the compressor capacity is initiated.
The weight matrix on the manipulated variables is given by $Q_1 = diag(q_1, q_2, q_3, q_4, q_5, q_6)$. Assuming that it is 100 times less expensive (in terms of wear) to open the valves than to change the compressor capacity, we set the weights on $\delta_{valve,1}$ and $\delta_{valve,2}$ to $q_1 = q_3 = \frac{100}{100} = 1$. The rest of the weights are set to small

[1] A soft constraint means; that the variable is penalized heavily if it crosses the constraint, it however remains feasible in contrast to a hard constrained variable

positive values > 0.
The soft constraints on the temperature bounds are taken into account by introducing slack variables for the upper $\overline{S}$ and the lower $\underline{S}$ bounds and a large penalty, $p = 10^4$.

6.4.3 Simulation Results

This section presents control experiments simulated on the nonlinear model described in Section 6.2.1. To illustrate the performance improvements that can be achieved by using a desynchronizing MPC scheme, the control performance resulting from a traditional controller (as described in Section 6.1.2) is compared with the desynchronizing MPC scheme. To illustrate the problems that often arise with the traditional control scheme, we have chosen a refrigeration system with two equally sized display cases that have a pronounced tendency for synchronization.
The traditional controller comprises a hysteresis based temperature controller with $[T_{lower}, T_{upper}] = [0, 4]$ and a PI-type suction pressure controller with a dead band of ± 0.2 bar around the reference of 4.2 bar. The MPC uses a horizon of $N = 10$. The prediction horizon is chosen such that it approximately corresponds to one switching period.

The lower part of Figure 6.6 depicts the air temperatures in the two display cases when using the traditional control scheme. Initially, the two temperatures exhibit an offset which vanishes within the first hour due to the attraction to synchronization described in Section 6.3. When the valves of the display cases get synchronized it leads to large variations in the suction pressure as shown in the lower part of Figure 6.7. As depicted in Figure 6.8, the compressor controller tries in vain to suppress these variations when they exceed the dead band of ± 0.2 bar causing excessive switching and wear. Unless something is done to de-synchronize the valves, they will remain synchronized.
The upper part of Figure 6.6 shows the temperatures in the display cases when employing the desynchronizing MPC. The two temperatures coincide in the beginning and the valves are thus synchronized. However, after only 20 min, the switching of the valves is de-synchronized, resulting in smaller variations in the suction pressure as can be seen in the upper part of Figure 6.7. These reduced variations not only result from the de-synchronization, but also from the significantly reduced undershoot in the air temperatures[2]. The traditional controller fails to respect the lower bound as it cannot predict the undershoot in contrast to MPC. By predicting the undershoot, the cooling capacity of the enclosed refrigerant in the evaporator plus the capacity "stored" in the evaporator wall is included, the energy consumption is thereby reduced, as the mean air temperature is increased (within the bounds). Finally, as can be seen in Figure 6.8, the large penalty on the compressor switching reduces the number of switch transitions considerably with respect to the traditional control scheme. By counting the number of switches

[2]The small undershoot in T_{air} for MPC, despite the soft constraints, is mainly caused by the coarse sampling.

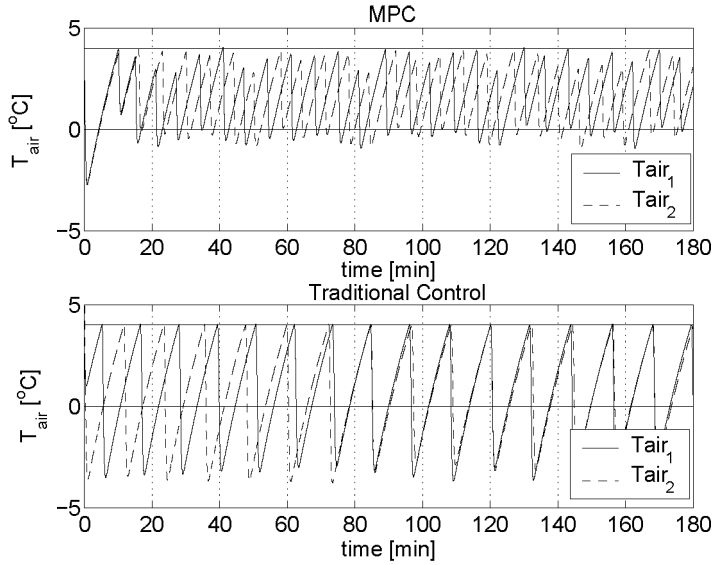

Figure 6.6: T_{air} in the 2 display cases, controlled respectively with the desynchronizing MPC and a traditional hysteresis controller.

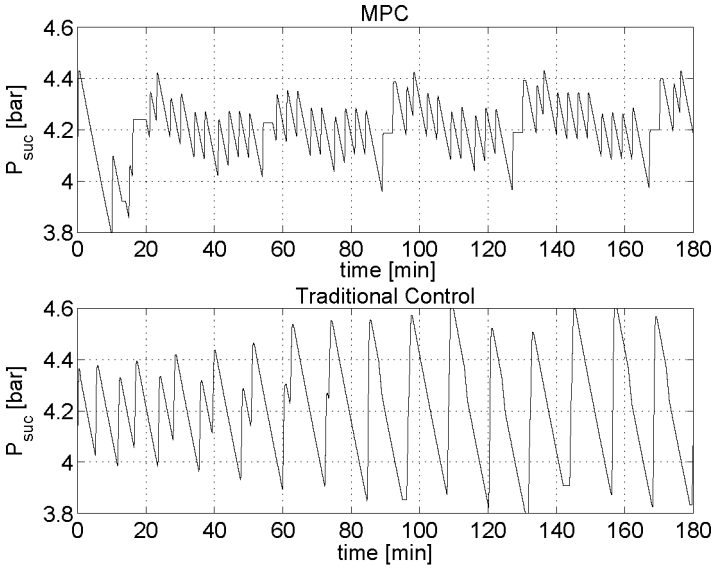

Figure 6.7: P_{suc} in the suction manifold, controlled respectively with the desynchronizing MPC and a traditional PI controller with a dead band on ± 0.2 bar.

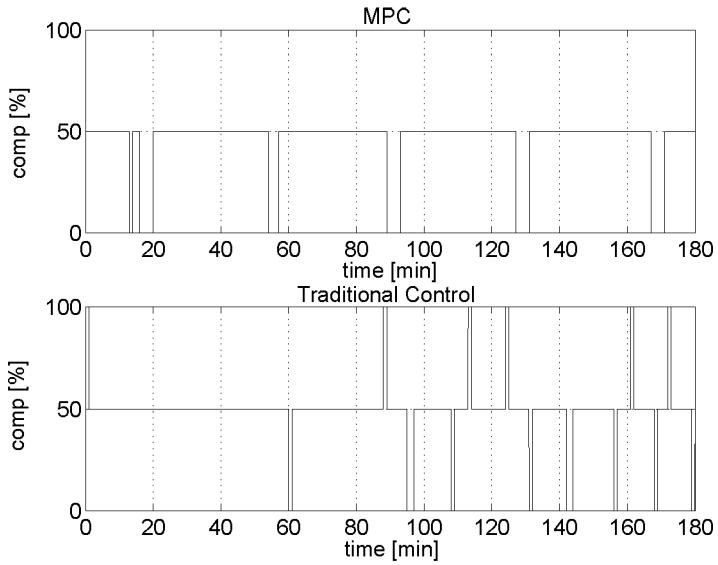

Figure 6.8: The compressor control input $comp$ (compressor capacity) using respectively the desynchronizing MPC and a traditional PI controller with a dead band on ± 0.2 bar.

after 100 min, where a steady operation is reached for both systems, it can roughly be seen that the number of steps is reduced by a factor 5.
To solve the optimal control problem online at each time step, CPLEX 9.0 was run on a Pentium IV 2.0 GHz computer. For $T_{samp} = 1$ min and a horizon of $N = 10$, the computation time is in average 3.9 sec and always less than 9.7 sec rendering an online implementation of the MPC scheme computationally feasible that is for a system consisting of two display cases. Extending the case study to larger systems is conceptually straight forward, however the method is limited by the fact that a MI-LP has to be solved, hence the complexity grows with the size of the system and thereby also the required computation time. Furthermore the switches are bounded to take place on samples and cannot occur in between samples, hence the switching is limited to a few restricted time instances, which limits the obtainable performance especially if a larger systems are considered. For systems larger systems initiatives therefore must be taken to decompose the optimization problem into a number of smaller problems, e.g. by grouping the display cases into fewer subsystems. However in that case a performance decay must be anticipated, as this would result in a sub-optimal solution. Finally, if needed, the explicit piecewise affine state feedback controller might be derived by pre-solving the optimal control problem offline for all states. This method is however by far limited more by the complexity of the problem.

6.5 Conclusion Part II

In the second part of the thesis dynamical optimizing control for refrigeration systems was considered. Firstly the phenomenon of synchronization in distributed control systems consisting of a number of interconnected hysteresis controlled subsystems was studied. Secondly a control scheme that desynchronizes the operation was proposed. In supermarket refrigeration systems synchronization turns out to cause a severe degradation in the control performance. Motivated by this the proposed desynchronizing control scheme was applied on a supermarket refrigeration system. In the following the main conclusion are drawn based on the accomplishments and contributions of Part II.

- In Chapter 5 a novel description of the phenomenon of synchronization of coupled hysteresis controlled subsystems was introduced. Here we studied the causes and effects of synchronization in a simple interconnected linear system consisting of a number of coupled hysteresis controlled subsystem. We found that the attraction to synchronization heavily depends on the feedback from the subsystem; the larger the feedback the higher attraction to synchronization, that is however if the feedback is negative. If on the other hand feedback is positive it turns out that the subsystems desynchronize. By introducing coupling strengths we found that even if the undisturbed switching frequencies in the subsystems are not alike, they will synchronize, if the coupling strength is sufficiently high. We furthermore found that there, in general, are two equilibriums; a stable where the subsystems are synchronized and an unstable where they are desynchronized. By utilizing this discovery we proposed a desynchronizing feedback control law, that changes the sign of the feedback, hence stabiles the unstable equilibrium and thus desynchronizes the operation of the hysteresis controlled subsystems.
  By studying recent work for synchronization of coupled continuous nonlinear systems, we found that many of the findings for the coupled hysteresis controlled systems are alike. An example of two coupled nonlinear oscillators exhibited the same dependency of the coupling strengths and also turned out to have two equilibria; a stable where the oscillators are synchronized and an unstable where they are exactly desynchronized. Furthermore this work brought the attention to the importance of the interconnecting structure, as this is a crucial precondition for synchronization to occur. We showed that the interconnecting digraph for the introduced structure of the coupled hysteresis controlled subsystems (Eq.(5.6) - Eq.(5.8)) under certain conditions fulfilled the precondition to the interconnecting structure.

- In Section 5.1.3 a general discrete-time framework for coupled hysteresis controlled subsystems was introduced, Eq.(5.6) - Eq.(5.8). In Section 5.3 a novel approach for desynchronization was proposed. The idea is to formulate a CFTOC

problem based on the introduced discrete-time framework, that penalizes the effects of synchronization hard. The CFTOC is employed in an MPC scheme, hence solved at each time-instance. The hereby computed optimal control sequences, thus minimize the variance on the resulting effects of the feedback from the subsystems (u_{sub}), using a minimal exogenous control effort (Δu_{exo}). The manipulatable control inputs are assumed to be the switches in the subsystems and the exogenous control input.

- In Chapter 6 we derived a linear model of a supermarket refrigeration system, that has the same structure as the introduced general linear hysteresis control system (Eq.(5.6) - Eq.(5.8)). We showed by analyzing the model, that the connection structure fulfilled the preconditions for synchronization. By studying respectively a nonlinear and the linear model, we found that the parameters determining the "natural" switching frequency, in general, are alike for a majority of the display cases. Furthermore since the display cases all are located in the supermarket sales area and they all operates at the same evaporation pressure ($\sim$ suction pressure) the operational conditions are alike. Finally groups of display cases containing goods requiring similar storage temperatures, are operated with the same hysteresis bounds. All in all a supermarket refrigeration system consists of various groups of display cases operating at similar switching frequencies, thus increasing the risk of synchronization.
  By studying the linearized model we found that the coupling strengths are similar for all of the display cases, however the size of the feedback is not. This indicated that large display cases contribute more to synchronization, furthermore that if a number of display cases has synchronized they attract other display cases within wider range of switching frequency to synchronize as well. We furthermore found that the size of the applied cooling capacity in the display cases ($\dot{Q}_{e,i}$), each time the inlet valve opens, are determinative for the attraction to synchronization. Furthermore the variations on the suction pressure e.g. caused by a stepwise control of the compressor capacities are important for the attraction to synchronization. All in all we substantiated that the preconditions for synchronization are present in a supermarket system, and that the controllable variables affecting synchronization is the suction pressure and the hysteresis bounds.

- The linearized model of the supermarket refrigeration system described in Section 6.2.2 was cast into the MLD form. The result is a hybrid model of low complexity that is sufficiently accurate to serve as a prediction model for the desynchronizing MPC-scheme and which is computationally tractable.
  The case study of a supermarket refrigeration system illustrated the performance limitations of traditional control schemes and furthermore proved that the proposed desynchronizing MPC was able to desynchronize the operation of the display cases, taking into account the interactions between the display cases and the compressor, respecting the temperature constraints, minimizing the variations in

the suction pressure, and reducing the switching in the compressor bank. This led to a lower wear in the compressor and a higher energy efficiency of the supermarket refrigeration system. The design and tuning of the cost function was easy and intuitive, and the extension of the case study to larger refrigeration systems is conceptually straightforward. However the method is limited by the fact that a MI-LP has to be solved, hence the complexity grows with the size of the system and thereby also the required computation time. Furthermore coarse sample instances limits obtainable performance especially for larger systems, as the switching is bounded to take place on samples.

Chapter 7

Discussion and Recommendations

In this thesis system optimizing control of refrigeration systems were considered. The optimizing control was divided into two layers namely a set-point optimizing layer and a dynamical optimizing layer. New approaches within both areas were presented and tested on respectively a dedicated refrigeration test rig and as a case study on a supermarkets refrigeration model. The conclusions for each of these two parts can be found at the ending of Part I and II and will therefore not be restated here. In the following we will discuss the obtained results and finally a number recommendation for further research will be given.

7.1 Discussion and Perspectives

The vision behind starting up this project was the idea of incorporating more "intelligence" in the control of refrigeration systems. One way of incorporating "intelligence" is to make use of mathematical models in the control. By incorporating the models directly in the control system the "stored information" in the models becomes available for the control system at all time. But how to handle all this information and how can consistent control actions be computed based on this? Furthermore in the future refrigeration systems it is likely that "softer" qualities will be asked for in the control system. For example how is the refrigeration system controlled such that the right food quality is obtained? This might be a question of balancing moist, temperature and light, quantities that cannot be controlled individually and not all directly. Moreover the right food quality is perhaps obtained by balancing cost of operation with the length of the shelf life. Nevertheless the problem is to figure out the right control action based on the available

information of the past, the present and the future such that the objectives are complied with best possible while meeting the system limitation. A structured way of dealing with this is to pose the problem as an optimization problem; by putting a "price" on the individual objectives, the control action that results in the "cheapest" operation can be computed. Though the optimization problem can be solved there is still a huge challenge in developing models that comprises these "soft" qualities as well static as dynamical.
This project has contributed to the process of integrating more "intelligence" in the refrigeration control systems, i.e. by moving towards a system optimizing control. In this thesis we have structured the optimization in two layers separated by difference in dynamics, i.e. a set-point optimizing layer and a dynamical optimizing layer.
In the first part of the thesis, concerning set-point optimizing control, a novel method is proposed. In the development of the method the focus has been on deriving a simple and general method, that with ease can be applied on various compositions of the same class of systems, such as refrigeration systems. The method was applied for minimization of energy consumption in refrigeration systems, however the generality of the method allows other steady state objectives to be optimized as well. This could be objectives aligned with what was mentioned above, such as optimizing food quality or ultimately economical goals, i.e. maximizes profit. Nevertheless different complexity levels in the implementation of the method can be imagined. A simple implementation can be one that only includes the constrain satisfaction possibly combined with the LTA control scheme and a complex can be one that includes several objectives as those mention above and furthermore accommodates changes in system parameters.
In the second part of this thesis, covering dynamical optimization, the main emphasis is laid on analyzing the phenomena of synchronization of hysteresis controlled subsystems. A method for desynchronization based on a model predictive control setup is proposed. The method was applied for desynchronization of the two hysteresis based temperature controllers in a supermarkets refrigeration system. It was hereby possible to improve the energy efficiency and minimize the wear. Extending this case study to larger systems is conceptually straight forward, however the method is limited by the growing complexity and thereby also the required computation time. For larger systems simplification therefore must be made to make it practically feasible. Though this method might not be practically feasible for commercial systems at present, the development of as well optimization algorithms and speed of processors, might make it feasible in the future. Nevertheless the proposed method for desynchronization and the preliminary analysis of synchronization has contributed to the understanding of the problem, given a benchmark for potential performance improvement and contributed to a number of patent applications (Larsen and Thybo (2004*a*) and Thybo (2005)).

7.2 Recommendation

In the following section recommendations and ideas for future work and research is stated.

- An interesting aspect for further research of the in Chapter 3, proposed optimization method, is the question of stability. It would be interesting to determine how much slower than the system dynamics, the steady state optimization should be, for the optimization to converge. Furthermore to investigate how the parameter adaption affects the shape of the cost function, i.e. what are the allowable bounds for the variation in the parameter adaptation and how much slower than the steady state optimization should the parameter adaptation be to insure convergence?
- In Chapter 3 a method, for set-point optimization taking systems constrains in to account, was proposed. It would be interesting to see how effective the optimizing scheme would be to uphold operational feasibility under extreme conditions in practice.
- Other objectives than energy consumption could be taken into account in the set-point optimization e.g. defrosting of evaporators, food quality, shelf life, maintenance, failures etc., however in that case a more appropriate common measure of cost could be in terms of money. For example what is the price of a reduced shelf life versus the profit of a reduced energy consumption? Nevertheless before such set-point optimization can be introduced, there is a huge challenge in deriving new models that describe the dependency between set-points and objectives.
- In Chapter 5 dynamical optimization was considered especially synchronization of coupled hysteresis controlled subsystems. In (Lin *et al.* (2005*a*)) a theorem for synchronization in coupled nonlinear systems with *time* dependent interconnecting structures is stated, it would be interesting to investigate whether this theorem could be expanded to cover systems with *state* dependent interconnecting structure. Hereby a larger class of hybrid systems could be considered including hysteresis controlled systems.
  It would furthermore be interesting to investigate whether a more constructive theorem could be developed for oscillating systems, that describes a relation between the coupling strength and the difference in frequencies for when synchronization would occur.
- In Chapter 5 we saw that the complexity of the MLD models is highly depended on how the system and control problem is stated. It would be interesting to investigate whether automated methods for generating minimal representations of MLD models in terms of the number of booleans, could be developed.
- In Chapter 6 the desynchronizing MPC was tested on a small scale supermarkets refrigeration system, however for larger system the complexity grows. It would

therefore be interesting to investigate how the system model could be simplified further and how the optimization problem could be sectioned into a number of less complex parallel subproblems, that could be solved either on- or off-line.

- The use of hysteresis control in the display cases is motivated mainly by two points, it ensures an uniform temperature distribution in the display cases and causes a less harmful frost build up on the evaporators. However if the frost build up and temperature distribution in the display case could be modelled, continuous valued control schemes that would not lead to synchronization could be developed. The modelling would properly lead to a set of partial differential equations, it could therefore be interesting to investigate how to control not a point temperature but a temperature distribution in a thermal system such as in a display case.

Bibliography

Åström, K. J. and B. Wittenmark (1989). *Adaptive Control*. Addison-Wesley.

Bemporad, A. (1997). Reference Governors: On-line Set-Point Optimization Techniques for Constraint Fulfillment. PhD thesis. Universit'a di Firenze. Firenze.

Bemporad, A. and M. Morari (1999). Control of Systems Integrating Logic, Dynamics and Constraints. *Automatica* **35**(3), 407–427.

Bemporad, A., M. Morari, V. Dua and E.N. Pistikopoulos (2002). The Explicit Linear Quadratic Regulator for Constrained Systems. *Automatica* **38**(1), 3–20.

Boyd, S. and L. Vandenberghe (n.d.). *Convex Optimization*.

C. E. Garcia, D. M. Prett and M. Morari (1989). Model Predictive Control: Theory and Practice - a Survey. *Automatica* **25**, 335–348.

Camacho, E. F. and C. Bordons (2003). *Model Predictive Control*. Springer.

Carabogdan, G., A. Badea and A. Leca (1983). A Simulation Model of the Transient Performance of a Heat Pump. *International Journal of Refrigeration* **6**, 11–19.

Chang, H. and C. Shih (2005). Simulation and Optimization for Power Plant Flue Gas CO2 Absorption-Stripping Systems. *Separation Science and Technology* **40**, 877–909.

Christiansen, D. (1997). *Electronics Engineers' Handbook, 4th edition*. McGraw Hill Inc.

Danfoss A/S, Technical litterature (2004*a*). *Compressor Pack Controller AK2-PC-301A*. Danfoss A/S, DK. http:// www.danfoss.com / BusinessAreas / RefrigerationAndAirConditioning / Documentation.htm.

Danfoss A/S, Technical litterature (2004*b*). *Multicase Controller AK2-CC-303A*. Danfoss A/S, DK. http:// www.danfoss.com / BusinessAreas / RefrigerationAndAirConditioning / Documentation.htm.

Danfoss A/S, Technical litterature (2005). *Concept and design guide AK2 series*. Danfoss A/S, DK. http:// www.danfoss.com / BusinessAreas / RefrigerationAndAirConditioning / Documentation.htm.

Dixon, S. L. (1998). *Fluid Mechanics and Thermodynamics of Turbomachinery, (4th edn)*. Butterworth Heinemann.

Dua, V. and E.N. Pistikopoulos (2000). An algorithm for the solution of multiparametric mixed integer linear programming problems. *Annals of Operations-Research* pp. 123–139.

Duwaish, H. and W. Naeem (2001). Nonlinear model predictive control of Hammerstein and Wiener Models using genetic algorithms. In proc.: *Conference on Control Applications*. Mexico City, Mexico.

Edgar, T. F. and D. M. Himmelblau (2001). *Optimization of Chemical Processes, (2nd edn)*. McGraw-Hill.

Efstratiadis, A., D. Koutsoyiannis and D. Xenos (2004). Minimizing water cost in water resource management of Athens. *Urban Water Journal* **1**, 3–15.

Fahlén, P. (1996). Frosting and Defrosting of Air-Coils. PhD thesis. Department of Building Services Engineering - Chalmers University of Technology. Göteborg.

Faramarzi, R. T. (2004). Investigation of Secondary Loop Supermarket Refrigeration Systems. Technical report. California Energy Commision, Public Interest Energy Research Program. http://www.energy.ca.gov/pier/final_project_reports/500-04-013.htm.

Gharb, R. B. C. (2001). Economic Optimization of EOR Processes Using Knowledge-Based System: Case Studies. *Petroleum Science and Technology* **19**, 797–823.

Gordon, B. W., S. Liu and H. H. Asada (1999). Dynamic Modeling of Multiple-Zone Vapor Compression Cycles using Variable order Representations. In proc.: *American Control Conference*. San Diego, California.

Grossmann, I. and M. Morari (1984). Operability, resiliency, and flexibility - process design objectives for a changing world. In proc.: *2nd International Conference on Foundations of Computer Design*. Austin TX, USA.

Gruhle, W. D. and R. Isermann (1985). Modelling and Control of a Refigerant Evaporator. In proc.: *American Control Conference*. Boston, USA.

Gunawardena, J. (2003). *Chemical reaction network theory for in-silico biologist, lecture notes*. Bauer Center for Research, Harvard University. Cambrigde, MA, USA.

Halvorsen, I.J. and S. Skogestad (1998). Use of Feedback for Indirect Optimizing Control: Application to Petlyuk Distillation. In proc.: *5th IFAC Symposium on Dynamics and Control of Process Systems (DYCOPS-5)*. Corfu, Greece.

Hayes, J. P. (1993). *Introduction to digital logic design*. Addison-Wesley.

Heemels, W. P. M. H., B. De Schutter and A. Bemporad (2001). Equivalence of hybrid dynamical models. *Automatica*.

HYSCOM (n.d.). IEEE CSS Technical Committee on Hybrid Systems. http://www.dii.unisi.it /hybrid / ieee.

ILOG, Inc. (2003). *CPLEX 9.0 User Manual*. Gentilly Cedex, France.

Incropera, F. P. and D. P. DeWitt (1985). *Fundamentals of Heat and Mass Transfer (2nd edn)*. John Wiley and Sons.

Jakobsen, A. and B. D. Rasmussen (1998). Energy-optimal speed control of fans and compressors in a refrigeration system. In proc.: *Eurotherm Seminar*. Nancy, France.

Jakobsen, A. and M. J. Skovrup (2001). Forslag til energioptimal styring af kondenseringstryk - Carlsberg Case (*in danish*). Case report from the ESO-project. Technical report. MEK, DTU. http://www.et.web.mek.dtu.dk/ESO/Index.htm.

Jakobsen, A. and M. J. Skovrup (2004). Simulation Model of Supermarket Refrigeration System. Technical report. IPU - Køle- og Energiteknik. http://www.ipu.dk/kt/indexke.php.

Jakobsen, A., B. D. Rasmussen, M. J. Skovrup and J. Fredsted (2001). Development of energy optimal capacity control in refrigeration systems. In proc.: *International Refrigeration Conference*. Purdue, USA.

Jiang, T., B. Chen, X. He and P. Stuart (2003). Application of steady-state detection method based on wavelet transform. *Computers and Chemical Engineering* **27**, 569–578.

Klein, S. A. and F. L. Alvarado (2002). *EES - Engineering Equation Solver*. F-Chart Software, USA. http://www.fchart.com.

Larsen, L. F. S. and C. Thybo (2004*a*). *A Model Prediction Controlled Refrigeration System*. Patent application pending, No: PA 2004 01494. Danfoss A/S, DK.

Larsen, L. F. S. and C. Thybo (2004*b*). Potential energy savings in refrigeration systems using optimal setpoints. In proc.: *Conference on Control Applications*. Taipei, Taiwan.

Larsen, L. F. S. and J. R. Holm (2002). Modelling and Control of Refrigeration Systems. *Master Thesis*.

Larsen, L. F. S. and J. R. Holm (2003). Modelling and Multi-Variable Control of Refrigeration Systems. In proc.: *ECOS*. Copenhagen, Denmark.

Larsen, L. F. S., C. Thybo, J. Stoustrup and H. Rasmussen (2003). Control Methods Utilizing Energy Optimizing Schemes in Refrigeration Systems. In proc.: *European Control Conference*. Cambrigde, UK.

Larsen, L. F. S., C. Thybo, J. Stoustrup and H. Rasmussen (2004). A Method for Online Steady State Energy Minimization, with Application to Refrigeration Systems. In proc.: *Conference on Decision and Control*. Paradise Island, Bahamas.

Larsen, L. F. S., T. Geyer and M. Morari (2005). Hybrid MPC in Supermarket Refrigeration Systems. In proc.: *16th IFAC World Congress*. Prague, Czech Republic.

Lefkowitz, I. (1966). Multilevel approach applied to control system design. *Trans. of ASME, Series B, Journal of Basic Engineering*.

Liavas, A. P., G. V. Moustakides, G. Henning, E. Z. Psarakis and Peter Husar (1998). A Periodogram-Based Method for the Detection of Steady-State Visually Evoked Potentials. *Transactions on Biomedical Engineering* **45**, 242–248.

Lin, J., A. S. Morse and B. D. O. Anderson (2005*a*). The multi-agent rendezvous problem - part 1 the synchronous case. *Submitted to SIAM Journal on Control and Optimization*.

Lin, Z., B. Francis and M. Maggiore (2005*b*). On the state agreement problem for dynamical multible nonlinear dynamical systems. In proc.: *16th IFAC World Congress*. Prague, Czech Republic.

Lin, Z., B. Francis and M. Maggiore (2005*c*). State agreement Problem for Coupled Nonlinear Systems with Time-varying Interaction. *Submitted to SIAM Journal on Control and Optimization*.

Maciejowski, J. M. (2002). *Predictive Control with Constraints*. Prentice Hall.

Mayne, D.Q., J.B. Rawlings, C.V. Rao and P.O.M. Scokaert (2000). Constrained model predictive control: Stability and Optimality. *Automatica* **36**(6), 789–814.

Meyer, M. and A. Sonnenmoser (1993). A hysteresis current control for parallel connected line-side converters of an inverter locomotive. In proc.: *Fifth European Conference on Power Electronics and Applications*.

Milosevic, M., J. Allmeling and G. Andersson (2004). Interaction Between Hysteresis Controlled Inverters used in Distributed Generation Systems. In proc.: *Presented at the IEEE PES General Meeting*. Denver, Colorado.

Moases, Y. and S. Rajsbaum (2002). A layered analysis of consensus. *SIAM Journal on Computing* **31**, 989–1021.

Mølbak, T. (2003). Integrated model based optimization of a power production system. In proc.: *ECOS*. Copenhagen, DK.

Morari, M. (2002). Hybrid system analysis and control via mixed integer optimization. In proc.: *IFAC Symposium on Dynamics and Control of Process Systems*. pp. 1–12.

Morari, M., Y. Arkun and G. Stephanopoulos (1980). Studies in the Synthesis of Control Structures for Chemical Processes; Part I: Formulation of the Problem. Process Decomposition and the Classification of the Control Tasks. Analysis of the Optimizing Control Structures. *AIChE J.* **26**, 220–232.

Parkum, J. and C. Wagner (1994). Identification and Control of a Dry-expansion Evaporator. In proc.: *10th IFAC symposium on system identification*. Copenhagen, Denmark.

Petersen, A. and P. A. Lund (2004). Modelling and Control of Refrigeration System. *Master Thesis*.

Pogromsky, A., G. Santoboni and H. Nijmeijer (2002). Partial synchronization: from symmetry towards stability. *Physica D*.

Qin, S. J. and T. A. Badgwell (2003). A Survey of Industrial Model Predictive Control Technology. *Control Engeneering Practice* **11**, 733–764.

Raman, R. and I.E. Grossmann (1991). Relation between MILP modeling and logical inference for chemical process synthesis. *Computers and Chemical Engineering* **15**(2), 73–84.

Rossiter, J. A. (2000). *Model Based Predictive Control A Practical Approach*. CRC Press.

Skogestad, S. (2000). Plantwide Control: The Search for the Self-optimizing Control Structure. *Journal of Process Control* **10**, 487–507.

Skovrup, M. J. (2000). *Thermodynamic and Thermophysical Properties of Refrigerants - Software package in Borland Delphi, Version 3.00*. Department of Energy Engineering, Technical University of Denmark, DK. http://www.et.web.mek.dtu.dk/WinDali/Files/RefEqns_3.10.zip.

Sonntag, R. E., C. Borgnakke and G. J. Van Wylen (1998). *Fundamentals of Thermodynamics (5th edn)*. John Wiley and Sons.

Stoecker, W. F. (1985). *Refrigeration and Air Conditioning*. McGraw-Hill.

Svensson, M. S. (1994). Studies on On-line Optimizing Control, with Application to a Heat Pump. PhD thesis. Institutt for kuldeteknikk - NTH. Trondheim.

Thybo, C. (2005). *A method for controlling a refrigeration system*. Patent application pending, No: PA 2005 00411. Danfoss A/S, DK.

Thybo, C. and R. I. Zamanabadi (2003*a*). Detecting condenser faults in commercial refrigeration systems. In proc.: *ECC*. Cambrigde, UK.

Thybo, C. and R. I. Zamanabadi (2003*b*). Fault detection and diagnosis in refrigeration systems - a summeray of latest results. In proc.: *International Congress of Refrigeration*. Washington D.C., USA.

Torrisi, F.D., A. Bemporad and D. Mignone (2000). HYSDEL — A Tool for Generating Hybrid Models. Technical Report AUT00-03. Automatic Control Laboratory ETH Zurich. http://control.ee.ethz.ch.

Tyler, M.L. and M. Morari (1999). Propositional logic in control and monitoring problems. *Automatica* **35**(4), 565–582.

Xiang-Dong, H., S. Liu and H. H. Asada (1997). Modelling of Vapor Compression Cycles for Multivariable Feedback Control of HVAC Systems. *Journals of Dynamic Systems, Measurement and Control* **119**, 183–191.

Yaqun, H., L. Shan, L. Maixi, K. Yali and L. Huaiyu (2002). A Profit-Oriented Expert System for Coal Washery Optimization. *Coal Preparation* **22**, 93–107.

Appendix A

Test System

The test refrigeration system has been buildt supported by sponsorships from Danfoss A/S, Danfoss Drives A/S, Siemens A/S, Grundfos A/S and Findan A/S. In the following a detailed description of the design of the test refrigeration system will be given. Large part of the description given here is extracted from Petersen and Lund (2004).

A.1 Construction of the Test Refrigeration System

The test refrigeration system can be divided into three parts namely:

- The refrigeration system
- The secondary side, i.e. the heat load circuit
- The control interface module.

In the following a detailed description of these parts will be given.

A.1.1 The Refrigeration System

A detail overview of the primary and secondary side is depicted in Figure A.2 and Figure A.1 depicts the entire system.
The components by which the refrigeration system has been constructed will be went over in the following and afterwards the sensors will be described.

Figure A.1: Picture of the test refrigeration system

A.1.1.1 Expansion Valves

There are two expansion valves on the refrigeration system, a thermostatic and an electronic expansion valve. It is possible by opening and closing the manual valves $v12$ and $v12b$ (see Figure A.2) to switch operation such that either the electronic or the thermostatic expansion valve is used.
Following types of valves has been used:

- A thermostatic valve, **Danfoss TEN 2**.
- An electronic expansion valve, **MCV HVAC** from Danfoss.

A.1.1.2 Compressor

The compressor is a **Danfoss-Maneurop MTZ32**, which is a reciprocating piston compressor. The compressor has a displacement volume of 53.86 cm^3. The motor shaft speed, is controlled by an adjustable frequency drive. The low-pressure vapor is used to cool down the compressor before it is compressed inside the cylinder. A pressostat is

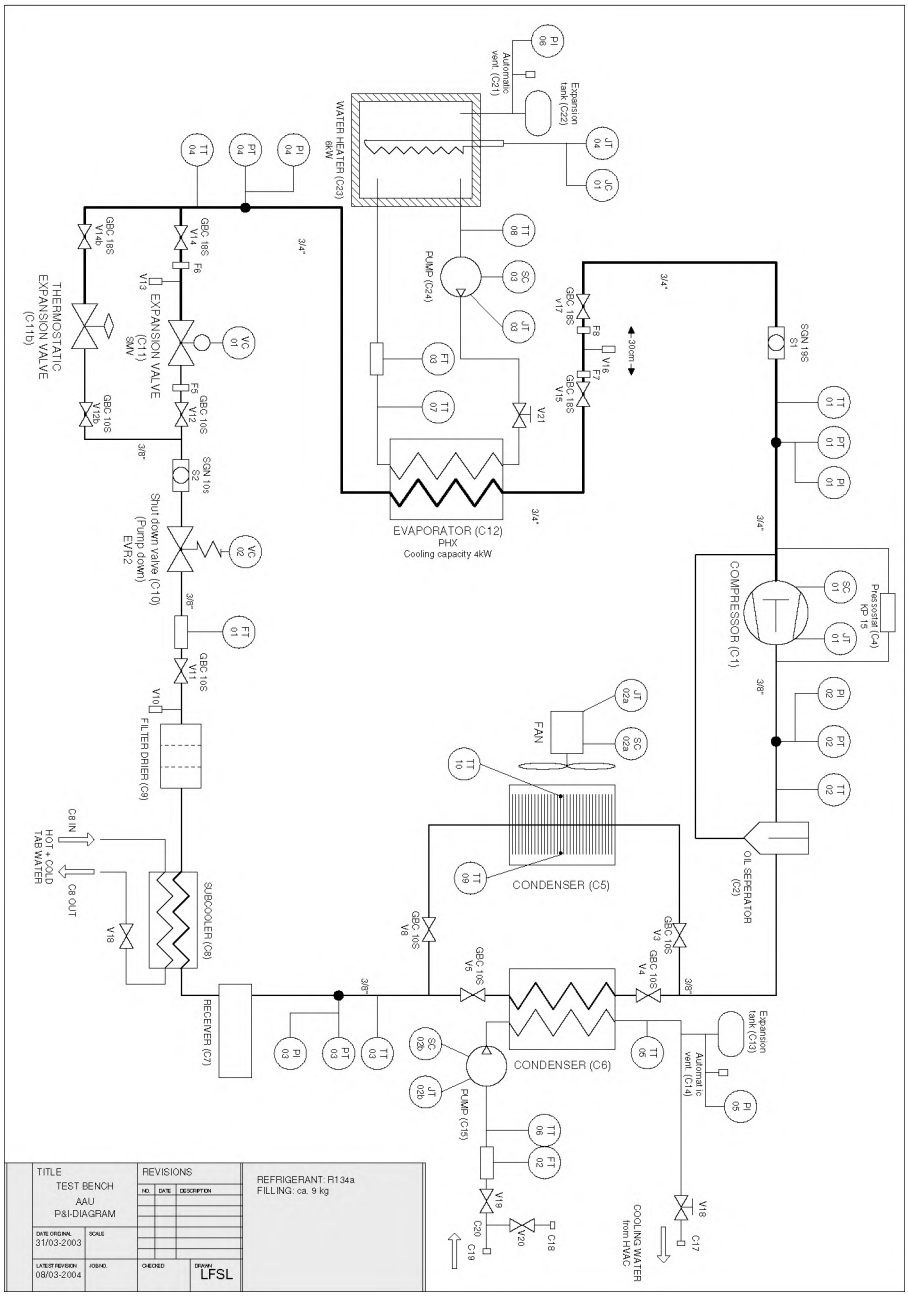

Figure A.2: Detailed layout of test refrigeration system

Figure A.3: Receiver (left) and Compressor (right).

placed across the compressor, cutting off the power supply to the entire system (except the data acquisition) when the pressure thresholds are violated, thereby preventing damage to the system. The pressostat will engage when the condensing pressure exceeds 12 bar, or the evaporating pressure drops below 2 bar. The compressor is depicted in Figure A.3

A.1.1.3 Receiver

A receiver is placed between the condenser and the expansion valves. The receiver establishes a buffer zone to compensate for varying need of refrigerant depending on the point of operation. The receiver is depicted to the left of the compressor in Figure A.3.

A.1.1.4 Condenser

The condenser is an **ECO, type ACE**. It is equipped with a 500 mm diameter fan, which is vertically aligned (see Figure A.4). The fan speed is controlled by an adjustable frequency drive allowing a fan speeds of 0-50 s^{-1}. The air flows across the condenser tubes guided by a number of the aluminium fins that furthermore ensure a large heat transferring area.

Figure A.4: Condenser seen from above.

A.1.1.5 Subcooler

The subcooler is placed between the condenser and the expansion valve. The function of the subcooler, is to cool down the condensed refrigerant. The refrigerant is cooled down by leading cold tap water past the refrigerant in a small heat exchanger. Additional energy is transmitted from the refrigerant to the tap water, cooling down the refrigerant creating larger subcooling. This is normally not used but can, if necessary, be turned on.

A.1.1.6 Evaporator

The evaporator is a **GEA, M2520L2G2X**. The refrigerant and the secondary medium (water) are separated in separate flow chambers. The flow chambers are constructed from pressed stainless steel plates. The plates are soldered together, and isolated from the ambient by a 30 mm thick layer of polyurethane foam. The refrigerant and secondary medium passes through the evaporator in opposite direction. The top of the evaporator is depicted in Figure A.5. The tube are in- and outlet of respectively water and refrigerant.

A.1.1.7 Frequency Drives

Two adjustable frequency drives are utilized in the cooling plant. a **VLT 5000**, controlling the rotational speed of the compressor and a **ADAP KOOL AKD 5000**, controlling the rotational speed of the condenser fan. The drives are both manufactured by Danfoss A/S. The adjustable frequency drive operates in open loop, as all regulation is performed in the control module (Section A.1.3). For the compressor the low limit rotational speed

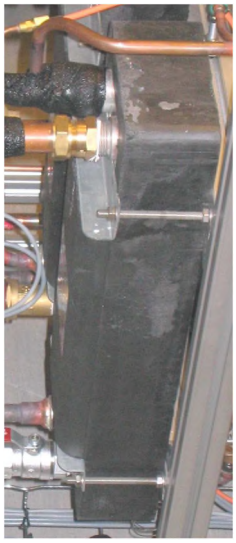

Figure A.5: The evaporator.

is sat to 35 s^{-1}, to ensure a sufficient lubrication when the compressor is running.
The frequency drives also measures power consumption in respectively the compressor and the condenser fan.

A.1.1.8 Flow Transmitter

The flow transmitter on the refrigerant side is a **Siemens SITRANS F M MAGFLO**. The measuring device is a MASS 2100, and the signal converter is a MAG 6000. The Mass 2100 is able to measure the mass flow of a liquid substance passing through. It utilizes the coriolis force to calculate the mass flow. The sensor converts the flow into an electrical voltage, proportional to the mass flow.

A.1.1.9 Pressure Transmitter

The pressure transmitters are manufactured by Danfoss A/S, and of the type **AKS 33**. They produce a signal between 0 and 10 volts proportional to the pressure.

A.1.1.10 Temperature Transmitter

The temperature transmitters are of the type **PT 1000** and manufactured by Danfoss. They produce a signal between 0 and 10 volts proportional to the temperature. They

are mounted onto the copper tubes, and isolated from the ambient by a layer of insulating material. The temperature transmitters do not have direct thermal contact with the refrigerant, but measures the copper tube temperature instead. This introduces a small time constant in the measurements.
The same kind of temperature sensors are used on the heat load circuit.

A.1.2 Heat Load Circuit

The function of the heating load circuit, is to simulate a cooling storage. By heating the water in the water tank, the temperature of the water led into the evaporator increases. This can be interpreted as a temperature change in a cooling storage. The components of the heating load circuit are outlined in the following.

A.1.2.1 Water Heater

The water heater is a **Metro, type 620**. It has a capacity of 60 liters. A 6 kW heating element is placed in the tank. The heating element delivers an adjustable power of 0-6 kW to the water.

A.1.2.2 Water Pump

The water pump is a **Grundfos UPE 25-40**. It provides a water flow proportional to an analog input signal. The input signal is not connected to the control module, so the water flow is presently set manually on the pump.

A.1.3 Control Interface Module

The control interface module establishes an interface between the refrigerate system, and the user. It is comprised by both hardware and software. A flow chart of the control interface module is depicted in Figure A.6. The Software is installed on the host PC, where the SIMULINK control diagram is compiled into an executable file, which is downloaded to the target PC through a LAN.

A.1.3.1 Target PC

A 3 GHz target PC equipped with two PCI National Instruments DAQ (NI-6024E DAQ), and 512 MbRAM is mounted on the cooling plant. Each DAQ has two output channels, and 8 differential or 16 single ended input channels. Each channel is sampled with 12 Bit.

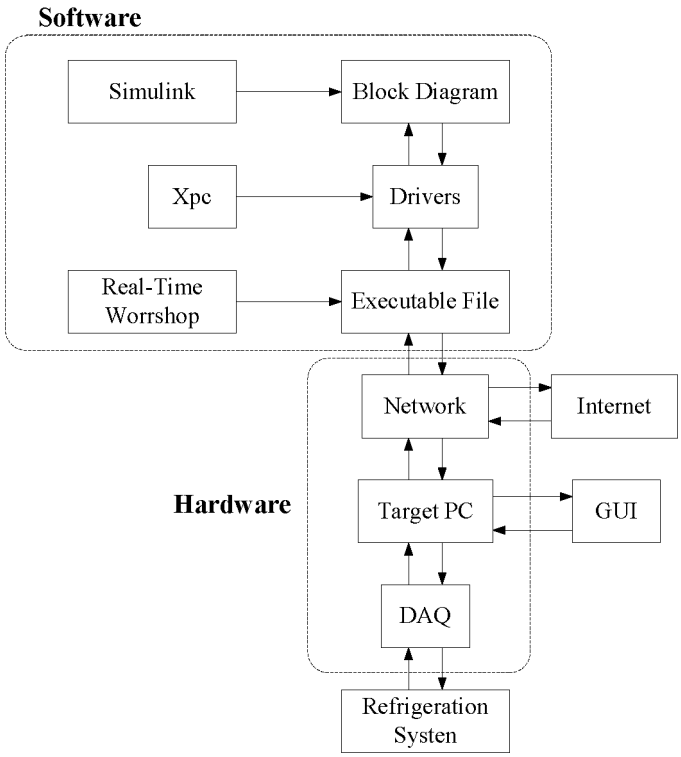

Figure A.6: Flowchart illustrating how the control module is constructed.

A.1.3.2 Software

For control of both the cooling circuit and heating load circuit, it has been chosen to interface the circuits using the XPC-toolbox for SIMULINK. The XPC-toolbox contains a set of block diagram representations of various hardware components, among which the National Instrument DAQ's can be found.
Mathworks have furthermore developed the Real-Time Workshop, which is an automatic code generator for a variety of platforms. By using Real-Time Workshop, it is possible to implement the controller in block-diagram form, as Real-Time Workshop will translate the SIMULINK diagram into C-code, which is afterwards compiled into an executable file using a C-compiler. The executable file is then uploaded on the target PC through a LAN. This construction enables control experiments to be conducted on the refrigeration system through the internet.

Appendix B

Derivation of Gradients

In Section 4.3 the gradient of $J = \dot{W}_C + \dot{W}_{CF} + \dot{W}_{EF}$ is used. In the following the derivation of

$$\frac{dJ}{dx_{ss}}\Big|_{o_{ss}} = \begin{bmatrix} \frac{d\dot{W}_C}{dP_c} & \frac{d\dot{W}_{CF}}{dP_c} & \frac{d\dot{W}_{EF}}{dP_c} \\ \frac{d\dot{W}_C}{dP_e} & \frac{d\dot{W}_{CF}}{dP_e} & \frac{d\dot{W}_{EF}}{dP_e} \end{bmatrix}_{\dot{Q}_e = const}$$

will be went over. Each of the three elements $[\frac{d\dot{W}_C}{dP_c}, \frac{d\dot{W}_C}{dP_e}]^T$, $[\frac{d\dot{W}_{CF}}{dP_c}, \frac{d\dot{W}_{CF}}{dP_e}]^T$, and $[\frac{d\dot{W}_{EF}}{dP_c}, \frac{d\dot{W}_{EF}}{dP_e}]^T$ will be derived individually. During the derivation it is assumed that the superheat (T_{sh}) and the subcooling (T_{sc}) is constant. The superheat is a controlled variable which makes it a good assumption, whereas the subcooling is varying. However the subcooling is normally not varying at lot and the variations has only an infinitesimal impact on the total power consumption.

Derivation of Eq.(4.19), that is $[\frac{d\dot{W}_C}{dP_c}, \frac{d\dot{W}_C}{dP_e}]^T$.
Inserting Eq.(4.9) in Eq.(4.8) gives:

$$\dot{W}_C = \frac{\dot{Q}_e}{\eta_{is}} \cdot \frac{h_{is}(P_e, P_c) - h_{oe}(P_e)}{h_{oe}(P_e) - h_{oc}(P_c)} \tag{B.1}$$

By direct differentiations of Eq.(B.1), following is obtained:

$$\begin{bmatrix} \frac{d\dot{W}_C}{dP_c} \\ \frac{d\dot{W}_C}{dP_e} \end{bmatrix} = \begin{bmatrix} \frac{\dot{Q}_e}{\eta_{is}} \cdot \frac{1}{h_{oe}-h_{oc}} \left(\frac{\partial h_{ic}}{\partial P_c} + \frac{\partial h_{oc}}{\partial P_c} \frac{h_{is}-h_{oe}}{h_{oe}-h_{oc}} \right) \\ \frac{\dot{Q}_e}{\eta_{is}} \cdot \frac{1}{h_{oe}-h_{oc}} \left(\frac{\partial h_{is}}{\partial P_e} - \frac{\partial h_{oe}}{\partial P_e} - \frac{\partial h_{oe}}{\partial P_e} \frac{h_{is}-h_{oe}}{h_{oe}-h_{oc}} \right) \end{bmatrix} \tag{B.2}$$

By inserting Eq.(B.1) in Eq.(B.2), Eq.(4.19) can be obtained.

Derivation of Eq.(4.20) and Eq.(4.21).
In the following we will only derive the derivative $\frac{d\dot{W}_{CF}}{dP_c}$ by using by using the same procedure, the rest of the derivatives in Eq.(4.20) and Eq.(4.21) can be found.
By using Eq.(4.11) and Eq.(4.12) the derivative $\frac{d\dot{W}_{CF}}{dP_c}$ can be found as:

$$\frac{d\dot{W}_{CF}}{dP_c} = \frac{\partial \dot{W}_{CF}}{\partial \dot{m}_{air,C}} \cdot \frac{\partial \dot{m}_{air,C}}{\partial P_c} = 3\frac{K_{1,CF}}{(K_{2,CF})^3}\dot{m}_{air,C}^2 \cdot \frac{\partial \dot{m}_{air,C}}{\partial P_c} \tag{B.3}$$

$\frac{\partial \dot{m}_{air,C}}{\partial P_c}$ can be found from Eq.(4.13), Eq.(4.14) and Eq.(2.12) hereby following is obtained:

$$0 = \dot{Q}_e + \dot{W}_C(1-f_q) - \dot{m}_{air,C}C_{p,air}(T_c - T_a) \cdot \left(1 - \exp\left(-\frac{\alpha_C \cdot \dot{m}_{air,C}^{m_C}}{\dot{m}_{air,C} \cdot C_{p,air}}\right)\right)$$

$$\Updownarrow$$

$$\underbrace{\dot{m}_{air,C}\left(1 - \exp\left(-\frac{\alpha_C \cdot \dot{m}_{air,C}^{m_C}}{\dot{m}_{air,C} \cdot C_{p,air}}\right)\right)}_{f(\dot{m}_{air,C})} = \underbrace{\frac{\dot{Q}_e + \dot{W}_C(1-f_q)}{C_{p,air}(T_c - T_a)}}_{g(P_c)}$$

From this following can be deduced:

$$\frac{\partial f}{\partial P_c} = \frac{\partial f}{\partial \dot{m}_{air,C}}\frac{\partial \dot{m}_{air,C}}{\partial \dot{P}_c} = \frac{\partial g}{\partial P_c} \Longrightarrow \frac{\partial \dot{m}_{air,C}}{\partial \dot{P}_c} = \frac{\partial g}{\partial P_c}\left(\frac{\partial f}{\partial \dot{m}_{air,C}}\right)^{-1} \tag{B.4}$$

Since $f(\dot{m}_{air,C}) = \dot{m}_{air,C}\left(1 - \exp\left(-\frac{\alpha_C \cdot \dot{m}_{air,C}^{m_C}}{\dot{m}_{air,C} \cdot C_{p,air}}\right)\right)$ we obtain:

$$\begin{aligned}\frac{\partial f}{\partial \dot{m}_{air,c}} &= 1 - \exp(-\frac{\alpha_C \cdot \dot{m}_{air,C}^{m_C}}{\dot{m}_{air,C} \cdot C_{p,air}})\left((1-m)\frac{\alpha_C \cdot \dot{m}_{air,C}^{m_C}}{\dot{m}_{air,C} \cdot C_{p,air}} + 1\right) \\ &= \frac{\dot{Q}_C - (1-m_C)UA_C(T_c - T_{aoc})}{(T_c - T_a)\dot{m}_{air,C} \cdot C_{p,air}}\end{aligned} \tag{B.5}$$

Furthermore $g(P_c) = \frac{\dot{Q}_e + \dot{W}_C(1-f_q)}{C_{p,air}(T_c - T_a)}$ thereby:

$$\frac{\partial g}{\partial P_c} = \frac{\frac{d\dot{W}_C}{dP_c}(1-f_q)(T_c - T_a) - \dot{Q}_c\frac{\partial T_c}{\partial P_c}}{C_{p,air}(T_c - T_a)^2} \tag{B.6}$$

By applying Eq.(B.4), Eq.(B.5) and Eq.(B.6) to Eq.(B.3) following is obtained:

$$\frac{d\dot{W}_{CF}}{dP_c} = \frac{3\dot{W}_{CF}}{\dot{Q}_c - UA_C(1-m_C)(T_c - T_{aoc})}\frac{d\dot{W}_C}{dP_c}(1-f_q) - \frac{\dot{Q}_c}{T_c - T_a}\frac{\partial T_c}{\partial P_c} \tag{B.7}$$

Finally by using Eq.(4.8) the derivative $\frac{d\dot{W}_{CF}}{dP_c}$ in Eq.(4.20) can be found.

Appendix C

HYSDEL Model

In this appendix the HYSDEL code used in the case example of a supermarket refrigeration system is provided. The model consist of two compressors that together forms 3 discrete capacities (0%, 50% and 100%) and two display cases each with an inlet valve that can be either open or closed.

```
SYSTEM Refrig_two_evap {
INTERFACE {

INPUT {
/* ----- COMPRESSOR & MANIFOLD-------------------------------------------------------------------------------------------*/
        BOOL Comp1,Comp2;                                       /* Discrete compressor capacities                */
/* ----- EVAPORATOR 1---------------------------------------------------------------------------------------------------*/
        BOOL valve_1;                                           /* Off/on Valve                          EVAP 1 */
        REAL topen_1;                                           /* Opening time of valve, when open      EVAP 1 */
/* ----- EVAPORATOR 2---------------------------------------------------------------------------------------------------*/
        BOOL valve_2;                                           /* Off/on Valve                          EVAP 2 */
        REAL topen_2;                                           /* Opening time of valve, when open      EVAP 2 */
}

STATE {
/* ----- COMPRESSOR & MANIFOLD -----------------------------------------------------------------------------------------*/
        REAL Psuc [1, 7];                                       /* Suction pressure in suction manifold          */
        REAL Comp_old [0,2];                                    /* Previous control action of compressor         */

    /* ----- EVAPORATOR 1--------------------------------------------------------------------------------------------*/
        REAL Dis_Twall_1 [-15,15];                              /* Discrete wall temperature             EVAP 1 */
        REAL Dis_Tgoods_1 [0,5];                                /* Discrete temperature of goods         EVAP 1 */
        REAL Dis_Qe_1 [0,3000];                                 /* Discrete Measured temperature of air  EVAP 1 */

    /* ----- EVAPORATOR 2--------------------------------------------------------------------------------------------- */
        REAL Dis_Twall_2 [-15,15];                              /* Discrete wall temperature             EVAP 2 */
        REAL Dis_Tgoods_2 [0,5];                                /* Discrete temperature of goods         EVAP 2 */
        REAL Dis_Qe_2 [0,3000];                                 /* Measured temperature of air           EVAP 2 */
}

OUTPUT {
        REAL out1,                                              /* Psuc                                          */
        out2,                                                   /* Tair_1                                        */
        out3,                                                   /* Tair_2                                        */
        out4,                                                   /* delt_comp                                     */
}

PARAMETER {
        REAL
/* ----- COMPRESSOR & MANIFOLD -----------------------------------------------------------------------------------------*/
```

```
        Te,                                                     /* Evaporation temperature     EXTERNAL PARAMETER*/
        he_in=2.096615e+005,                                    /* Enthalpy at inlet of evaporator              */
        he_out=3.623586e+005,                                   /* Enthalpy at outlet of evaporator             */
        A_suc_1 = -0.05810540416268,            /* Discrete state space model of suction manifold for comp1=50\%.*/
        A_suc_2 = -0.05810540416268,            /* Discrete state space model of suction manifold for comp2=50\%.*/
        B_suc = 1.318443840638573e-005,

/* ----- EVAPORATOR 1-------------------------------------------------------------------------------------------*/
        Qairload_1=900,                                     /* Direct load on air-curtain [W], Disturbance EVAP 1 */
        UA_refrig_1=15.4*150,                             /* Heat transfer coefficient refrigerant evap. wall EVAP 1 */
        UA_goodsair_1=60,                                   /* Heat transfer coefficient goods to air     EVAP 1 */
        UA_airwall_1=360,                                   /* Heat transfer coefficient air to wall      EVAP 1 */
        Twall_1,                /* Temperature of the evaporator wall (updated each time step)  EXTERNAL PARAMETER*/
        Qe_ind_1=UA_refrig_1*(Twall_1-Te),                  /* Cooling capacity of display case       EVAP 1 */
        /* Discrete state space model evaporator when valve = on                                      EVAP 1 */
        A11_1=0.99240812,      A12_1=-5.3170404e-008,   A13_1=0.007591876,
        A21_1=0,               A22_1=0.22313016,        A23_1=0,
        A31_1=0.043382149,     A32_1=-1.0906412e-005,   A33_1=0.95661785,
        B11_1=-0.0010695303, B12_1=0.00014642237,
        B21_1=27967.314,     B22_1=0,
        B31_1=-0.36954043,   B32_1=0.004358106,
        C11_1=1, C12_1=0,     C13_1=0,
        C21_1=0, C22_1=0.025, C23_1=0,
        C31_1=0, C32_1=0,     C33_1=1,
        D11_1=0, D12_1=0,
        D21_1=0, D22_1=0,
        D31_1=0, D32_1=0,

/* ----- EVAPORATOR 2-------------------------------------------------------------------------------------------*/
        Qairload_2=900,                                     /* Direct load on air-curtain [W], Disturbance EVAP 2 */
        UA_refrig_2=900,                                  /* Heat transfer coefficient refrigerant evap. wall EVAP 2 */
        UA_goodsair_2=60,                                   /* Heat transfer coefficient goods to air     EVAP 2 */
        UA_airwall_2=360,                                   /* Heat transfer coefficient air to wall      EVAP 2 */
        Twall_2,                                          /* Temperature of the evaporator wall  EXTERNAL PARAMETER*/
        Qe_ind_2= UA_refrig_2*(Twall_2-Te),                 /* Cooling capacity of display case       EVAP 2 */
       /* Discrete state space model evaporator when valve = on                                       EVAP 2 */
        A11_2=0.99240812,      A12_2=-5.3170404e-008,   A13_2=0.007591876,
        A21_2=0,               A22_2=0.22313016,        A23_2=0,
        A31_2=0.043382149,     A32_2=-1.0906412e-005,   A33_2=0.95661785,
        B11_2=-0.0010695303, B12_2=0.00014642237,
        B21_2=27967.314,     B22_2=0,
        B31_2=-0.36954043,   B32_2=0.004358106,
        C11_2=1, C12_2=0,     C13_2=0,
        C21_2=0, C22_2=0.025, C23_2=0,
        C31_2=0, C32_2=0,     C33_2=1,
        D11_2=0, D12_2=0,
        D21_2=0, D22_2=0,
        D31_2=0, D32_2=0;
}
} /* End INTERFACE*/

IMPLEMENTATION {
        AUX {
        REAL Energy_In;                                     /* Energy flow into manifold from evaporator      */
/* ----- COMPRESSOR & MANIFOLD ---------------------------------------------------------------------------------*/
        REAL z_psuc1,z_psuc2;                               /* Z-variable for compressor switches             */
        REAL delt_comp;                                     /* Change in compressor capacity                  */
/* ----- EVAPORATOR 1------------------------------------------------------------------------------------------*/
        REAL z_Twall_1,                                     /* variable for wall temperature           EVAP 1 */
        z_Tgoods_1,                                         /* variable for goods temperature          EVAP 1 */
        z_Qe_1,                                             /* variable for cooling cap. i evap.       EVAP 1 */
        Tair_1,                                             /* Air temperature                         EVAP 1 */
        Energy_out_1,                                       /* Energy flow out of evaporator           EVAP 1 */
        mout_1,                                             /* Mass flow out of evaporator             EVAP 1 */
        slack_Tair_upper_1,                  /* Slack variable for upper bound on the air temperature EVAP 1 */
        slack_Tair_lower_1;                  /* Slack variable for lower bound on the air temperature EVAP 1 */
/* ----- EVAPORATOR 2------------------------------------------------------------------------------------------*/
        REAL z_Twall_2,                                     /* variable for wall temperature           EVAP 2 */
        z_Tgoods_2,                                         /* variable for goods temperature          EVAP 2 */
        z_Qe_2,                                             /* variable for cooling cap. i evap.       EVAP 2 */
        Tair_2,                                             /* Air temperature                         EVAP 2 */
        Energy_out_2,                                       /* Energy flow out of evaporator           EVAP 2 */
        mout_2,                                             /* Mass flow out of evaporator             EVAP 2 */
        slack_Tair_upper_2,                  /* Slack variable for upper bound on the air temperature EVAP 2 */
        slack_Tair_lower_2;                  /* Slack variable for lower bound on the air temperature EVAP 2 */
}

DA {
/* ----- COMPRESSOR & MANIFOLD ---------------------------------------------------------------------------------*/
        z_psuc1 = { IF Comp1 THEN A_suc_1*Psuc
                             ELSE 0};
```

```
       z_psuc2 = { IF Comp2 THEN A_suc_2*Psuc
                           ELSE 0};
}

LINEAR {
/*----- EVAPORATOR 1-------------------------------------------------------------------------------------------------*/
      /* Discrete temperatures:                                                                                EVAP 1 */
    z_Tgoods_1=  A11_1*Dis_Tgoods_1 + A12_1*Dis_Qe_1 + A13_1*Dis_Twall_1 + B11_1*Qe_ind_1*topen_1 + B12_1*Qairload_1;
    z_Qe_1    =  A21_1*Dis_Tgoods_1 + A22_1*Dis_Qe_1 + A23_1*Dis_Twall_1 + B21_1*Qe_ind_1*topen_1 + B22_1*Qairload_1;
    z_Twall_1 =  A31_1*Dis_Tgoods_1 + A32_1*Dis_Qe_1 + A33_1*Dis_Twall_1 + B31_1*Qe_ind_1*topen_1 + B32_1*Qairload_1;
      /* Real air temperatures EVAP 1 */
    Tair_1=(Qairload_1+C11_1*z_Tgoods_1*UA_goodsair_1+C33_1*z_Twall_1*UA_airwall_1)/(UA_goodsair_1+UA_airwall_1);
      mout_1=Dis_Qe_1*C22_1/(he_out-he_in);                    /* Mass flow out of evaporator              EVAP 1 */
      Energy_out_1=mout_1*he_out;                              /* Energy flow out of evaporator            EVAP 1 */
/*----- EVAPORATOR 2-------------------------------------------------------------------------------------------------*/
      /* Discrete temperatures:                                                                                EVAP 2 */
    z_Tgoods_2=  A11_2*Dis_Tgoods_2 + A12_2*Dis_Qe_2 + A13_2*Dis_Twall_2 + B11_2*Qe_ind_2*topen_2 + B12_2*Qairload_2;
    z_Qe_2    =  A21_2*Dis_Tgoods_2 + A22_2*Dis_Qe_2 + A23_2*Dis_Twall_2 + B21_2*Qe_ind_2*topen_2 + B22_2*Qairload_2;
    z_Twall_2 =  A31_2*Dis_Tgoods_2 + A32_2*Dis_Qe_2 + A33_2*Dis_Twall_2 + B31_2*Qe_ind_2*topen_2 + B32_2*Qairload_2;
      /* Real air temperatures EVAP 2 */
    Tair_2=(Qairload_2+C11_2*z_Tgoods_2*UA_goodsair_2+C33_2*z_Twall_2*UA_airwall_2)/(UA_goodsair_2+UA_airwall_2);
      mout_2=Dis_Qe_2*C22_2/(he_out-he_in);                    /* Mass flow out of evaporator              EVAP 2 */
      Energy_out_2=mout_2*he_out;                              /* he_out Energy flow out of evaporator     EVAP 2 */

/*----- COMPRESSOR & MANIFOLD ---------------------------------------------------------------------------------------*/
       Energy_In =Energy_out_1+Energy_out_2;                    /* Energy flow in from all evaporators            */
       delt_comp=Comp_old-((REAL Comp1)+(REAL Comp2));          /* Change in compressor capacity                  */
}

/* CONSTRAINTS */
MUST {
      topen_1-(REAL valve_1)<=0;                               /* When valve open then opening time <1 HARD EVAP 1 */
      topen_1>=(REAL valve_1)*1/6;                            /* When valve open then opening time >10sec HARD EVAP 1 */
      topen_2-(REAL valve_2)<=0;                               /* When valve open then opening time <1 HARD EVAP 2 */
      topen_2>=(REAL valve_2)*1/6;                            /* When valve open then opening time >10sec HARD EVAP 2 */
      1e4*(Tair_1-4)<=slack_Tair_upper_1;                      /* Upper bound on Tair                   SOFT EVAP 1 */
      1e4*(0-Tair_1)<=slack_Tair_lower_1;                      /* Lower bound on Tair                   SOFT EVAP 1 */
      1e4*(Tair_2-4)<=slack_Tair_upper_2;                      /* Upper bound on Tair                   SOFT EVAP 2 */
      1e4*(0-Tair_2)<=slack_Tair_lower_2;                      /* Lower bound on Tair                   SOFT EVAP 2 */
}

CONTINUOUS {
/*----- COMPRESSOR & MANIFOLD ---------------------------------------------------------------------------------------*/
      Psuc = z_psuc1+z_psuc2+B_suc*Energy_In;                  /* Suction pressure in manifold                   */
      Comp_old= ((REAL Comp1)+(REAL Comp2));                   /* Change in compressor capacity                  */
/*----- EVAPORATOR 1-------------------------------------------------------------------------------------------------*/
      Dis_Twall_1 = z_Twall_1;                                 /* Discrete wall temperature             EVAP 1 */
      Dis_Tgoods_1= z_Tgoods_1;                                /* Discrete temperature of goods         EVAP 1 */
      Dis_Qe_1= z_Qe_1;                                        /* Discrete temperature of air           EVAP 1 */
/*----- EVAPORATOR 2-------------------------------------------------------------------------------------------------*/
      Dis_Twall_2 = z_Twall_2;                                 /* Discrete wall temperature             EVAP 2 */
      Dis_Tgoods_2= z_Tgoods_2;                                /* Discrete temperature of goods         EVAP 2 */
      Dis_Qe_2= z_Qe_2;                                        /* Discrete temperature of air           EVAP 2 */
}

OUTPUT {
      out1=Psuc;
      out2=Tair_1;
      out3=Tair_2;
      out4=50*delt_comp;
}


} /* End Implementation */

} /*SYSTEM Refrig_one_evap */
```

Appendix D

System Matrices

In Chapter 6 a linearized model of a supermarkets refrigeration system was derived, i.e. Eq.(6.16) and Eq.(6.17). In this appendix the matching continuous-time system matrices are stated.

For to i'th display case following system matrices are assigned. It is implied that the parameters that enters can variate between the individual display cases.

$$A_i = \begin{bmatrix} \frac{UA_{goods-air}}{M_{goods} \cdot C_{p,goods}}(UA_{goods-air} - 1) & \frac{UA_{air-wall} UA_{goods-air}}{M_{goods} \cdot C_{p,goods}} & 0 \\ \frac{UA_{air-wall} UA_{goods-air}}{M_{wall} \cdot C_{p,wall}} & \frac{UA_{air-wall}}{M_{wall} \cdot C_{p,wall}}(UA_{air-wall} - 1) & 0 \\ 0 & 0 & -\frac{1}{\tau_{fil}} \end{bmatrix} \tag{D.1}$$

$$B_i = \begin{bmatrix} 0 \\ 0 \\ \frac{UA_{wall-ref,max}}{\tau_{fil}} \end{bmatrix} \tag{D.2}$$

$$c_i = \begin{bmatrix} \dot{Q}_{airload} \frac{UA_{goods-air}}{M_{goods} \cdot C_{p,goods}} \\ \dot{Q}_{airload} \frac{UA_{air-wall}}{M_{wall} \cdot C_{p,wall}} \\ 0 \end{bmatrix} \tag{D.3}$$

$$C_i = \frac{1}{UA_{goods-air} + UA_{goods-air}} \begin{bmatrix} UA_{goods-air} & UA_{air-wall} & 0 \end{bmatrix} \tag{D.4}$$

$$d_i = \frac{\dot{Q}_{airload}}{UA_{goods-air} + UA_{goods-air}} \tag{D.5}$$

For the suction manifold following system matrices are assigned.

$$B_u = -\frac{R \cdot h_{out-suc,0} \cdot \rho_{suc,0}}{C_v \cdot V_{suc}} \tag{D.6}$$

$$B_\alpha = -\frac{R \cdot h_{oe,0}}{C_v \cdot V_{suc}(h_{oe,0} - h_{ie,0})} \underbrace{\begin{bmatrix} 0 & 0 & 1 & \dots & 0 & 0 & 1 \end{bmatrix}}_{3 \times n} \tag{D.7}$$

$$C_u = -\frac{dT_e}{dP_{suc}}\bigg|_{P_{suc,0}} \tag{D.8}$$

$$d_u = T_{wall,0} + \frac{dT_e}{dP_{suc}}\bigg|_{P_{suc,0}} P_{suc,0} - T_{e,0} \tag{D.9}$$